2011-12

Experimental study of fluid structure interaction effects on metal plates under fully developed laminar flow

Wong, Chee Chew

Monterey, California. Naval Postgraduate School

NAVAL POSTGRADUATE SCHOOL

MONTEREY, CALIFORNIA

THESIS

EXPERIMENTAL STUDY OF FLUID STRUCTURE INTERACTION EFFECTS ON METAL PLATES UNDER FULLY DEVELOPED LAMINAR FLOW

by

Chee Chew Wong

December 2011

Thesis Advisor:	Young W. Kwon
Thesis Co-Advisor:	Jarema M. Didoszak

Approved for public release; distribution is unlimited

THIS PAGE INTENTIONALLY LEFT BLANK

REPORT DOCUMENTATION PAGE			Form Approved OMB No. 0704–0188
Public reporting burden for this collection of information is estimated to average 1 hour per response, including the time for reviewing instruction, searching existing data sources, gathering and maintaining the data needed, and completing and reviewing the collection of information. Send comments regarding this burden estimate or any other aspect of this collection of information, including suggestions for reducing this burden, to Washington headquarters Services, Directorate for Information Operations and Reports, 1215 Jefferson Davis Highway, Suite 1204, Arlington, VA 22202–4302, and to the Office of Management and Budget, Paperwork Reduction Project (0704–0188) Washington DC 20503.			
1. AGENCY USE ONLY *(Leave blank)*	**2. REPORT DATE** December 2011	**3. REPORT TYPE AND DATES COVERED** Master's Thesis	
4. TITLE AND SUBTITLE Experimental Study of Fluid Structure Interaction Effects on Metal Plates Under Fully Developed Laminar Flow		**5. FUNDING NUMBERS**	
6. AUTHOR(S) Chee Chew Wong			
7. PERFORMING ORGANIZATION NAME(S) AND ADDRESS(ES) Naval Postgraduate School Monterey, CA 93943–5000		**8. PERFORMING ORGANIZATION REPORT NUMBER**	
9. SPONSORING /MONITORING AGENCY NAME(S) AND ADDRESS(ES) N/A		**10. SPONSORING/MONITORING AGENCY REPORT NUMBER**	
11. SUPPLEMENTARY NOTES The views expressed in this thesis are those of the author and do not reflect the official policy or position of the Department of Defense or the U.S. Government. IRB Protocol number ____N/A_____.			
12a. DISTRIBUTION / AVAILABILITY STATEMENT Approved for public release; distribution is unlimited		**12b. DISTRIBUTION CODE** A	

13. ABSTRACT (maximum 200 words)

The development of a reference test case with repeatable and accurate results is of paramount importance for the validation of numerical Fluid Structure Interaction (FSI) models and simulations. In this study, a new experimental facility was designed and constructed for the investigation of FSI between fully developed laminar flow and test section plate in an enclosed flow channel. Computational Fluid Dynamics (CFD) software was used to model laminar flow in a shallow rectangular duct to determine proper dimensions of the experimental apparatus. The FSI problem was then modeled in CFD using the predetermined dimensions. The experimental set up included construction of the duct, creation of a closed flow circuit and its instrumentation. The metal test plate was fitted with gages to gather real-time information on the strain levels during the experiment. Subsequently, the experiment was performed and the results were compared with the FSI modeling.

14. SUBJECT TERMS Fluid Structure Interaction, Flow Channel Experiment, FSI CFD Modeling			**15. NUMBER OF PAGES** 87
			16. PRICE CODE
17. SECURITY CLASSIFICATION OF REPORT Unclassified	**18. SECURITY CLASSIFICATION OF THIS PAGE** Unclassified	**19. SECURITY CLASSIFICATION OF ABSTRACT** Unclassified	**20. LIMITATION OF ABSTRACT** UU

NSN 7540–01–280–5500 Standard Form 298 (Rev. 8–98)
Prescribed by ANSI Std. Z39.18

THIS PAGE INTENTIONALLY LEFT BLANK

Approved for public release; distribution is unlimited

EXPERIMENTAL STUDY OF FLUID STRUCTURE INTERACTION EFFECTS ON METAL PLATES UNDER FULLY DEVELOPED LAMINAR FLOW

Chee Chew Wong
Civilian, Singapore Technologies Kinetics, Ltd.
B.E., Nanyang Technological University, 2006

Submitted in partial fulfillment of the
requirements for the degree of

MASTER OF SCIENCE IN MECHANICAL ENGINEERING

from the

NAVAL POSTGRADUATE SCHOOL
December 2011

Author: Chee Chew Wong

Approved by: Young W. Kwon
Thesis Advisor

Jarema M. Didoszak
Thesis Co-Advisor

Knox T. Millsaps
Chair, Department of Mechanical and Aerospace Engineering

THIS PAGE INTENTIONALLY LEFT BLANK

ABSTRACT

The development of a reference test case with repeatable and accurate results is of paramount importance for the validation of numerical Fluid Structure Interaction (FSI) models and simulations. In this study, a new experimental facility was designed and constructed for the investigation of FSI between fully developed laminar flow and test section plate in an enclosed flow channel. Computational Fluid Dynamics (CFD) software was used to model laminar flow in a shallow rectangular duct to determine proper dimensions of the experimental apparatus. The FSI problem was then modeled in CFD using the predetermined dimensions. The experimental set up included construction of the duct, creation of a closed flow circuit and its instrumentation. The metal test plate was fitted with gages to gather real-time information on the strain levels during the experiment. Subsequently, the experiment was performed and the results were compared with the FSI modeling.

THIS PAGE INTENTIONALLY LEFT BLANK

TABLE OF CONTENTS

THIS PAGE INTENTIONALLY LEFT BLANK

LIST OF FIGURES

ACKNOWLEDGMENTS

First and foremost, I would like to thank my wife, Callie, for her unfailing love and support throughout this period of studies. Finally, I thank Dr. Young W. Kwon and Jarema M. Didoszak for their dedicated mentorship in the course of this thesis work.

THIS PAGE INTENTIONALLY LEFT BLANK

I. INTRODUCTION

A. BACKGROUND

The interaction between a structure and a fluid in which it is submerged or a surrounding fluid flow is generally known as Fluid Structure Interaction (FSI). FSI problems exist in numerous applications of engineering such as the stability and response of aircraft wings, the flow of blood through arteries, the response of bridges and tall buildings to wind, the vibration of turbine and compressor blades, the oscillation of heat exchangers [1], and underwater explosion interaction with submerged structures [2–4].

With ever-increasing computational power, there is an ongoing extensive research on numerical methods for solving FSI problems. Some common techniques include the finite element method (FEM), boundary element method, arbitrary Lagrangian-Eulerian (ALE) and the lattice Boltzmann method (LBM). These techniques were used to solve fluid and structure equations either individually or coupled [5–8], and to develop coupling strategies for numerical simulations and coupling algorithms between computational fluid dynamics (CFD) and computational structural dynamics (CSD) solvers [9]. Despite the practical relevance of the prediction of coupled fluid and structural dynamics, much of the research in FSI problems has been numerical in nature. The validation of numerical models for FSI simulations with reference to test cases was rare.

In more recent research, there has been increased interest in the vibration of plates either in contact with or submerged in a fluid due to the accessibility of powerful numerical methods in FSI, simple geometry and relevancy in many marine, geotechnical and aerodynamics applications. Free vibration of plates interacting with a fluid has been investigated widely [10–12]. Time-dependent

response of a floating flexible plate due to an impulsive load [13] and high frequency behavior of thin plate structures in contact with a dense fluid were also examined [14].

B. OBJECTIVES

The objective of this present work is to design and develop a reference test case for the validation of numerical FSI models and simulations, including the design and construction of experimental apparatus. The interaction between a simple plate and a fluid flow under laminar, well-defined, uniform and fully developed inlet and outlet flow conditions was investigated. Phases of this work included modeling of fully developed laminar flow through a duct using CFD software, determining the appropriate dimensions of the duct and velocity of flow, construction of the experimental apparatus, forming a closed flow circuit, measurement and collection of strain levels. The findings of this work will serve as a baseline test case and database, which can be easily used to verify and validate different numerical and computational FSI models. A simple plate and duct geometry was used intentionally to enhance the reproducibility of the results and the measurement of moderate structure motion.

II. DESIGN OF EXPERIMENTAL APPARATUS

A. COMPUTATIONAL MODEL

As an initial step in the design of the experimental apparatus, fluid flow through a rectangular duct was modeled using the finite element analysis simulation code, ANSYS 13.0. The main objective of these simulations was to determine the location at which fully developed flow would be achieved, hence determining the appropriate dimensions for the actual experimental apparatus. This was done through the examination of flow velocity profiles at different planes.

The dimensions used for the duct were a length of 2 m, width of 0.2 m and height of 0.05 m, see Figure 1.

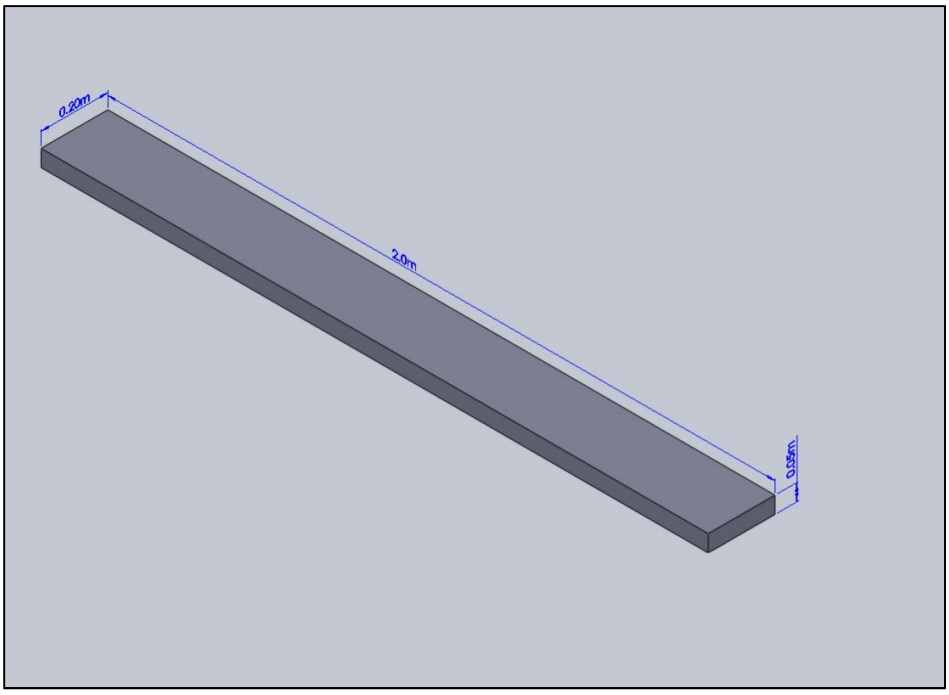

Figure 1. Rectangular Duct for Initial Simulation

As the requirement of the project was in the laminar regime, a fluid of high dynamic viscosity was chosen to attain Reynolds numbers (Re) of less than

2300. Propylene Glycol with a density of 965.3 kg/m^3 and dynamic viscosity of 0.06 kg/m s was used in the simulations. A uniform inlet velocity ranging from 0.3 to 0.8 m/s was specified as the inlet boundary condition in the +X direction for different runs of the simulation, while an outlet boundary condition of 0 Pa was set as the reference pressure. The flow velocity profiles at multiple points of the duct were taken from three planes, XZ plane, XY plane at center and XY plane at side as shown in Figure 2.

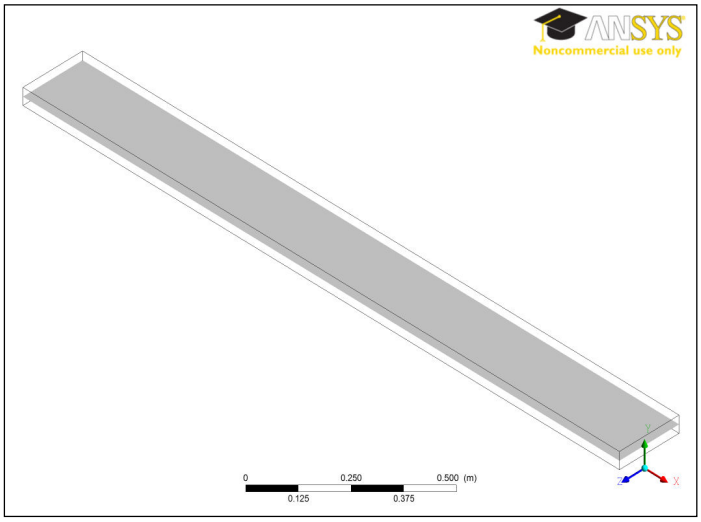

(a) XZ Plane

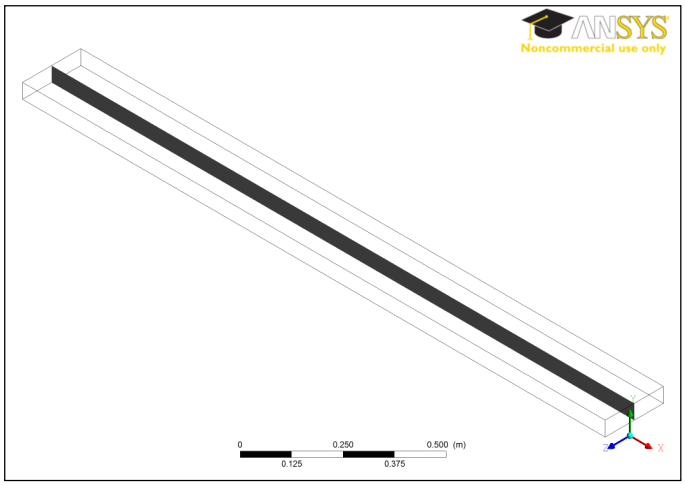

(b) XY Plane at Center

(continued)

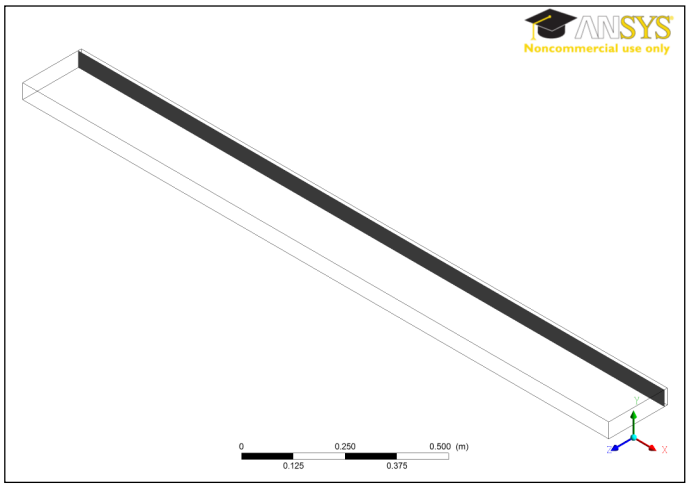

(c) XY Plane at Side

Figure 2. Planes at Which Velocity Profiles Were Taken

For illustration purposes, results taken for one of the runs (uniform inlet velocity of 0.8 m/s) are shown in Figures 3 to 8.

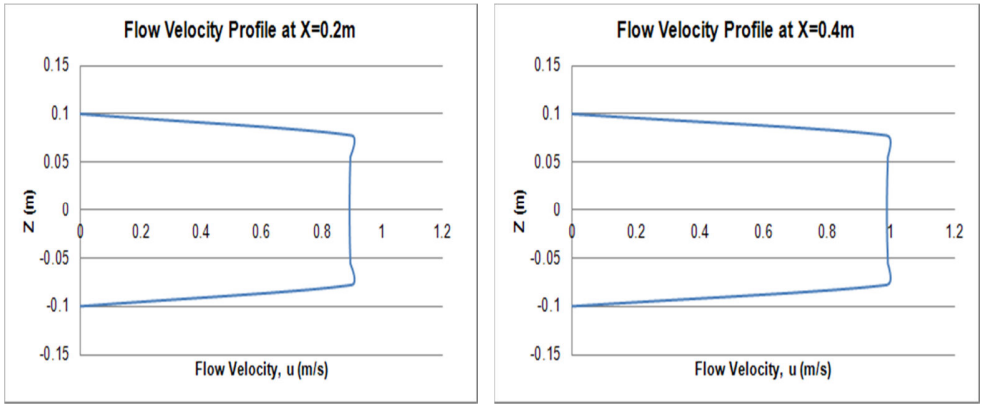

(continued)

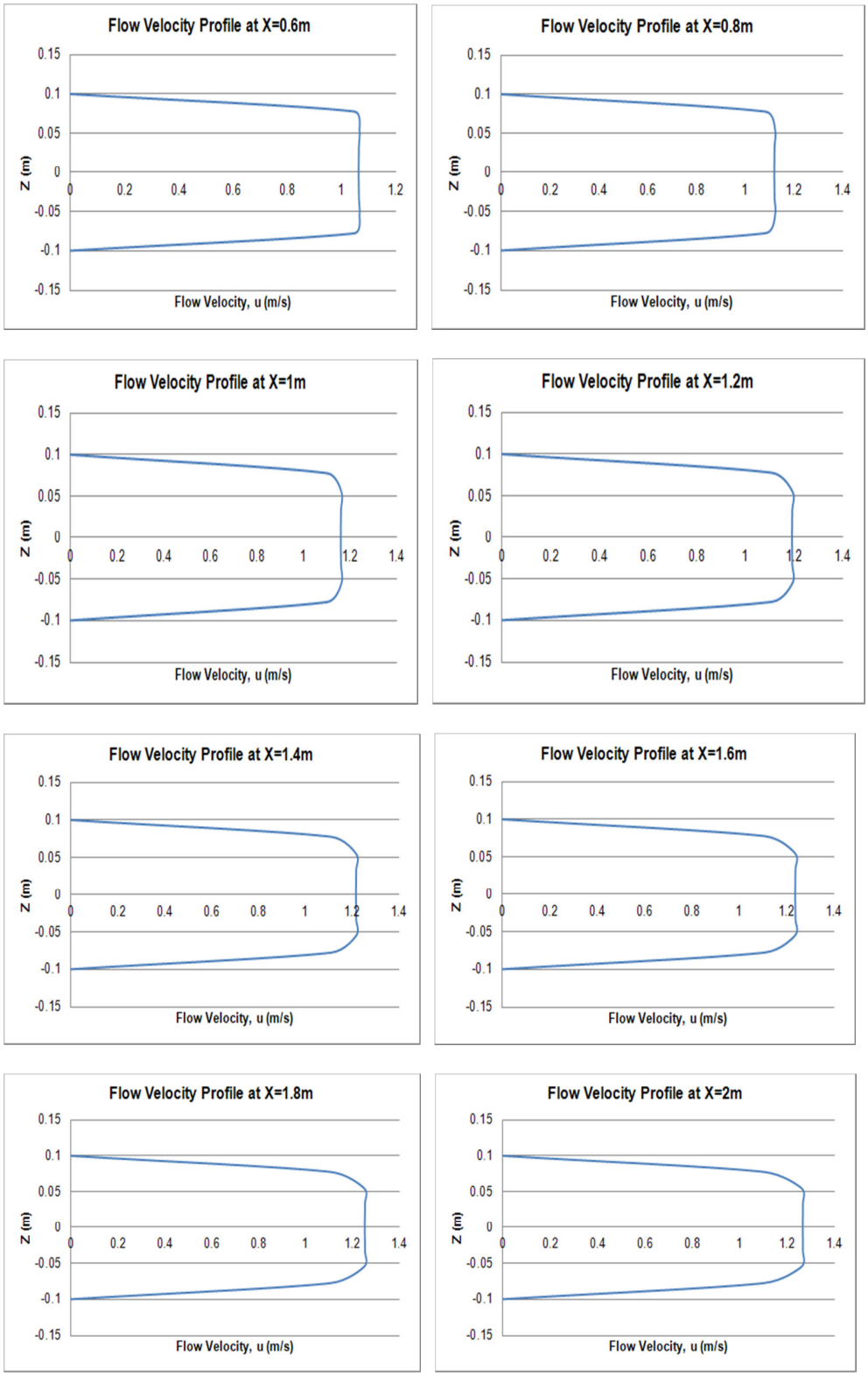

Figure 3. Flow Velocity Profiles at XZ Plane of Rectangular Duct

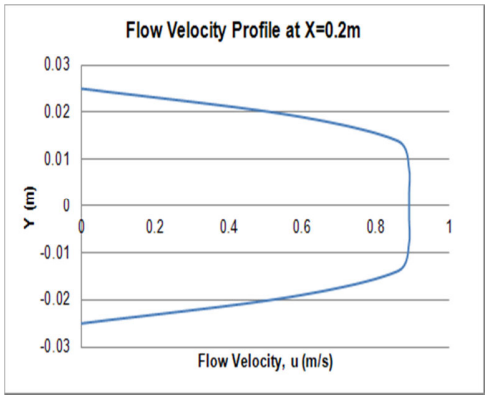
Flow Velocity Profile at X=0.2m
0.03
0.02
0.01
0
-0.01
-0.02
-0.03
Y (m)
0
0.2
0.4
0.6
0.8
1
Flow Velocity, u (m/s)

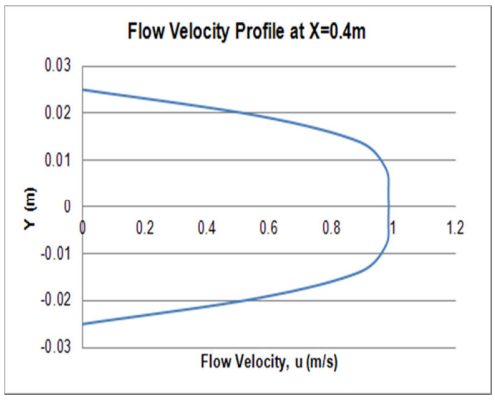
Flow Velocity Profile at X=0.4m
0.03
0.02
0.01
0
-0.01
-0.02
-0.03
Y (m)
0
0.2
0.4
0.6
0.8
1
1.2
Flow Velocity, u (m/s)

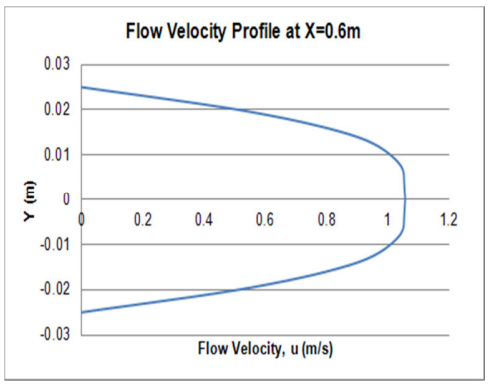
Flow Velocity Profile at X=0.6m
0.03
0.02
0.01
0
-0.01
-0.02
-0.03
Y (m)
0
0.2
0.4
0.6
0.8
1
1.2
Flow Velocity, u (m/s)

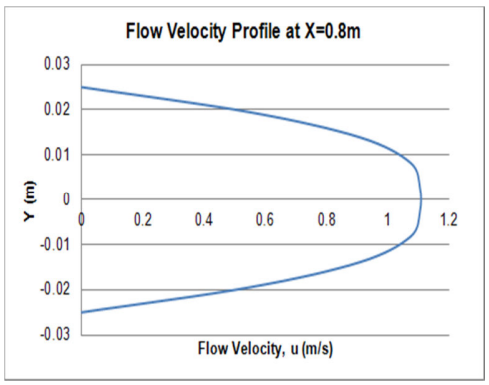
Flow Velocity Profile at X=0.8m
0.03
0.02
0.01
0
-0.01
-0.02
-0.03
Y (m)
0
0.2
0.4
0.6
0.8
1
1.2
Flow Velocity, u (m/s)

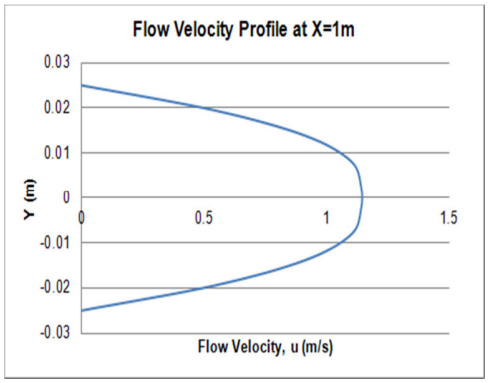
Flow Velocity Profile at X=1m
0.03
0.02
0.01
0
-0.01
-0.02
-0.03
Y (m)
0
0.5
1
1.5
Flow Velocity, u (m/s)

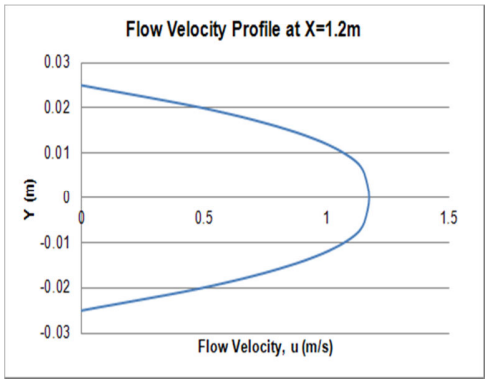
Flow Velocity Profile at X=1.2m
0.03
0.02
0.01
0
-0.01
-0.02
-0.03
Y (m)
0
0.5
1
1.5
Flow Velocity, u (m/s)

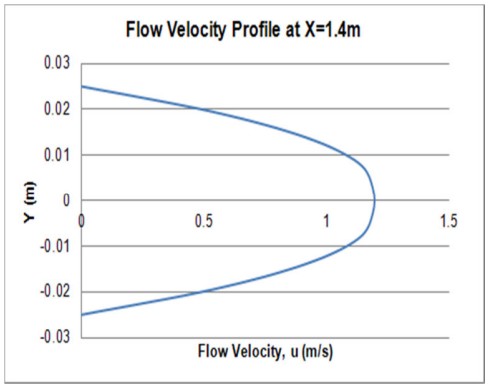
Flow Velocity Profile at X=1.4m
0.03
0.02
0.01
0
-0.01
-0.02
-0.03
Y (m)
0
0.5
1
1.5
Flow Velocity, u (m/s)

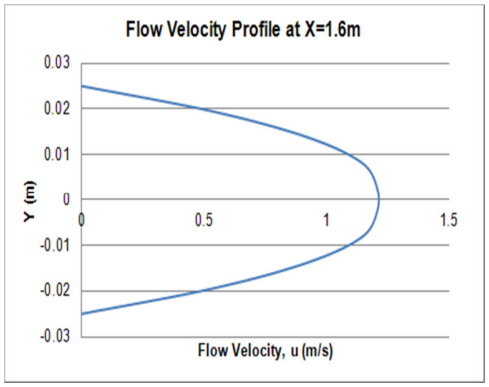
Flow Velocity Profile at X=1.6m
0.03
0.02
0.01
0
-0.01
-0.02
-0.03
Y (m)
0
0.5
1
1.5
Flow Velocity, u (m/s)

(continued)

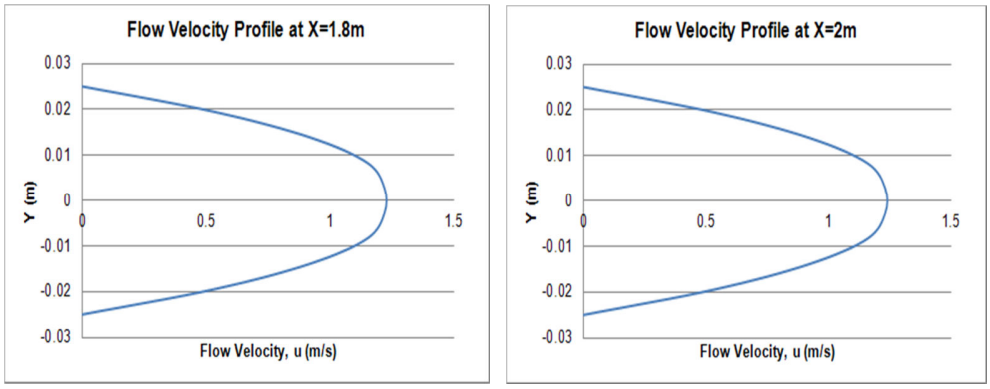

Figure 4. Flow Velocity Profiles at XY Plane at Center of Rectangular Duct

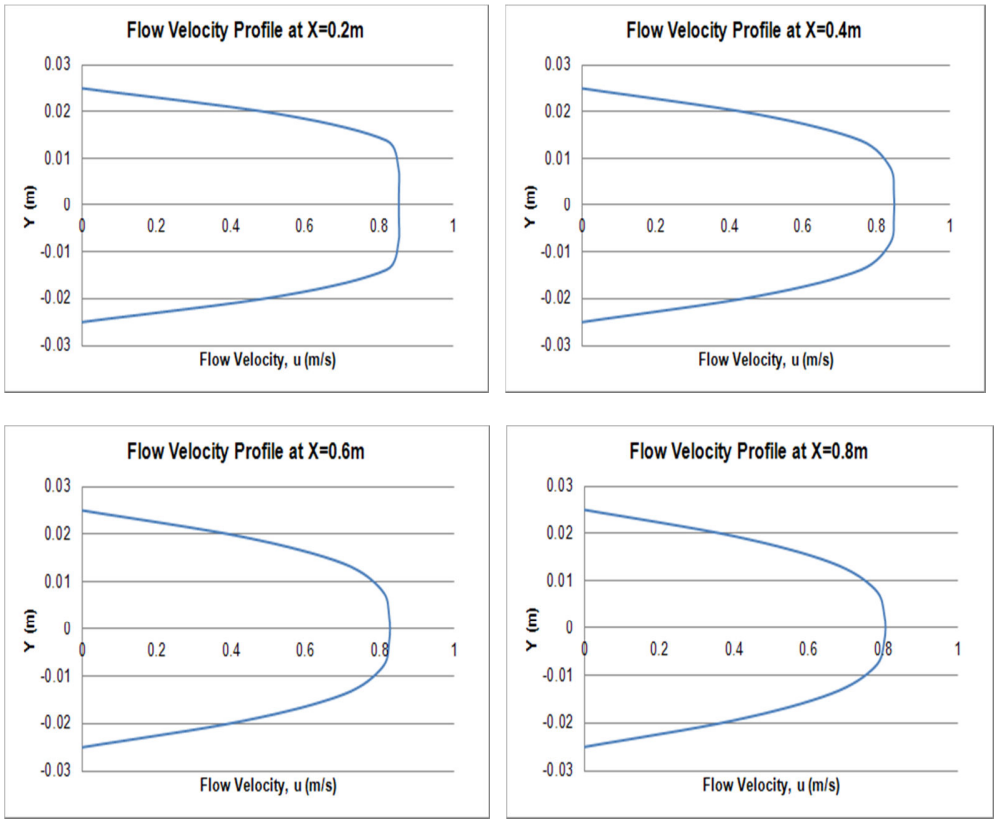

(continued)

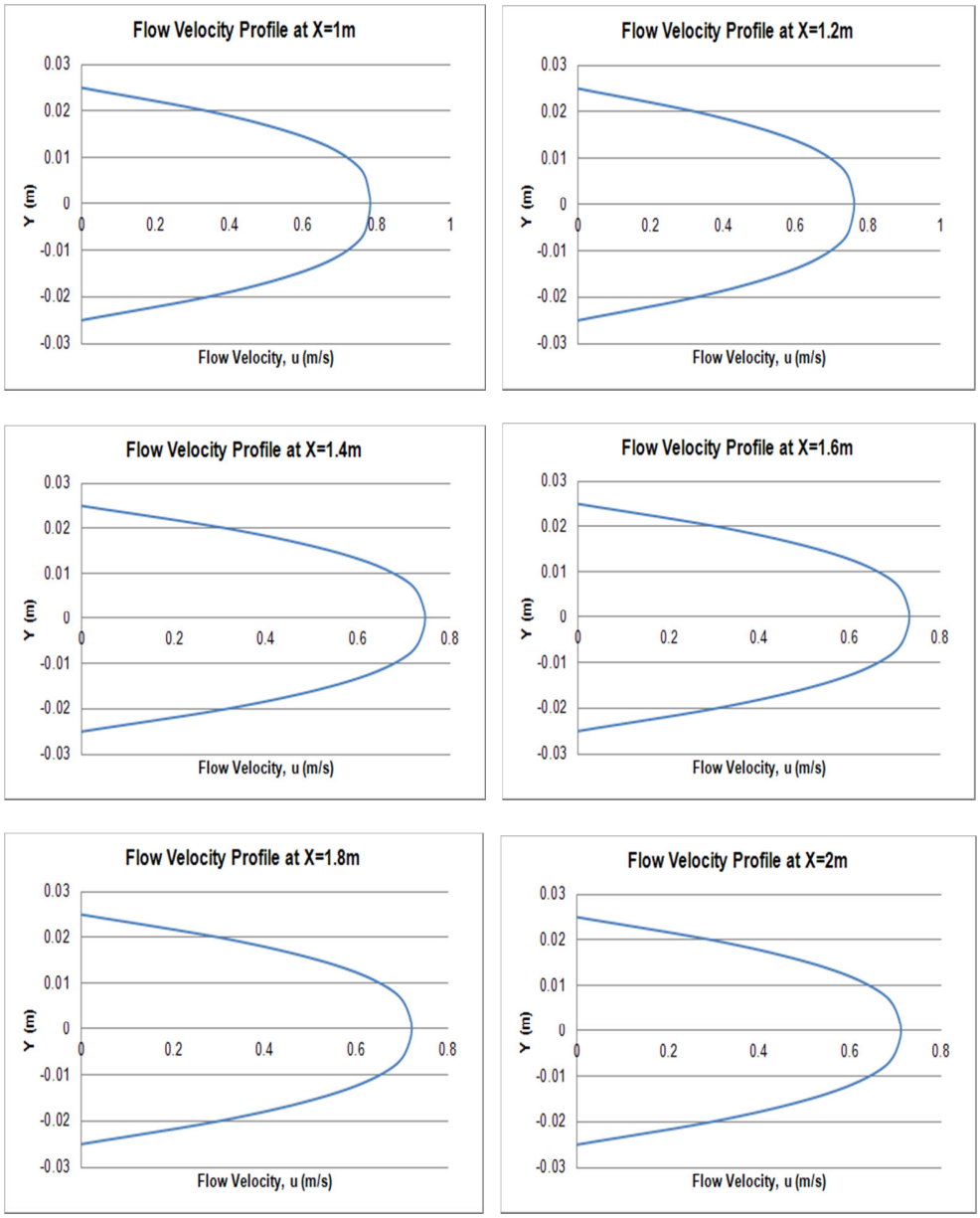

Figure 5. Flow Velocity Profiles at XY Plane at Side of Rectangular Duct

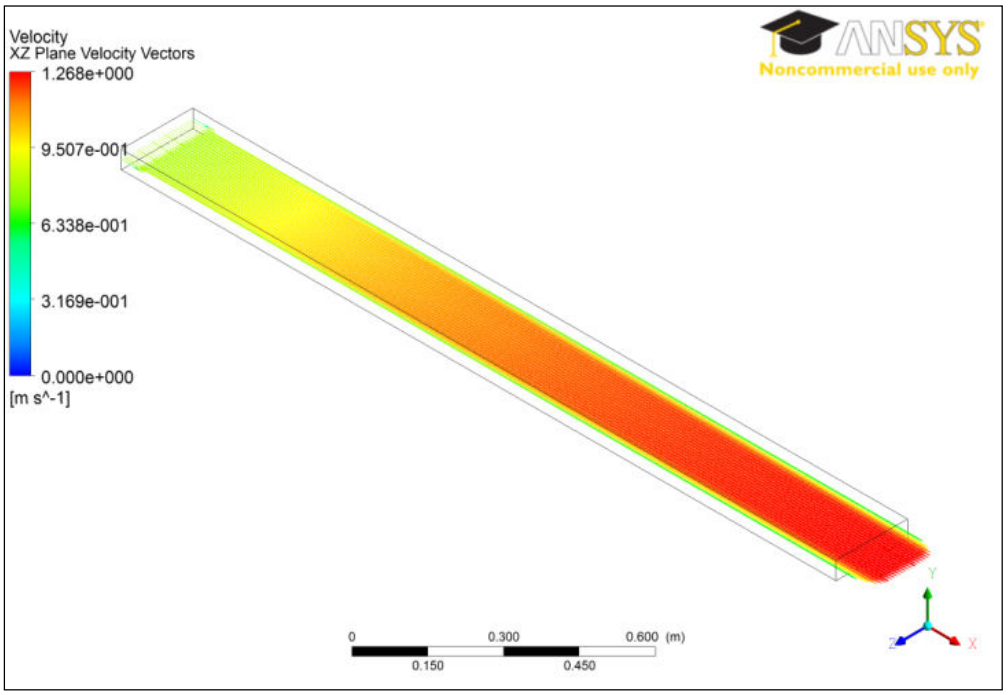

Figure 6. Velocity Vectors at XZ Plane of Rectangular Duct

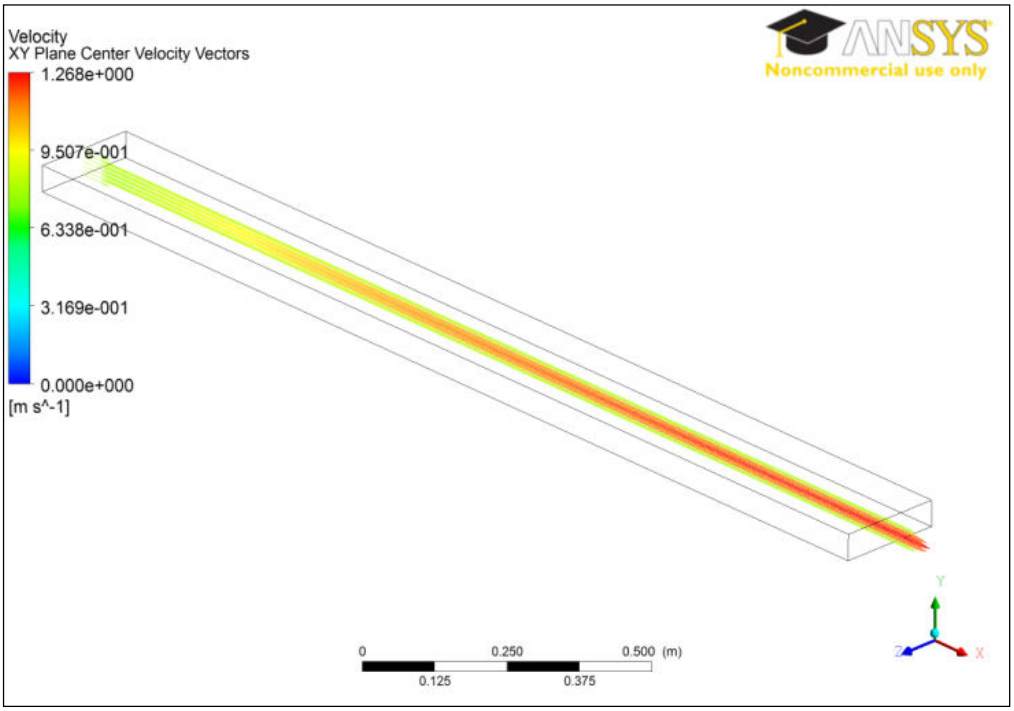

Figure 7. Velocity Vectors at XY Plane Center of Rectangular Duct

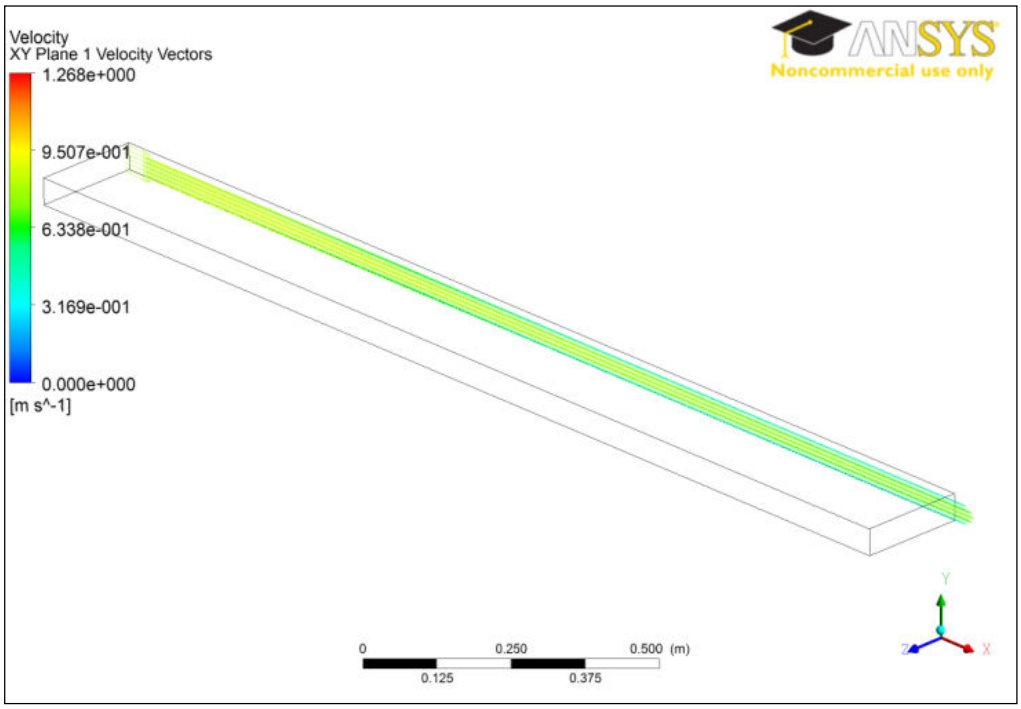

Figure 8. Velocity Vectors at XY Plane at Side of Rectangular Duct

As shown in the preceding group of figures, the flow in the duct was able to achieve near fully developed flow in most parts of the duct except at Z=0.2m, with a velocity magnitude variance of less than 2%.

A refined duct with length of 2.95 m, width of 0.25 m and height of 0.032 m was modeled in the next set of simulations. Diverging and converging sections with length of 0.15 m and end nose diameter of 0.025 m were added at the entrance and exit respectively to represent pipe connections from a pump and to a reservoir, see Figure 9.

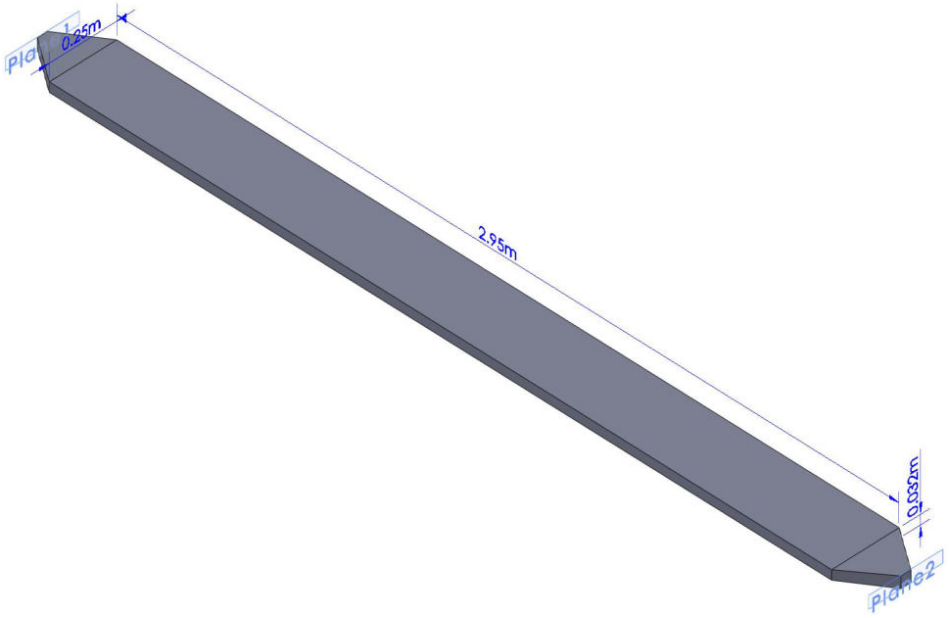

Figure 9. Duct with Diverging and Converging Sections

The same fluid and range of uniform inlet velocities were used for the simulations. The flow velocity profiles were taken at multiple points at the planes shown in Figure 2, with more points taken before and after the half of the duct. The results obtained are shown in Figures 10 to 15.

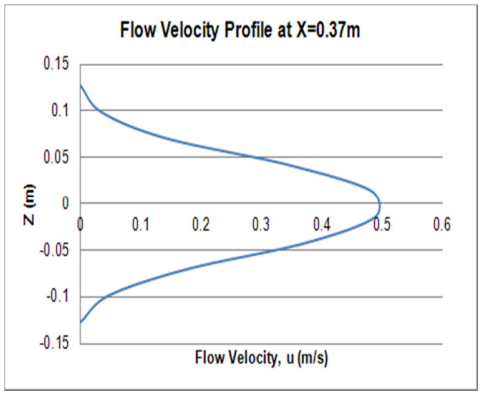
Flow Velocity Profile at X=0.37m
0.15
0.1
0.05
0
-0.05
-0.1
-0.15
Z (m)
0
0.1
0.2
0.3
0.4
0.5
0.6
Flow Velocity, u (m/s)

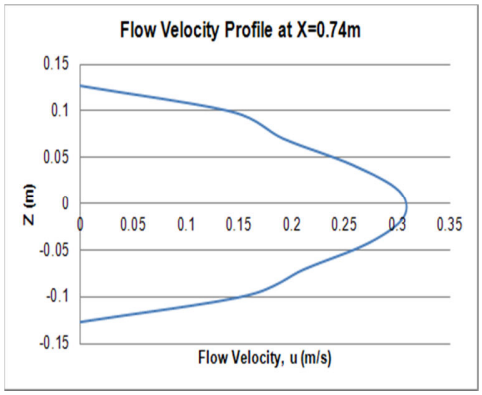
Flow Velocity Profile at X=0.74m
0.15
0.1
0.05
0
-0.05
-0.1
-0.15
Z (m)
0
0.05
0.1
0.15
0.2
0.25
0.3
0.35
Flow Velocity, u (m/s)

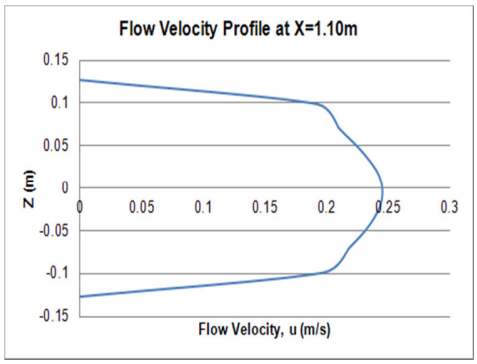
Flow Velocity Profile at X=1.10m
0.15
0.1
0.05
0
-0.05
-0.1
-0.15
Z (m)
0
0.05
0.1
0.15
0.2
0.25
0.3
Flow Velocity, u (m/s)

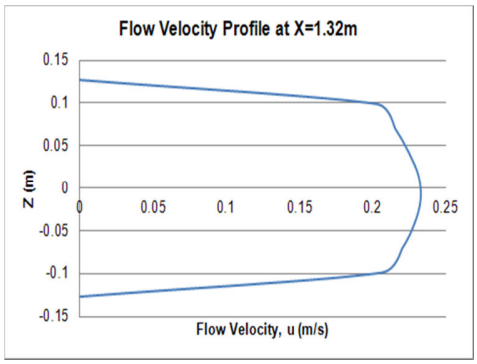
Flow Velocity Profile at X=1.32m
0.15
0.1
0.05
0
-0.05
-0.1
-0.15
Z (m)
0
0.05
0.1
0.15
0.2
0.25
Flow Velocity, u (m/s)

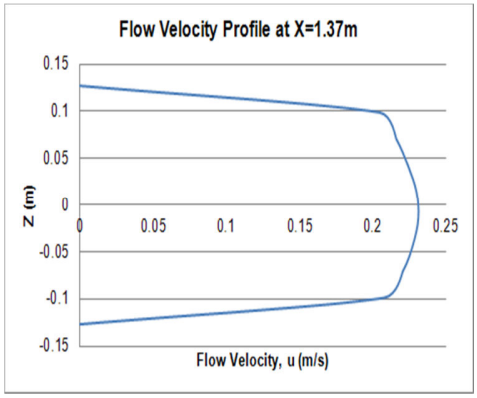
Flow Velocity Profile at X=1.37m
0.15
0.1
0.05
0
-0.05
-0.1
-0.15
Z (m)
0
0.05
0.1
0.15
0.2
0.25
Flow Velocity, u (m/s)

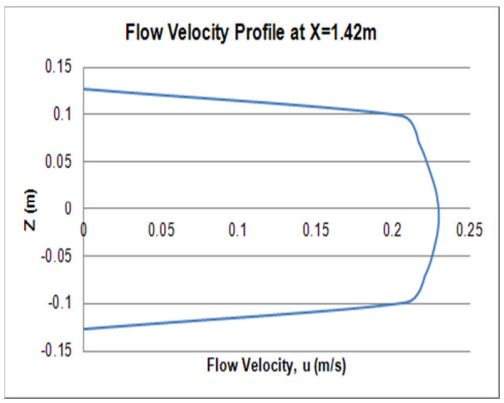
Flow Velocity Profile at X=1.42m
0.15
0.1
0.05
0
-0.05
-0.1
-0.15
Z (m)
0
0.05
0.1
0.15
0.2
0.25
Flow Velocity, u (m/s)

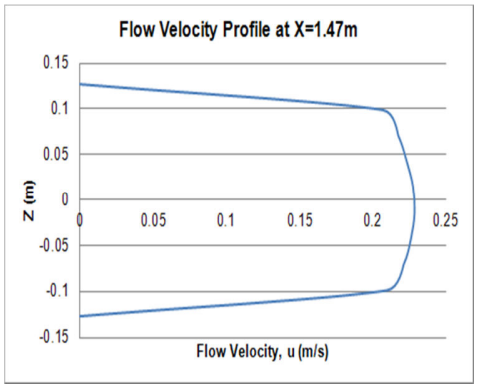
Flow Velocity Profile at X=1.47m
0.15
0.1
0.05
0
-0.05
-0.1
-0.15
Z (m)
0
0.05
0.1
0.15
0.2
0.25
Flow Velocity, u (m/s)

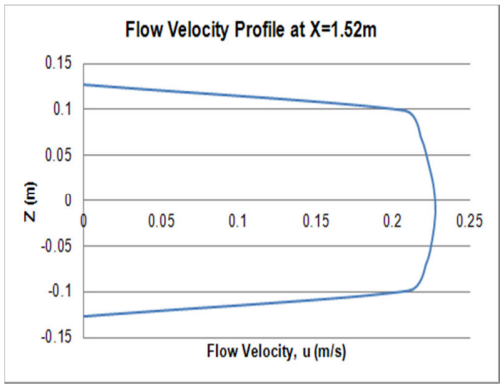
Flow Velocity Profile at X=1.52m
0.15
0.1
0.05
0
-0.05
-0.1
-0.15
Z (m)
0
0.05
0.1
0.15
0.2
0.25
Flow Velocity, u (m/s)

(continued)

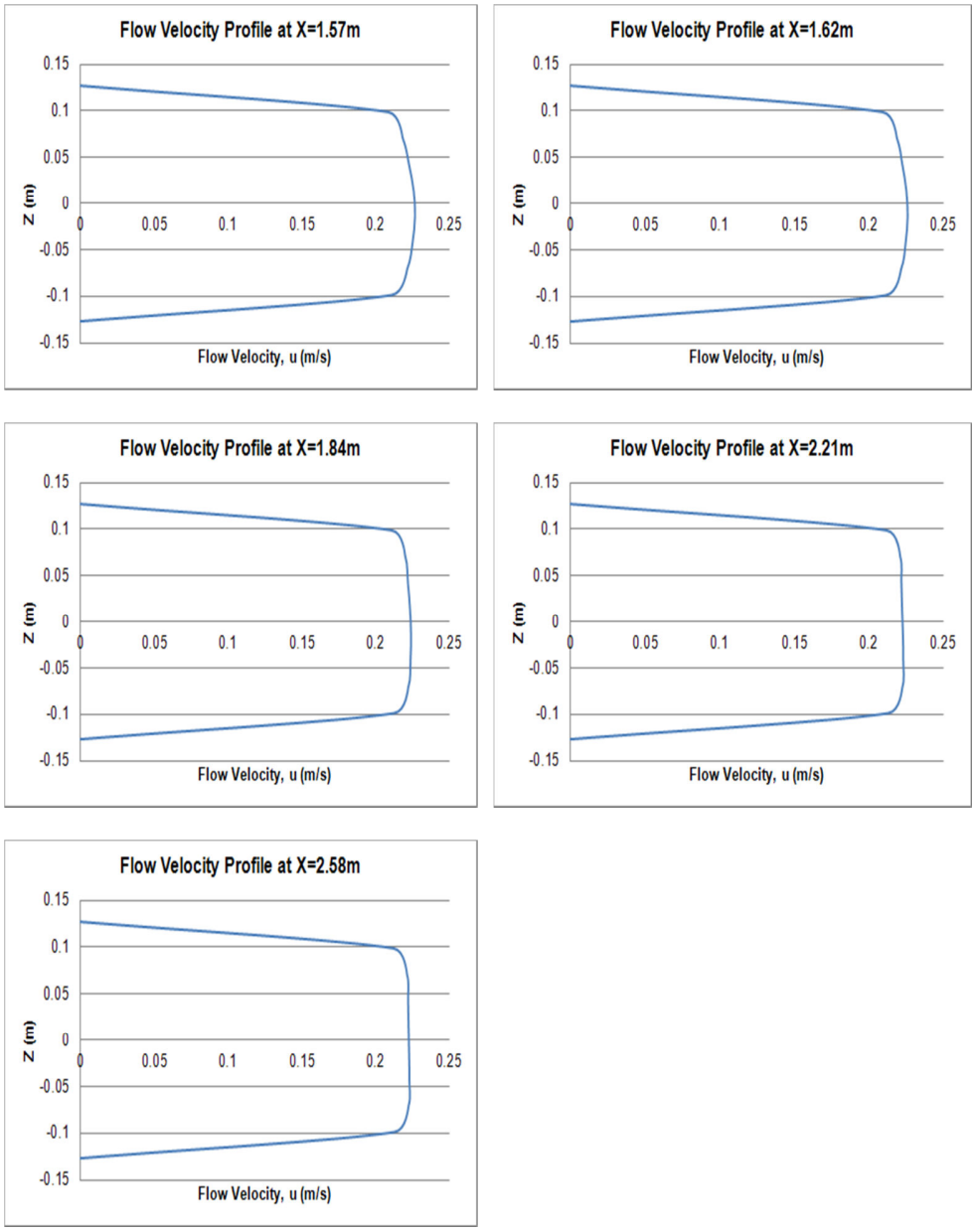

Figure 10. Flow Velocity Profiles at XZ Plane of Duct with Diverging and Converging Sections

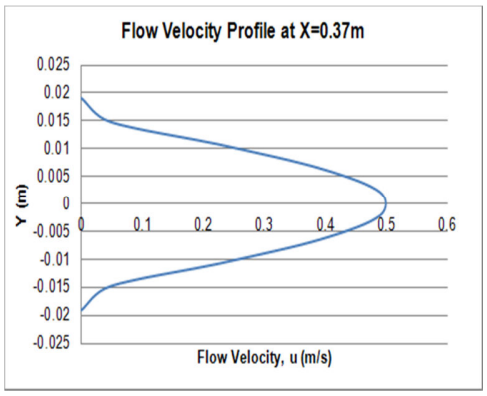
Flow Velocity Profile at X=0.37m
Y (m)
Flow Velocity, u (m/s)

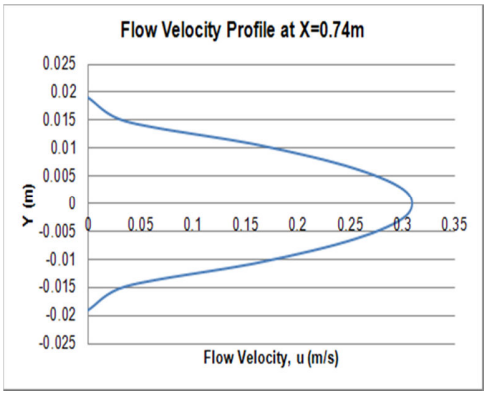
Flow Velocity Profile at X=0.74m
Y (m)
Flow Velocity, u (m/s)

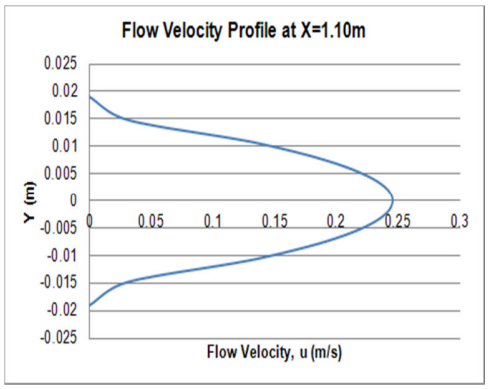
Flow Velocity Profile at X=1.10m
Y (m)
Flow Velocity, u (m/s)

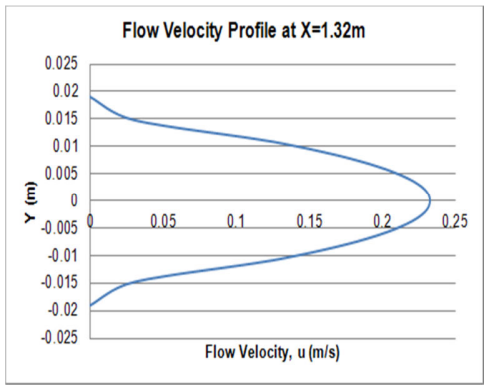
Flow Velocity Profile at X=1.32m
Y (m)
Flow Velocity, u (m/s)

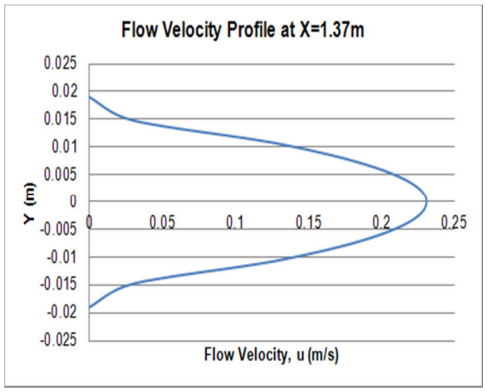
Flow Velocity Profile at X=1.37m
Y (m)
Flow Velocity, u (m/s)

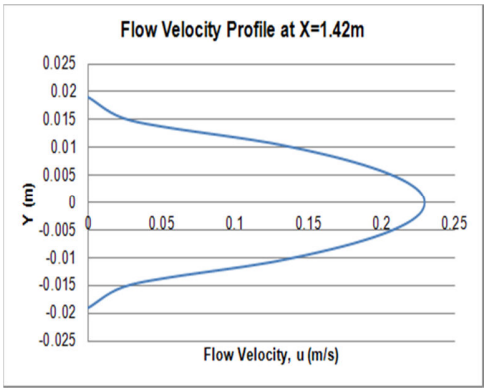
Flow Velocity Profile at X=1.42m
Y (m)
Flow Velocity, u (m/s)

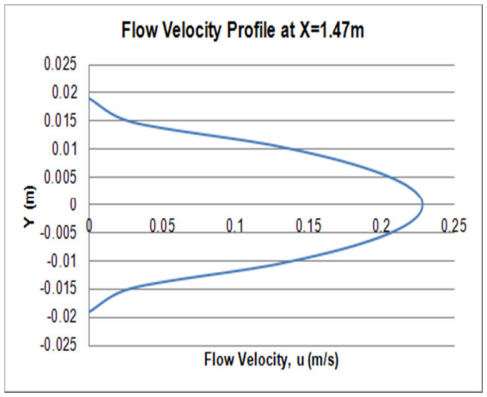
Flow Velocity Profile at X=1.47m
Y (m)
Flow Velocity, u (m/s)

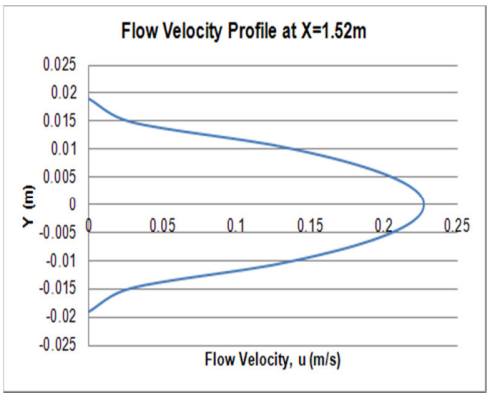
Flow Velocity Profile at X=1.52m
Y (m)
Flow Velocity, u (m/s)

(continued)

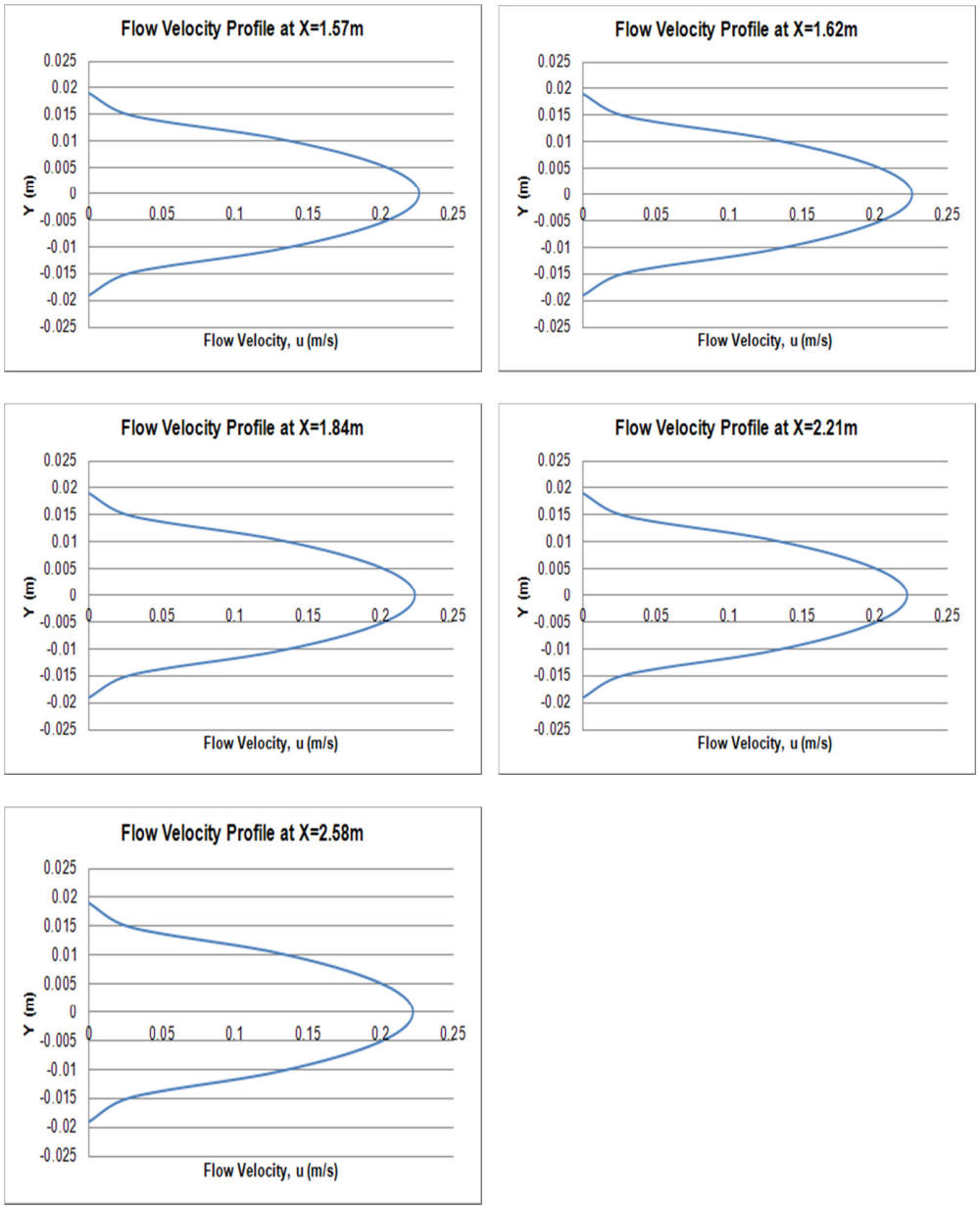

Figure 11. Flow Velocity Profiles at XY Plane at Center of Duct with Diverging and Converging Sections

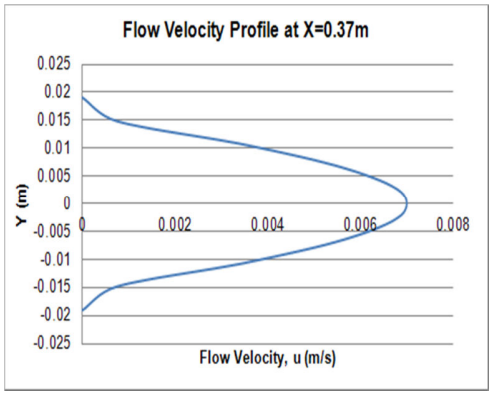
Flow Velocity Profile at X=0.37m
Y (m)
0.025
0.02
0.015
0.01
0.005
0
-0.005
-0.01
-0.015
-0.02
-0.025
0
0.002
0.004
0.006
0.008
Flow Velocity, u (m/s)

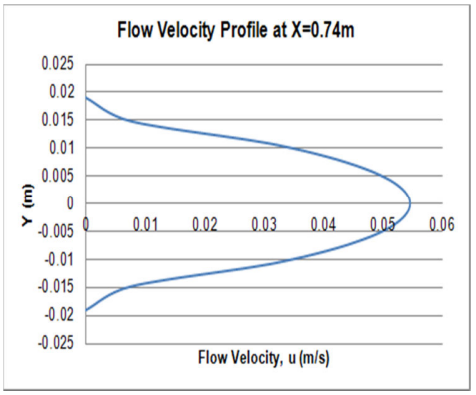
Flow Velocity Profile at X=0.74m
Y (m)
0.025
0.02
0.015
0.01
0.005
0
-0.005
-0.01
-0.015
-0.02
-0.025
0
0.01
0.02
0.03
0.04
0.05
0.06
Flow Velocity, u (m/s)

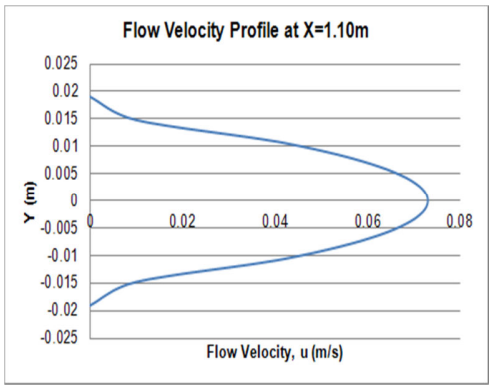
Flow Velocity Profile at X=1.10m
Y (m)
0.025
0.02
0.015
0.01
0.005
0
-0.005
-0.01
-0.015
-0.02
-0.025
0
0.02
0.04
0.06
0.08
Flow Velocity, u (m/s)

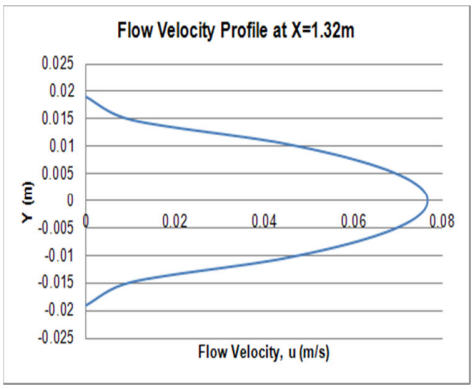
Flow Velocity Profile at X=1.32m
Y (m)
0.025
0.02
0.015
0.01
0.005
0
-0.005
-0.01
-0.015
-0.02
-0.025
0
0.02
0.04
0.06
0.08
Flow Velocity, u (m/s)

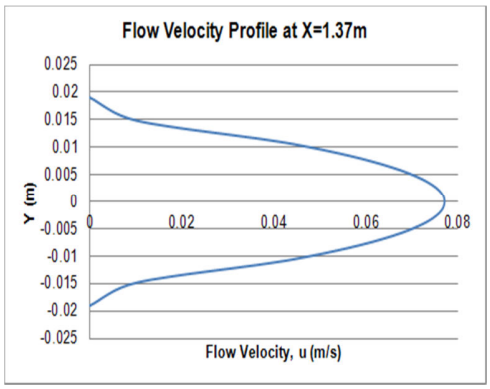
Flow Velocity Profile at X=1.37m
Y (m)
0.025
0.02
0.015
0.01
0.005
0
-0.005
-0.01
-0.015
-0.02
-0.025
0
0.02
0.04
0.06
0.08
Flow Velocity, u (m/s)

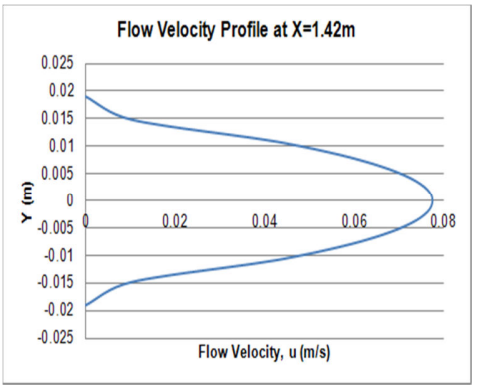
Flow Velocity Profile at X=1.42m
Y (m)
0.025
0.02
0.015
0.01
0.005
0
-0.005
-0.01
-0.015
-0.02
-0.025
0
0.02
0.04
0.06
0.08
Flow Velocity, u (m/s)

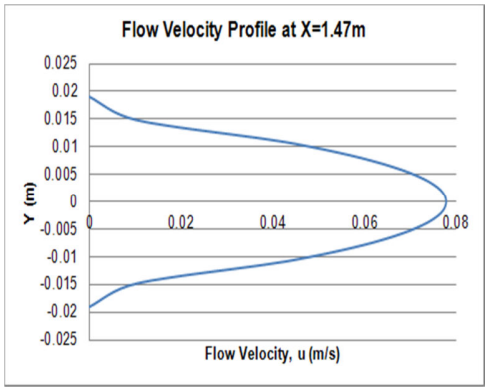
Flow Velocity Profile at X=1.47m
Y (m)
0.025
0.02
0.015
0.01
0.005
0
-0.005
-0.01
-0.015
-0.02
-0.025
0
0.02
0.04
0.06
0.08
Flow Velocity, u (m/s)

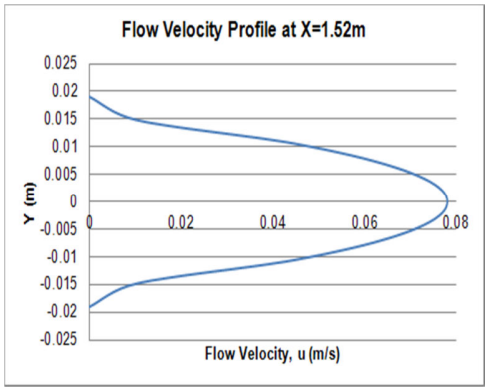
Flow Velocity Profile at X=1.52m
Y (m)
0.025
0.02
0.015
0.01
0.005
0
-0.005
-0.01
-0.015
-0.02
-0.025
0
0.02
0.04
0.06
0.08
Flow Velocity, u (m/s)

(continued)

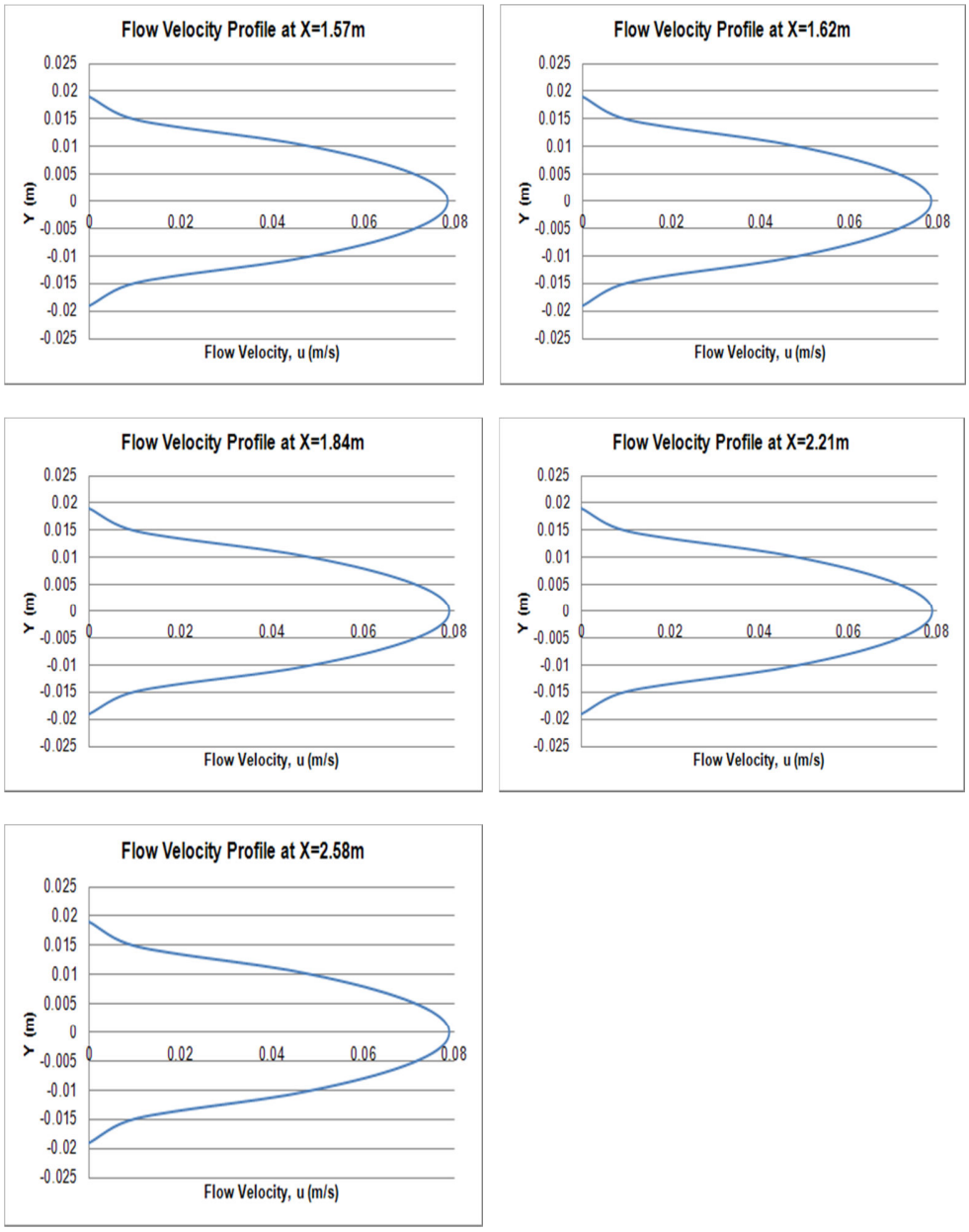

Figure 12. Flow Velocity Profiles at XY Plane at Side of Duct with Diverging and Converging Sections

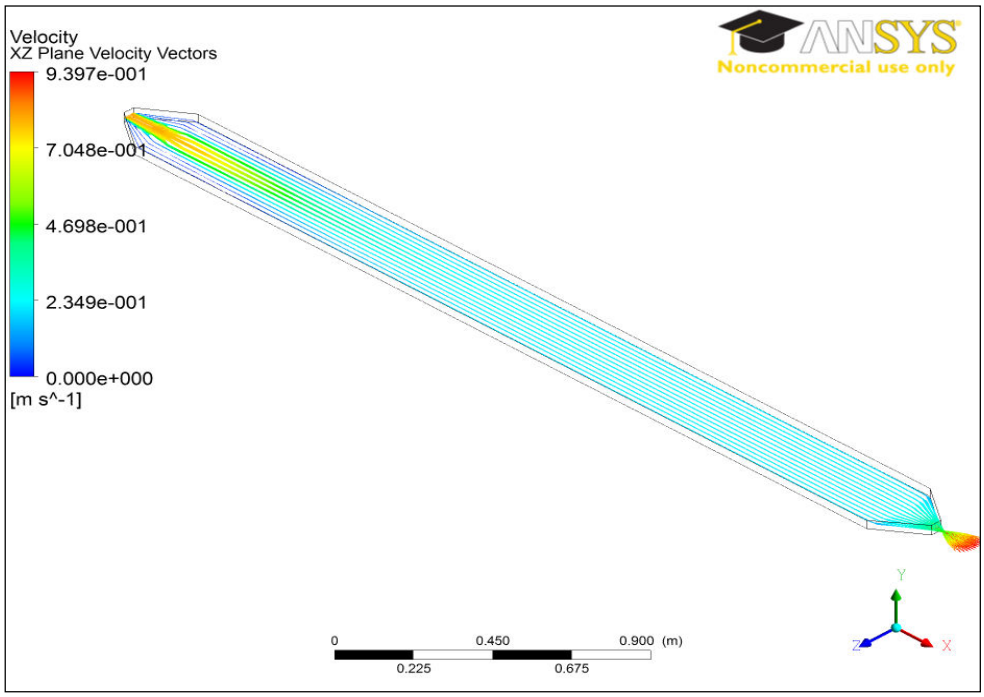

Figure 13. Velocity Vectors at XZ Plane of Duct with Diverging and Converging Sections

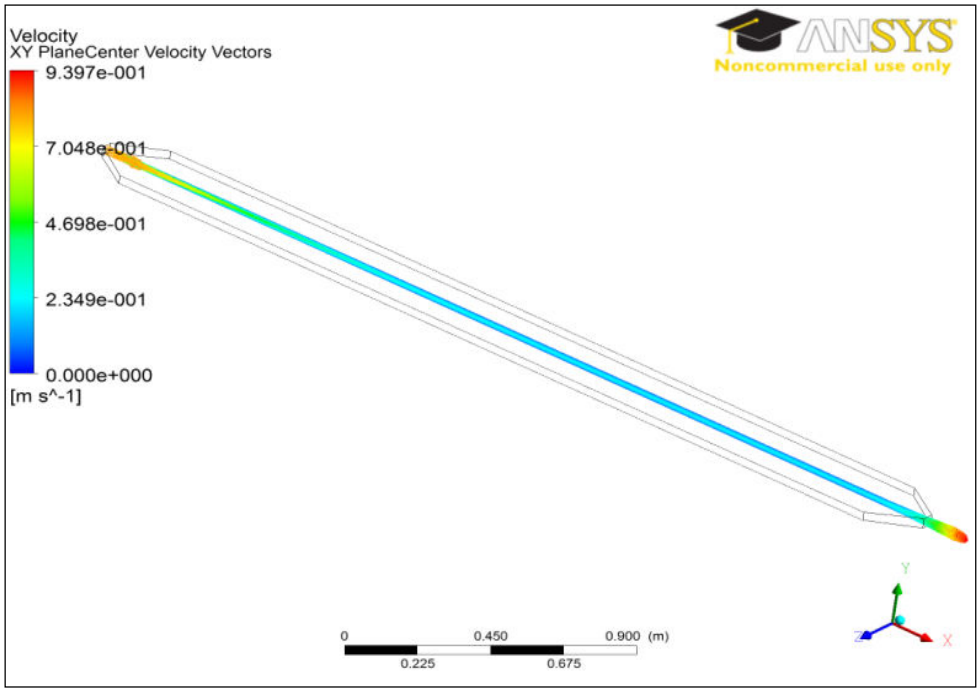

Figure 14. Velocity Vectors at XY Plane Center of Duct with Diverging and Converging Sections

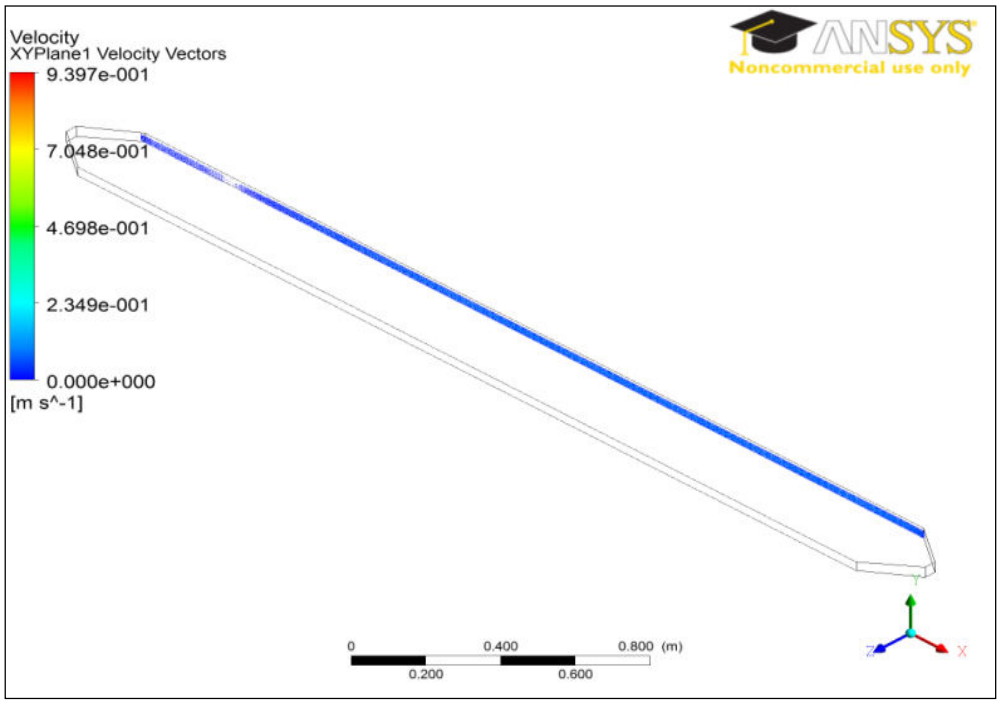

Figure 15. Velocity Vectors at XY Plane at Side of Duct with Diverging and Converging Sections

It can be seen from the various flow velocity profiles that the flow comes to near fully developed flow as it approaches the halfway point along of the duct. On the other hand, from the velocity vectors plots as shown in Figure 13, it is clear that there is a concentration of flow through the center of the duct in the initial portion of the duct as well as towards the end. This is due to the added diverging and converging inlet and outlet.

In the next iteration of design and simulation, the objective was to achieve a further distributed flow as early as possible. In an attempt to distribute the flow from the center, two sets of metallic honeycomb structures were added into the flow channel. The entrance portion was split into a 3-pipe inlet instead of one diverging section, as seen in Figure 16.

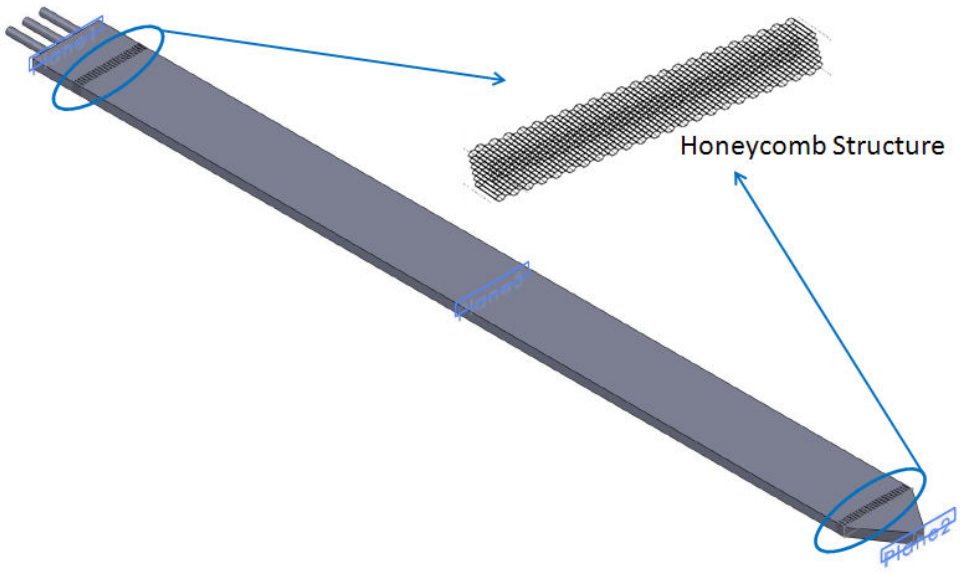

Figure 16. Honeycomb Structures and Split Pipe Entrance

The same fluid was used for all of the simulations. The uniform inlet velocity at each pipe inlet was set as 1 m/s. The flow velocity profiles were taken at multiple points along the planes shown in Figure 2, with more points examined before and after the midpoint of the duct. The results obtained are shown in Figures 17 to 22.

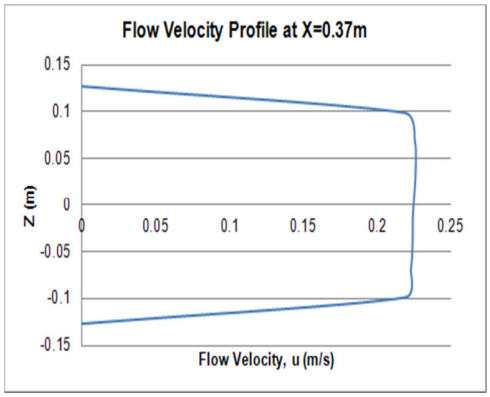
Flow Velocity Profile at X=0.37m
Z (m)
0.15
0.1
0.05
0
-0.05
-0.1
-0.15
0
0.05
0.1
0.15
0.2
0.25
Flow Velocity, u (m/s)

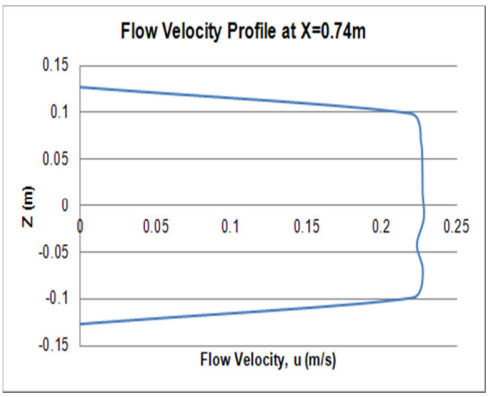
Flow Velocity Profile at X=0.74m
Z (m)
0.15
0.1
0.05
0
-0.05
-0.1
-0.15
0
0.05
0.1
0.15
0.2
0.25
Flow Velocity, u (m/s)

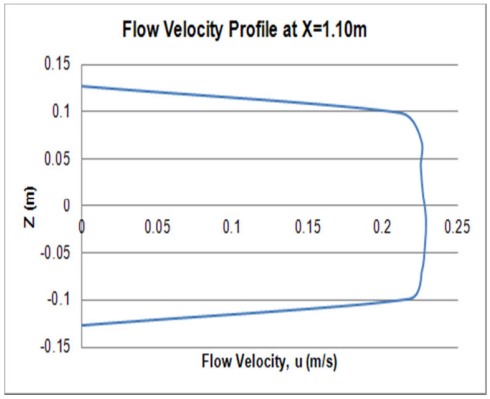
Flow Velocity Profile at X=1.10m
Z (m)
0.15
0.1
0.05
0
-0.05
-0.1
-0.15
0
0.05
0.1
0.15
0.2
0.25
Flow Velocity, u (m/s)

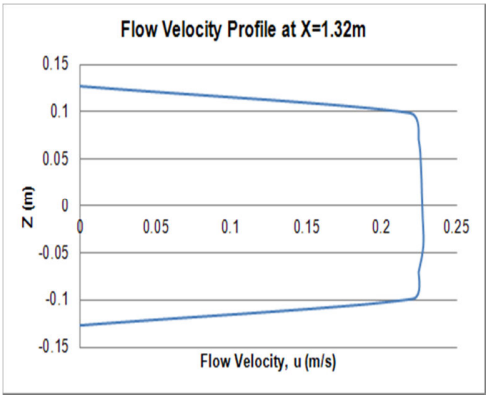
Flow Velocity Profile at X=1.32m
Z (m)
0.15
0.1
0.05
0
-0.05
-0.1
-0.15
0
0.05
0.1
0.15
0.2
0.25
Flow Velocity, u (m/s)

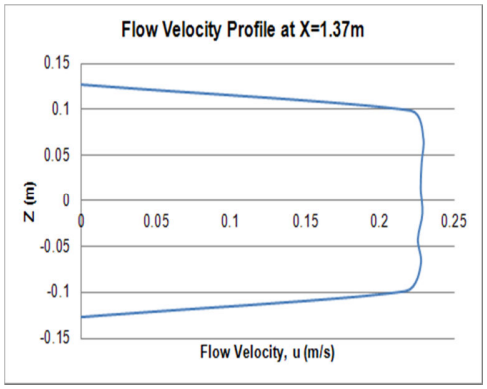
Flow Velocity Profile at X=1.37m
Z (m)
0.15
0.1
0.05
0
-0.05
-0.1
-0.15
0
0.05
0.1
0.15
0.2
0.25
Flow Velocity, u (m/s)

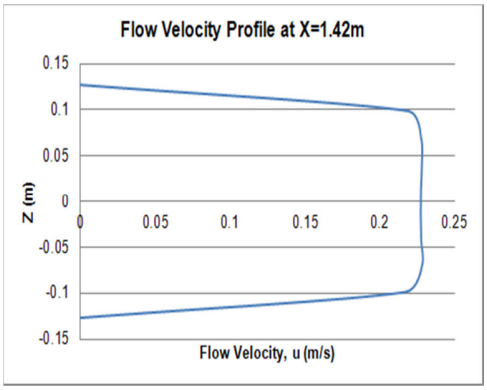
Flow Velocity Profile at X=1.42m
Z (m)
0.15
0.1
0.05
0
-0.05
-0.1
-0.15
0
0.05
0.1
0.15
0.2
0.25
Flow Velocity, u (m/s)

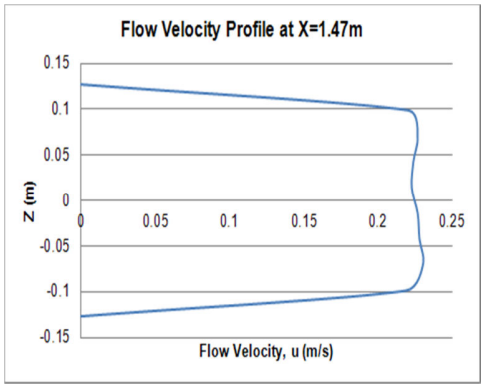
Flow Velocity Profile at X=1.47m
Z (m)
0.15
0.1
0.05
0
-0.05
-0.1
-0.15
0
0.05
0.1
0.15
0.2
0.25
Flow Velocity, u (m/s)

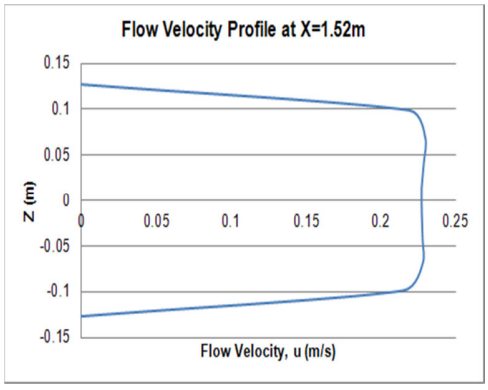
Flow Velocity Profile at X=1.52m
Z (m)
0.15
0.1
0.05
0
-0.05
-0.1
-0.15
0
0.05
0.1
0.15
0.2
0.25
Flow Velocity, u (m/s)

(continued)

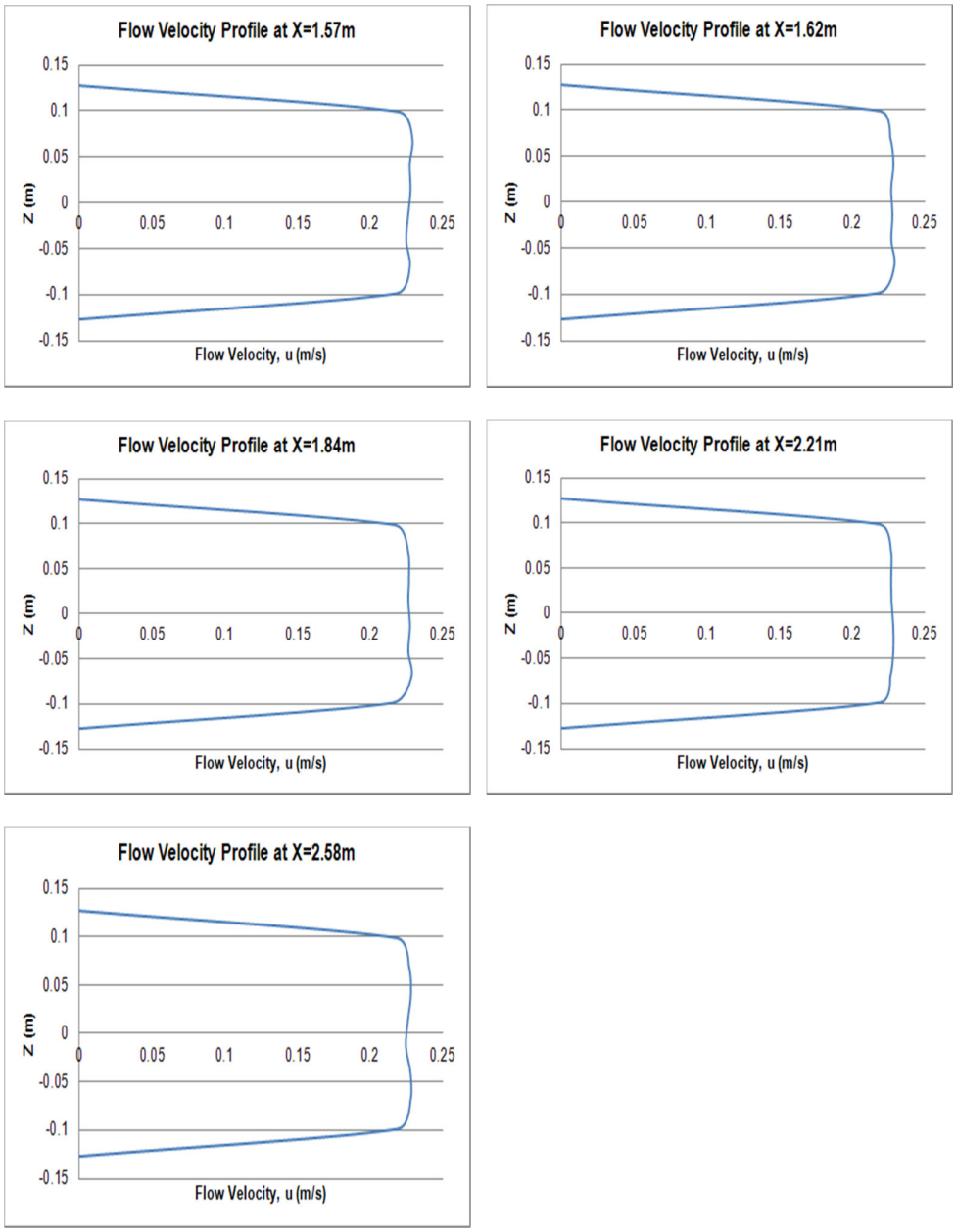

Figure 17. Flow Velocity Profiles at XZ Plane of Duct with Honeycomb Structures

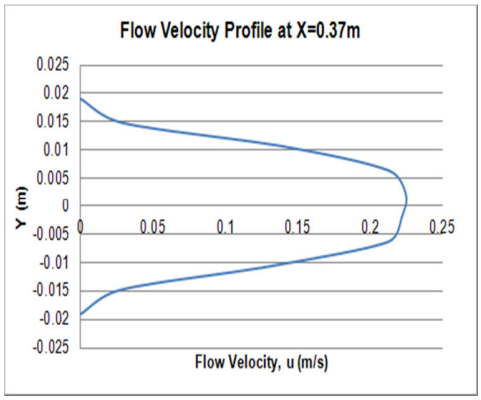
Flow Velocity Profile at X=0.37m
Y (m)
Flow Velocity, u (m/s)

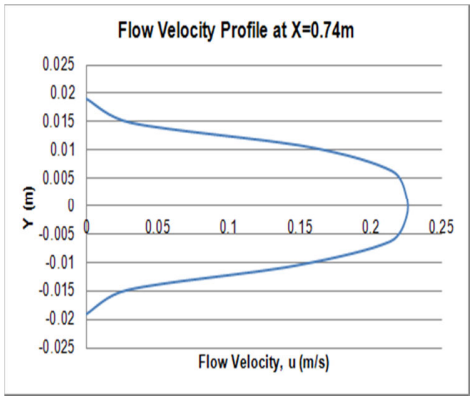
Flow Velocity Profile at X=0.74m
Y (m)
Flow Velocity, u (m/s)

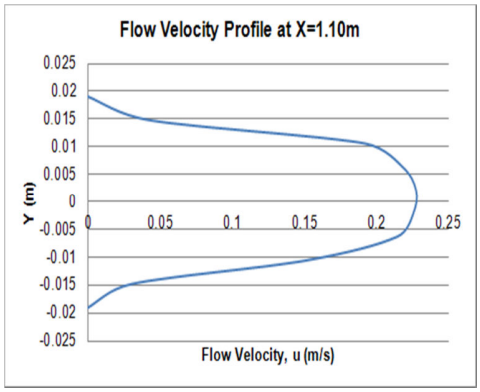
Flow Velocity Profile at X=1.10m
Y (m)
Flow Velocity, u (m/s)

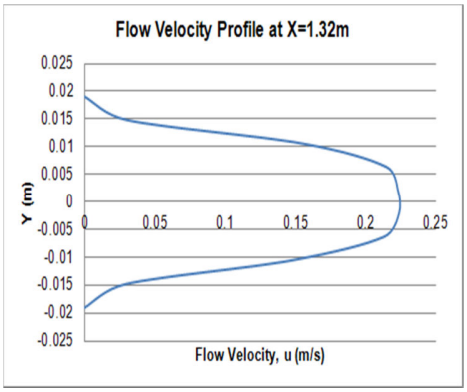
Flow Velocity Profile at X=1.32m
Y (m)
Flow Velocity, u (m/s)

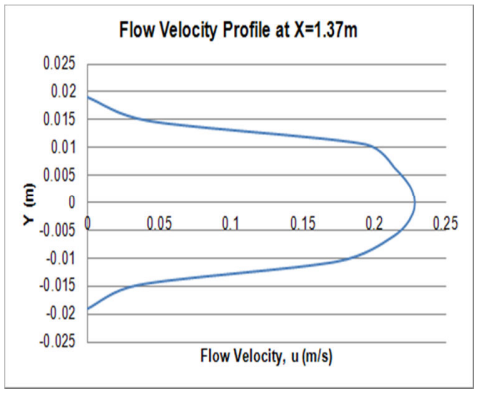
Flow Velocity Profile at X=1.37m
Y (m)
Flow Velocity, u (m/s)

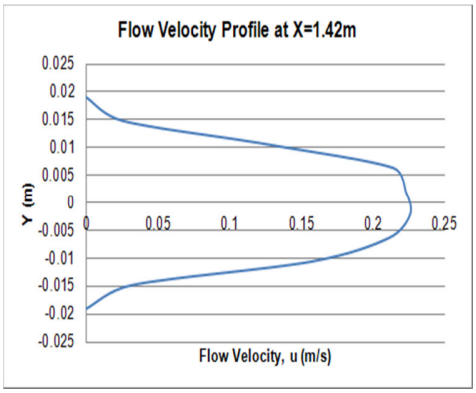
Flow Velocity Profile at X=1.42m
Y (m)
Flow Velocity, u (m/s)

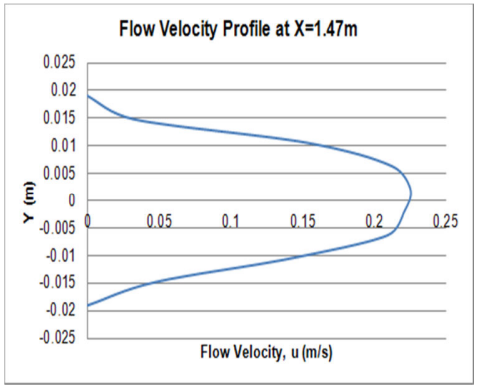
Flow Velocity Profile at X=1.47m
Y (m)
Flow Velocity, u (m/s)

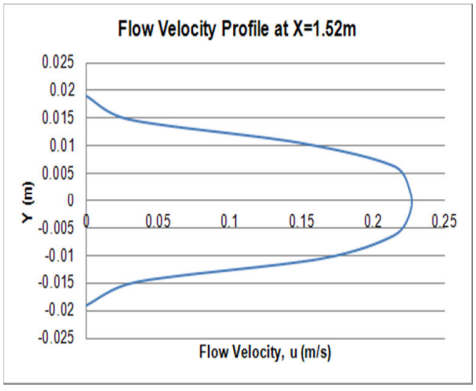
Flow Velocity Profile at X=1.52m
Y (m)
Flow Velocity, u (m/s)

(continued)

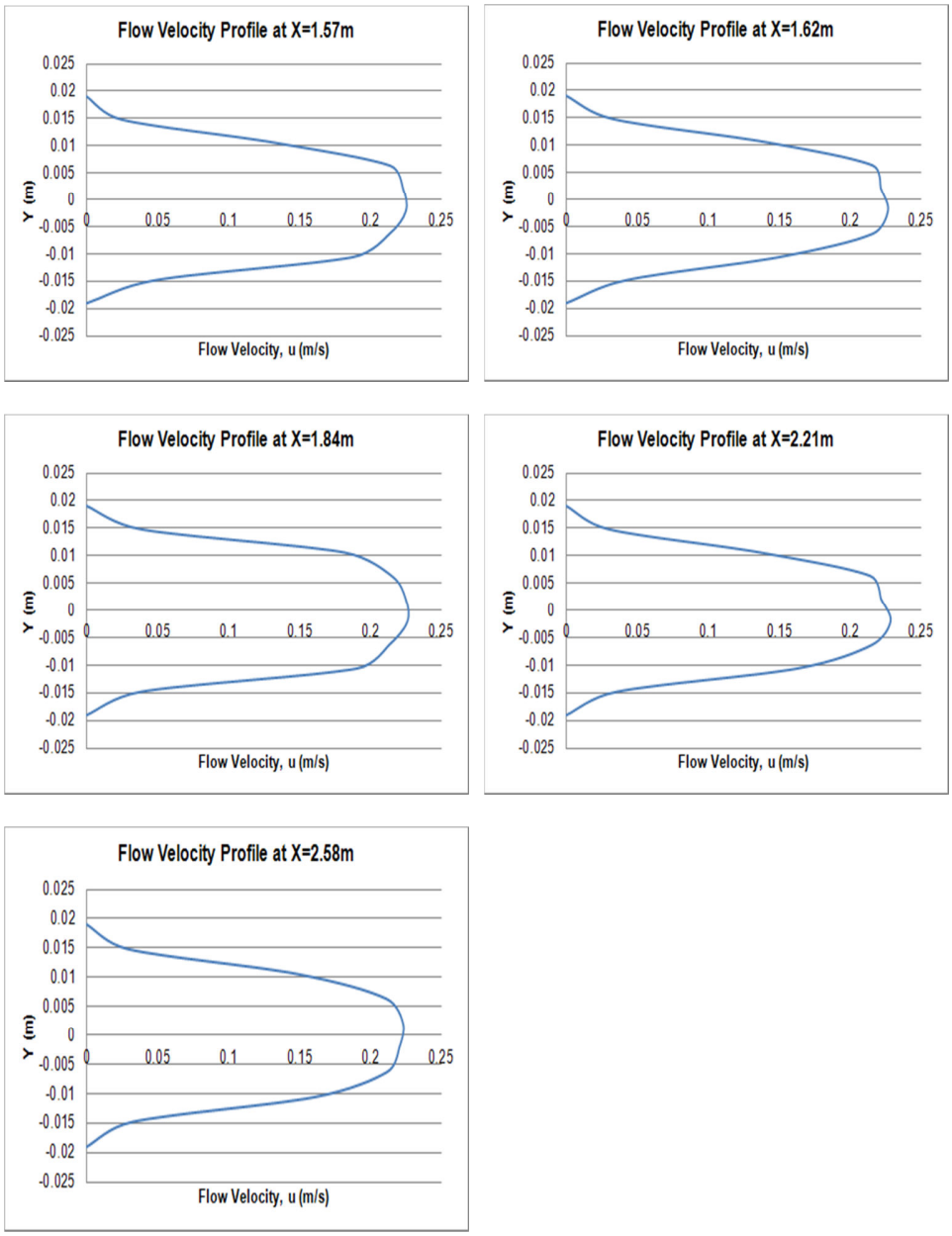

Figure 18. Flow Velocity Profiles at XY Plane at Center of Duct with Honeycomb Structures

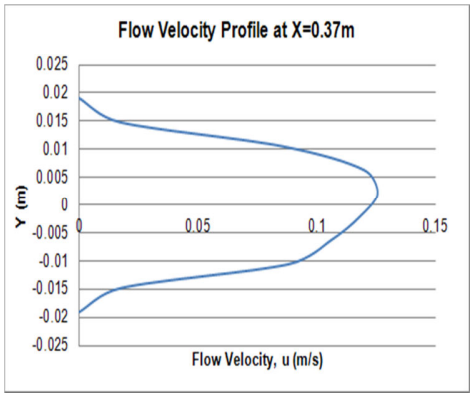
Flow Velocity Profile at X=0.37m
Y (m)
Flow Velocity, u (m/s)

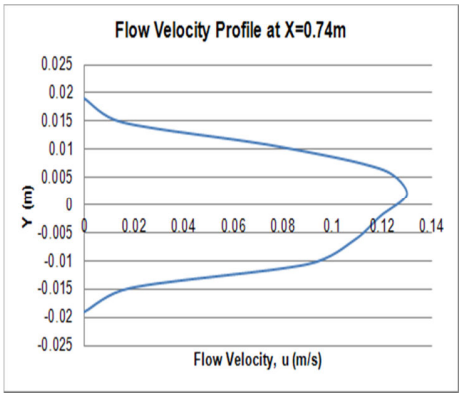
Flow Velocity Profile at X=0.74m
Y (m)
Flow Velocity, u (m/s)

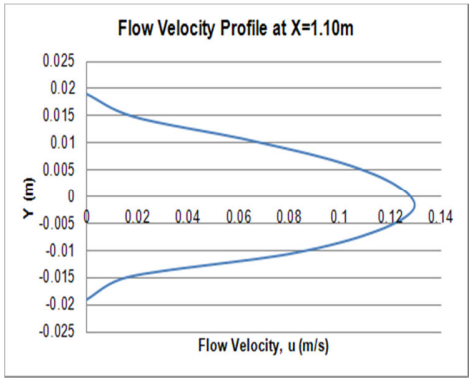
Flow Velocity Profile at X=1.10m
Y (m)
Flow Velocity, u (m/s)

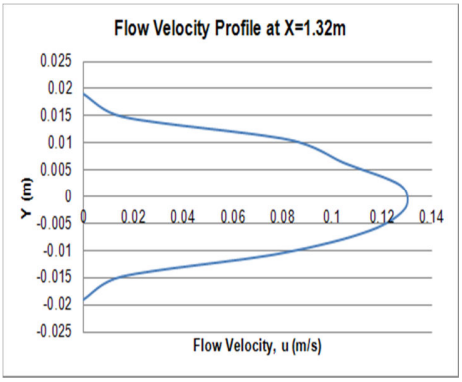
Flow Velocity Profile at X=1.32m
Y (m)
Flow Velocity, u (m/s)

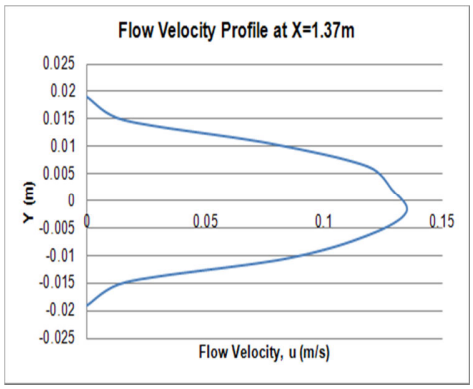
Flow Velocity Profile at X=1.37m
Y (m)
Flow Velocity, u (m/s)

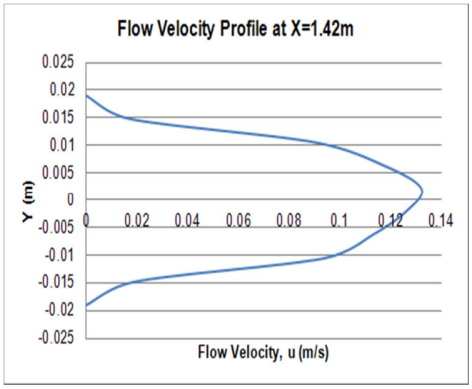
Flow Velocity Profile at X=1.42m
Y (m)
Flow Velocity, u (m/s)

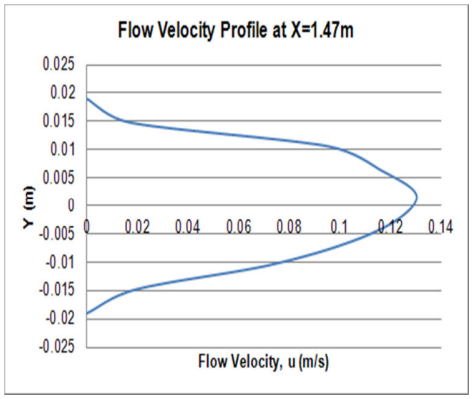
Flow Velocity Profile at X=1.47m
Y (m)
Flow Velocity, u (m/s)

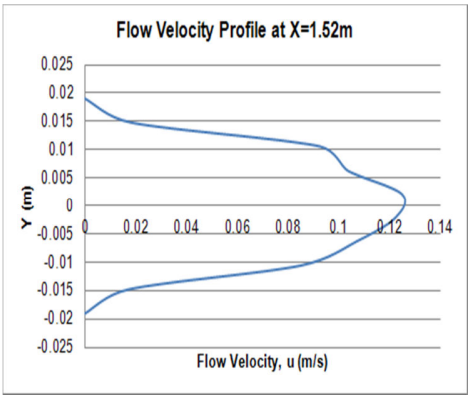
Flow Velocity Profile at X=1.52m
Y (m)
Flow Velocity, u (m/s)

(continued)

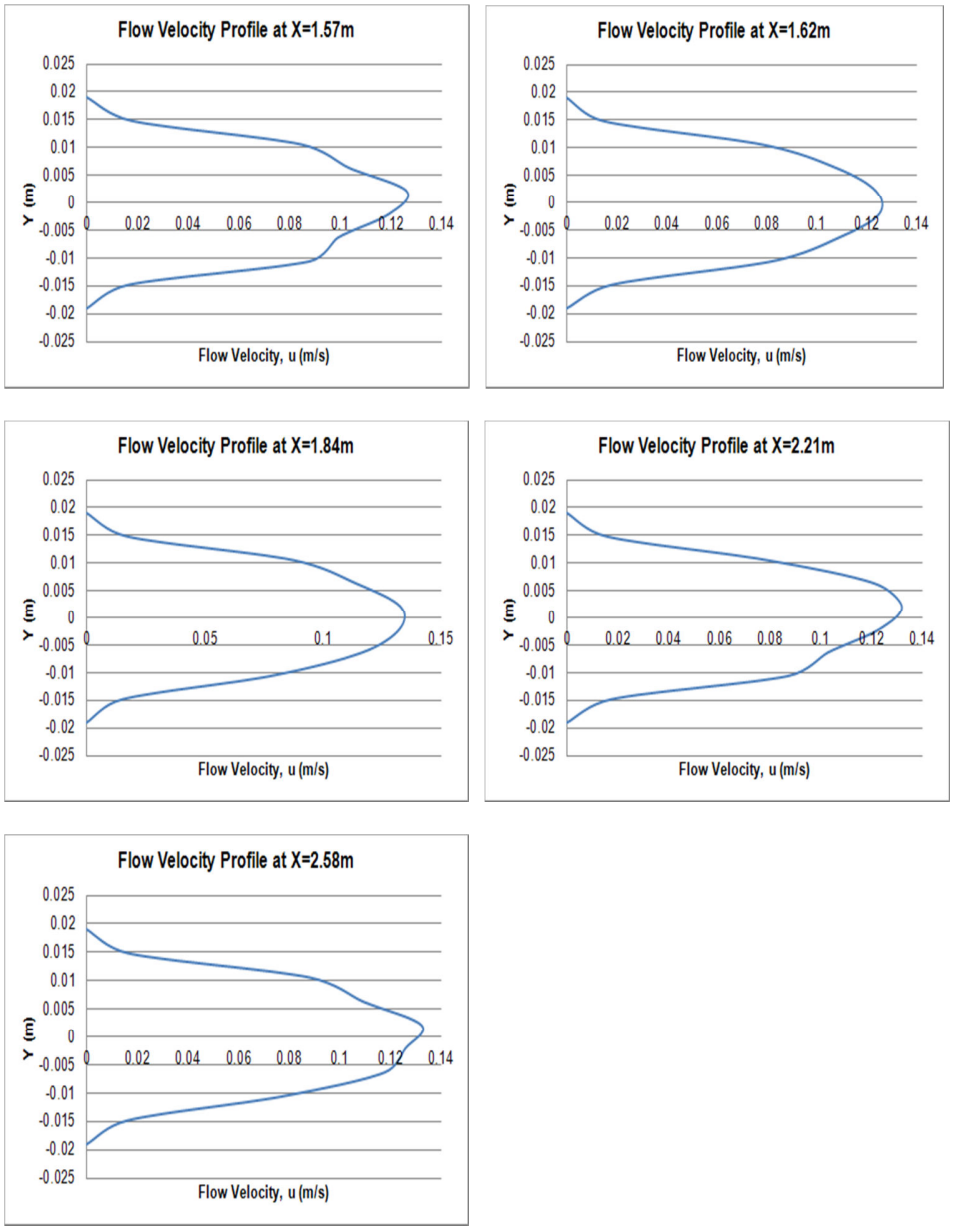

Figure 19. Flow Velocity Profiles at XY Plane at Side of Duct with Honeycomb Structures

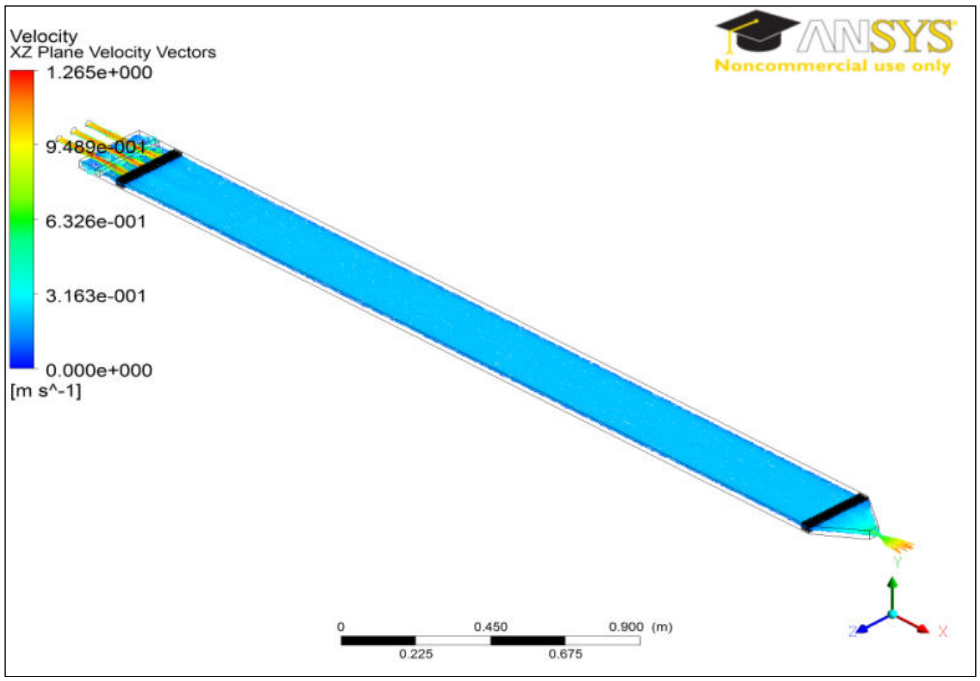

Figure 20. Velocity Vectors at XZ Plane of Duct with Honeycomb Structures

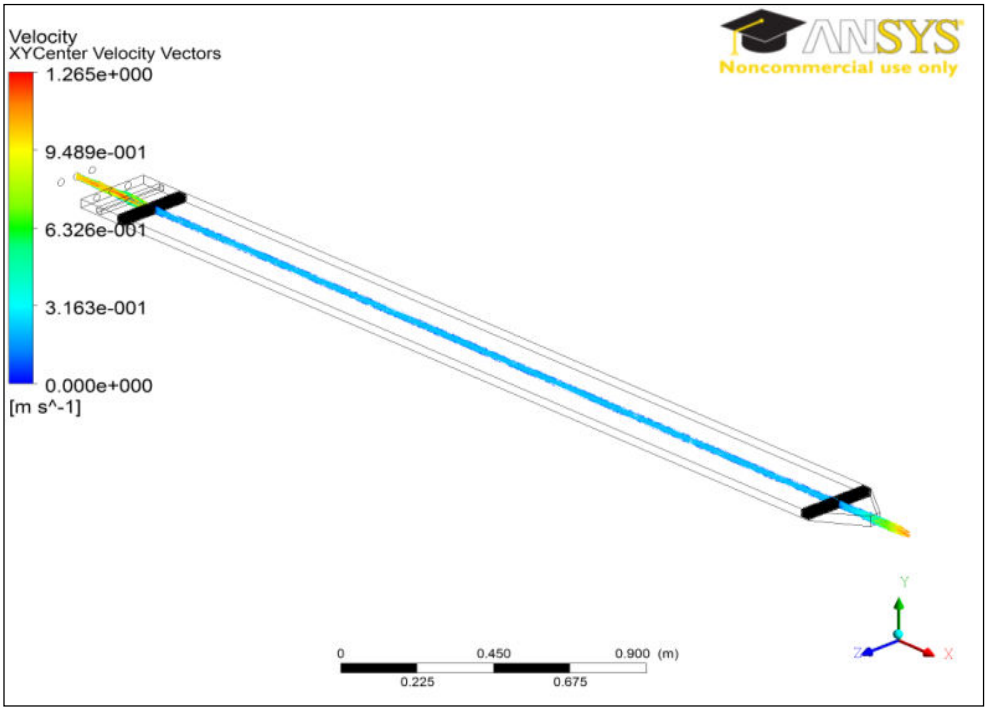

Figure 21. Velocity Vectors at XY Plane at Center of Duct with Honeycomb Structures

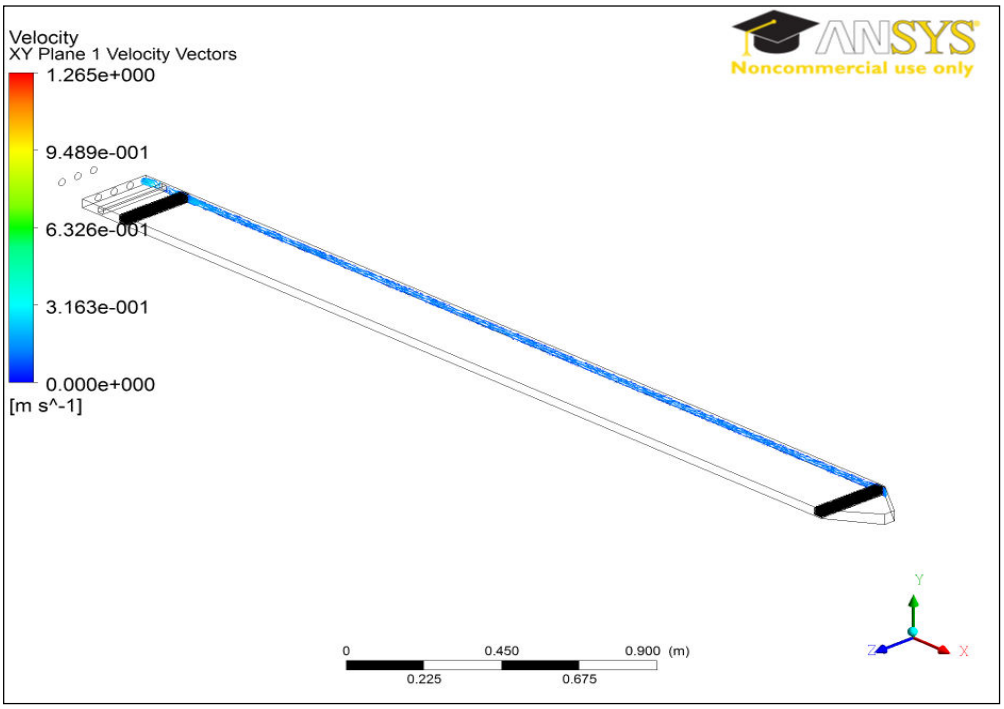

Figure 22. Velocity Vectors at XY Plane at Side of Duct with Honeycomb Structures

From the velocity vectors plot in Figure 20 and other velocity profiles, it was observed that the flow did not concentrate at the center and was near fully developed flow as it approaches the halfway point of the duct. This showed that the change of diverging entrance into a 3-pipe inlet and addition of honeycomb structures were effective in distributing the flow further.

In the next iteration of design and simulation, the overall dimensions and honeycomb structures were retained. Changes were made to the entrance to further split it into a 4-pipe inlet and the end converging section was modified into a drainage point in order to simplify the final design. Both inlet and outlet sections are 0.1524 m in length, giving a total duct length of 3.05 m, see Figure 23.

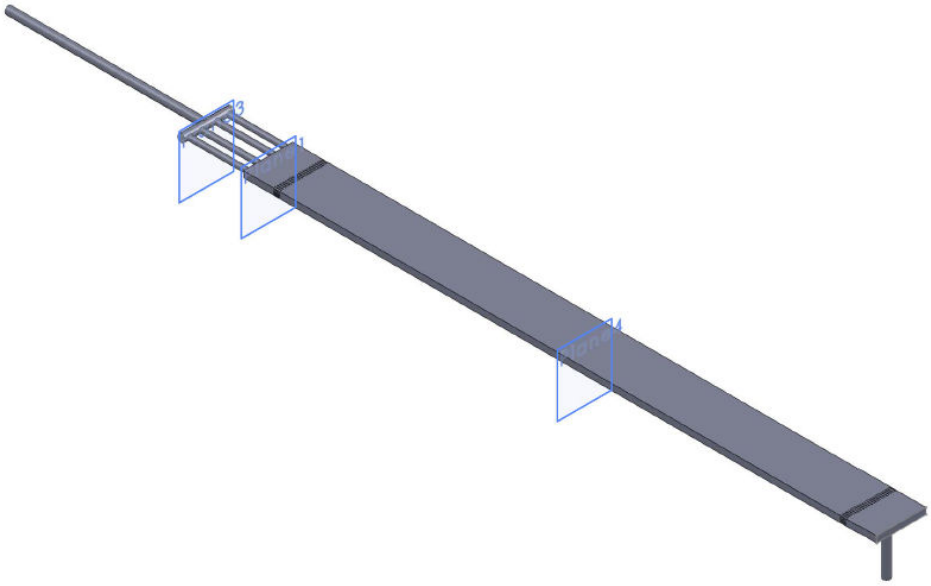

Figure 23. Final Duct Design

The same set of parameters and conditions were used to run the simulations and the results obtained are shown in Figure 24 to 29.

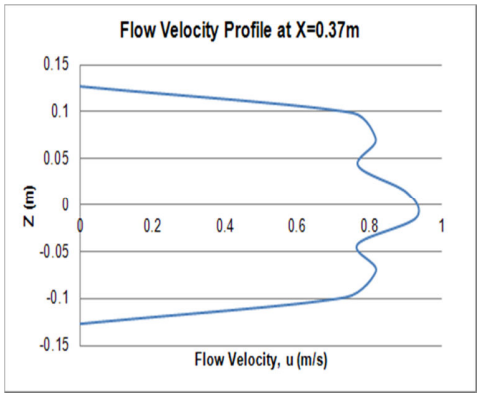
Flow Velocity Profile at X=0.37m
0.15
0.1
0.05
0
-0.05
-0.1
-0.15
Z (m)
0
0.2
0.4
0.6
0.8
1
Flow Velocity, u (m/s)

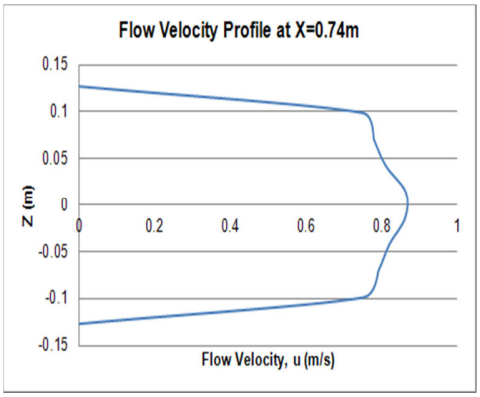
Flow Velocity Profile at X=0.74m
0.15
0.1
0.05
0
-0.05
-0.1
-0.15
Z (m)
0
0.2
0.4
0.6
0.8
1
Flow Velocity, u (m/s)

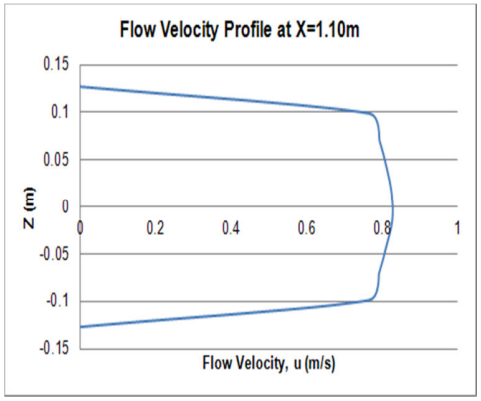
Flow Velocity Profile at X=1.10m
0.15
0.1
0.05
0
-0.05
-0.1
-0.15
Z (m)
0
0.2
0.4
0.6
0.8
1
Flow Velocity, u (m/s)

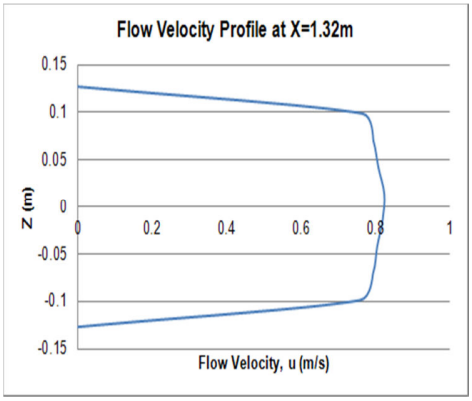
Flow Velocity Profile at X=1.32m
0.15
0.1
0.05
0
-0.05
-0.1
-0.15
Z (m)
0
0.2
0.4
0.6
0.8
1
Flow Velocity, u (m/s)

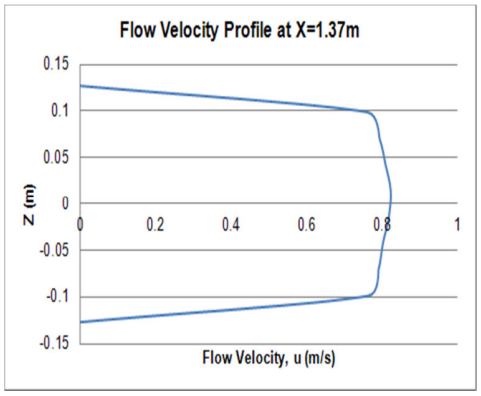
Flow Velocity Profile at X=1.37m
0.15
0.1
0.05
0
-0.05
-0.1
-0.15
Z (m)
0
0.2
0.4
0.6
0.8
1
Flow Velocity, u (m/s)

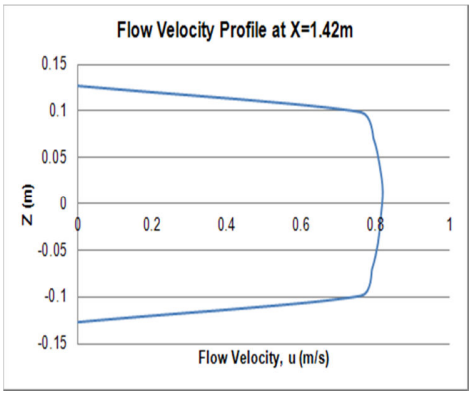
Flow Velocity Profile at X=1.42m
0.15
0.1
0.05
0
-0.05
-0.1
-0.15
Z (m)
0
0.2
0.4
0.6
0.8
1
Flow Velocity, u (m/s)

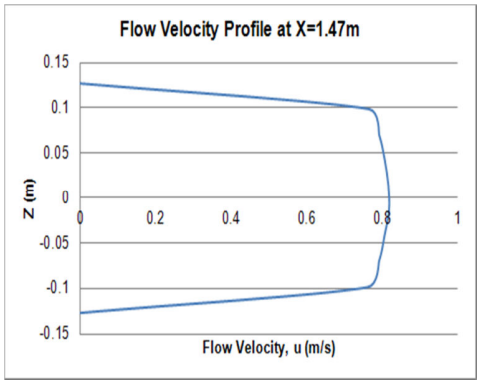
Flow Velocity Profile at X=1.47m
0.15
0.1
0.05
0
-0.05
-0.1
-0.15
Z (m)
0
0.2
0.4
0.6
0.8
1
Flow Velocity, u (m/s)

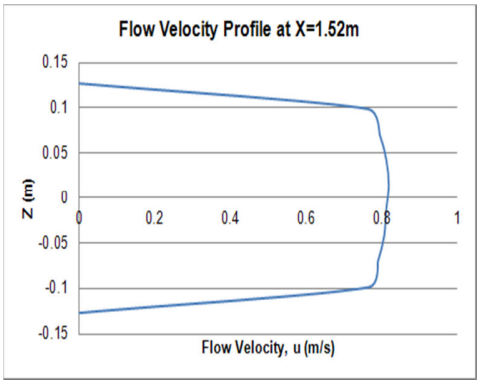
Flow Velocity Profile at X=1.52m
0.15
0.1
0.05
0
-0.05
-0.1
-0.15
Z (m)
0
0.2
0.4
0.6
0.8
1
Flow Velocity, u (m/s)

(continued)

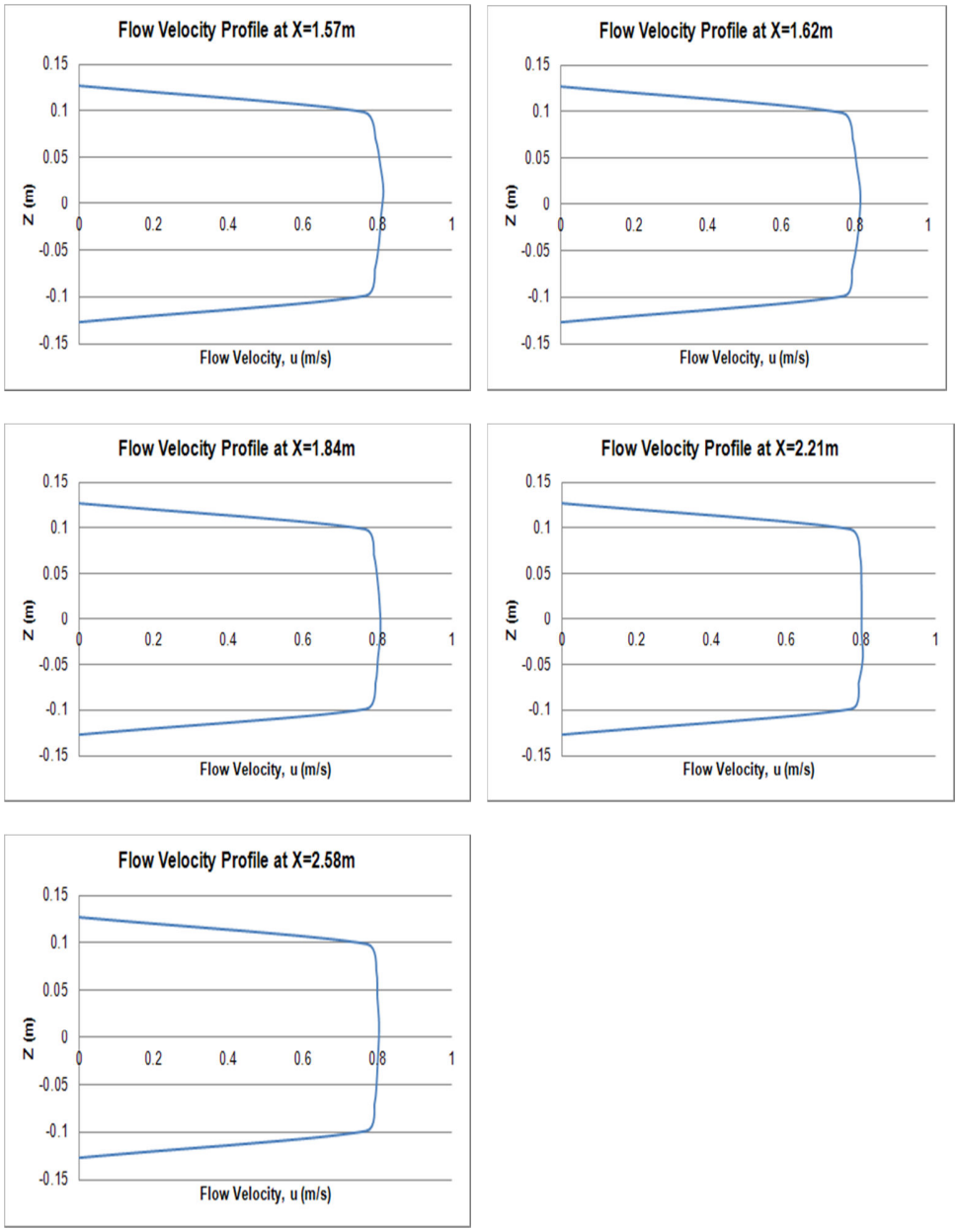

Figure 24. Flow Velocity Profiles at XZ Plane of Final Duct Design

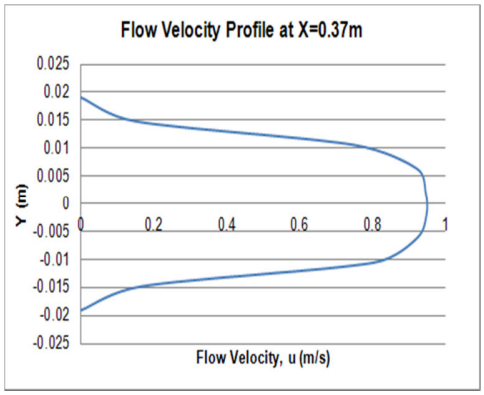
Flow Velocity Profile at X=0.37m
Y (m)
Flow Velocity, u (m/s)

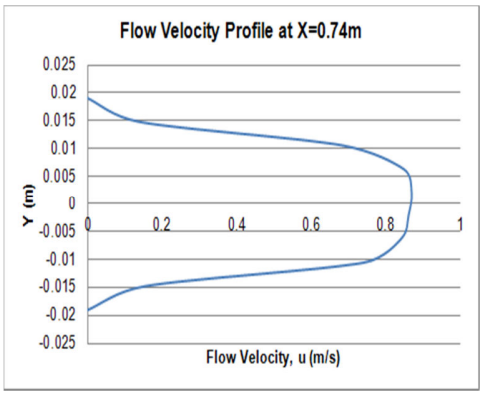
Flow Velocity Profile at X=0.74m
Y (m)
Flow Velocity, u (m/s)

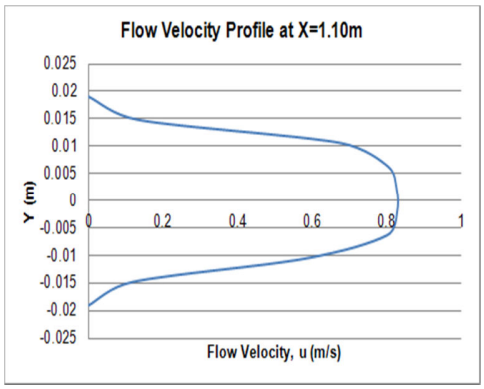
Flow Velocity Profile at X=1.10m
Y (m)
Flow Velocity, u (m/s)

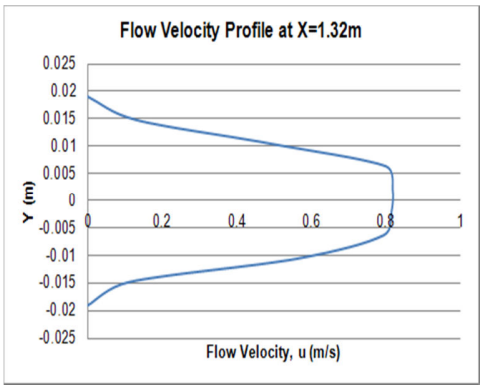
Flow Velocity Profile at X=1.32m
Y (m)
Flow Velocity, u (m/s)

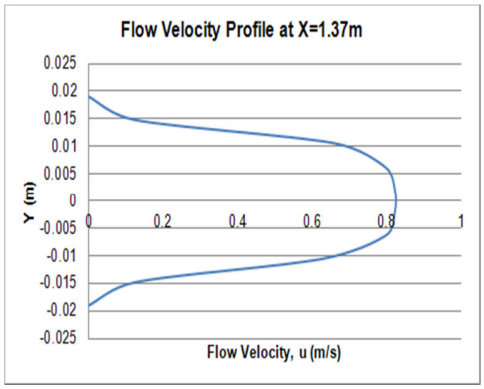
Flow Velocity Profile at X=1.37m
Y (m)
Flow Velocity, u (m/s)

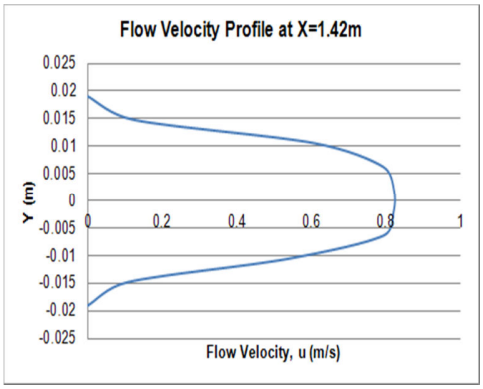
Flow Velocity Profile at X=1.42m
Y (m)
Flow Velocity, u (m/s)

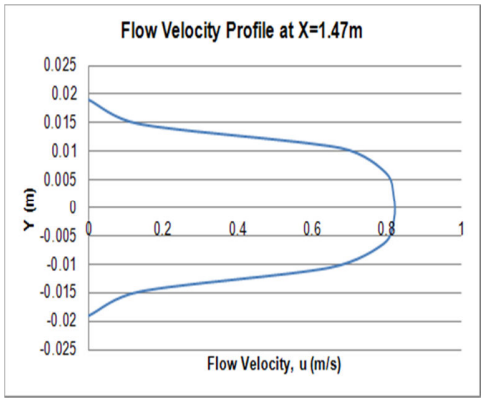
Flow Velocity Profile at X=1.47m
Y (m)
Flow Velocity, u (m/s)

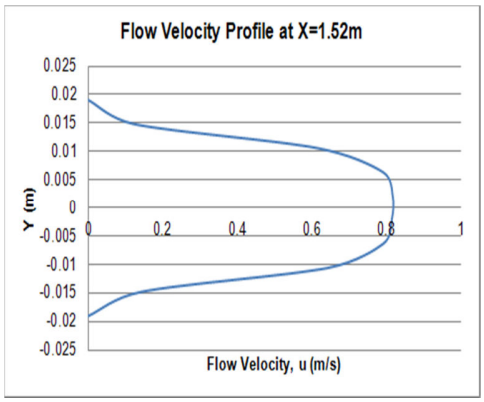
Flow Velocity Profile at X=1.52m
Y (m)
Flow Velocity, u (m/s)

(continued)

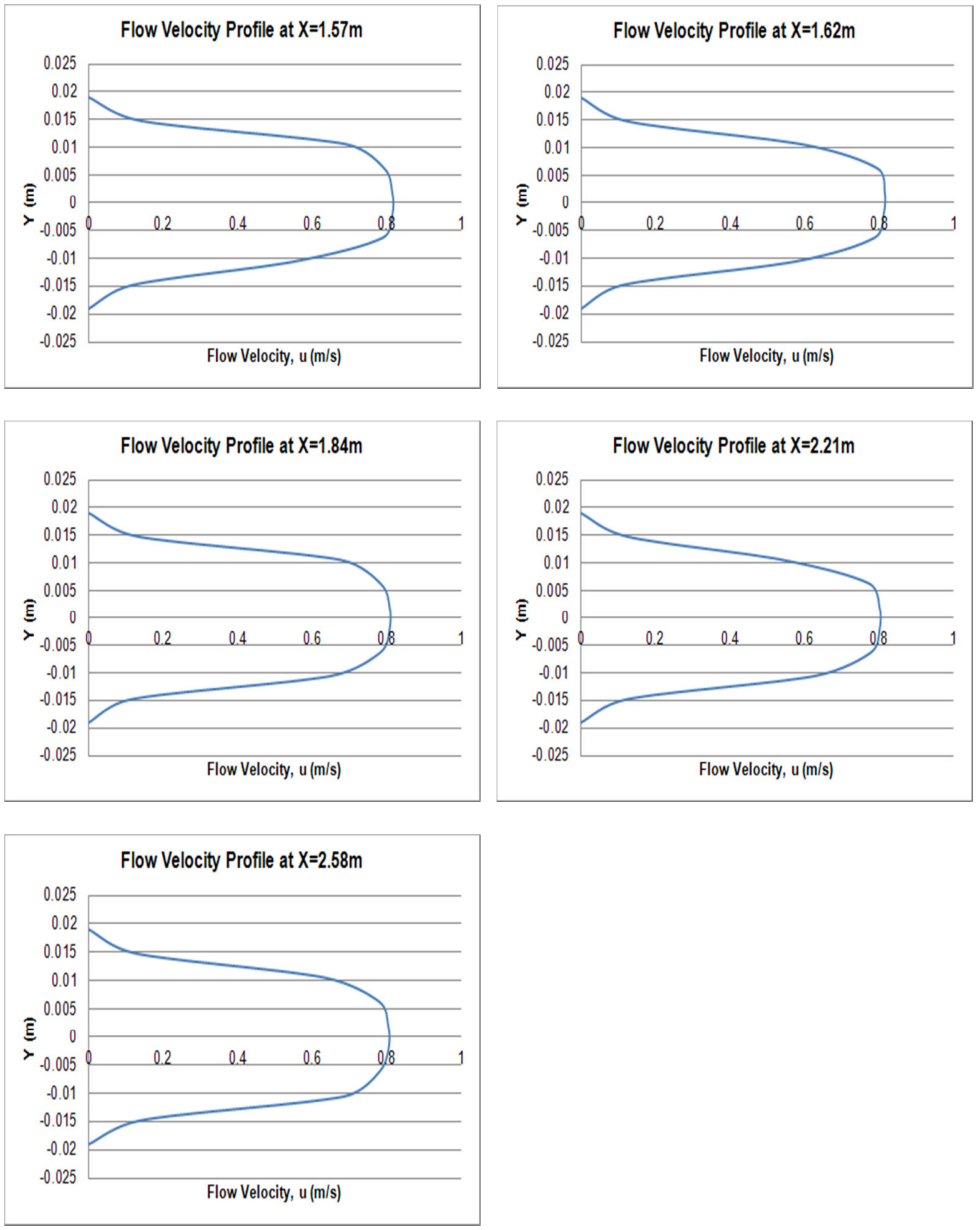

Figure 25. Flow Velocity Profiles at XY Plane at Center of Final Duct Design

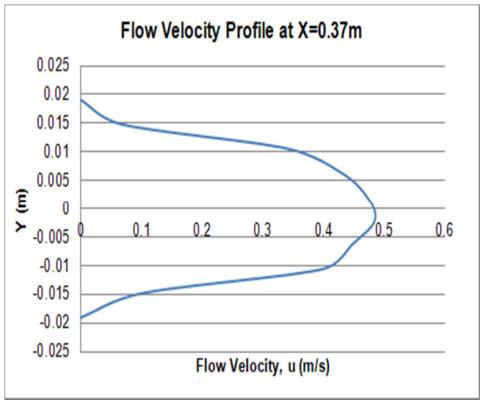
Flow Velocity Profile at X=0.37m
Y (m)
Flow Velocity, u (m/s)

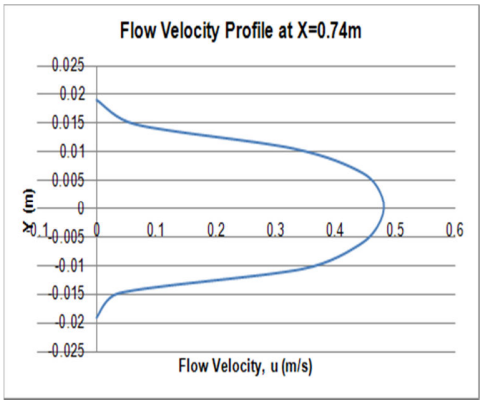
Flow Velocity Profile at X=0.74m
Y (m)
Flow Velocity, u (m/s)

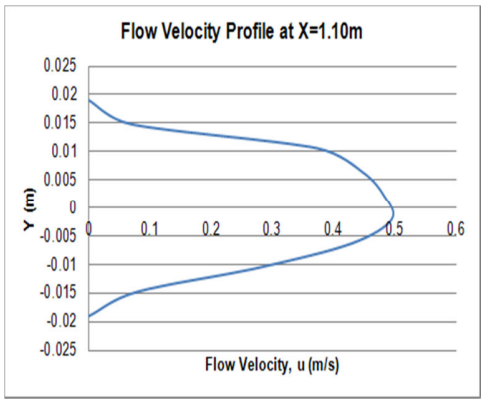
Flow Velocity Profile at X=1.10m
Y (m)
Flow Velocity, u (m/s)

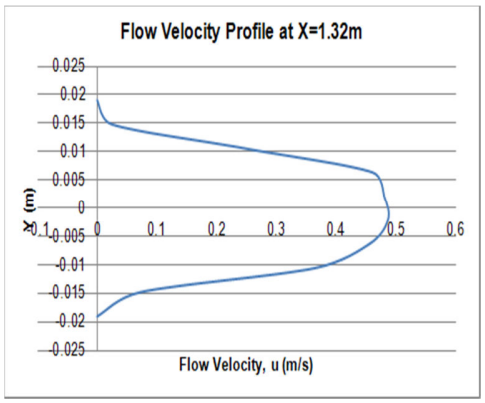
Flow Velocity Profile at X=1.32m
Y (m)
Flow Velocity, u (m/s)

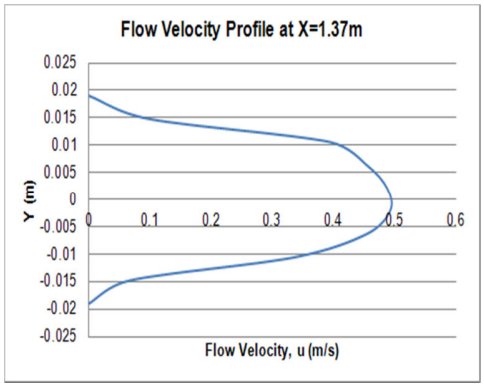
Flow Velocity Profile at X=1.37m
Y (m)
Flow Velocity, u (m/s)

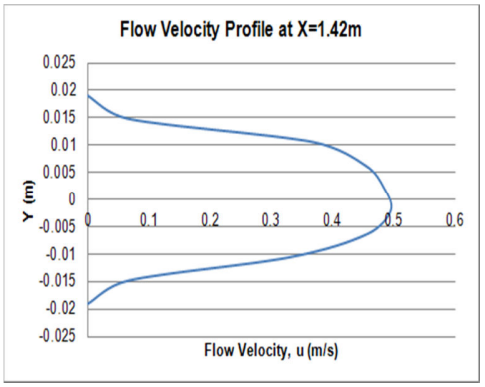
Flow Velocity Profile at X=1.42m
Y (m)
Flow Velocity, u (m/s)

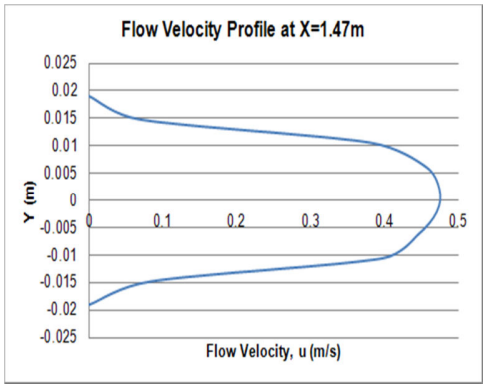
Flow Velocity Profile at X=1.47m
Y (m)
Flow Velocity, u (m/s)

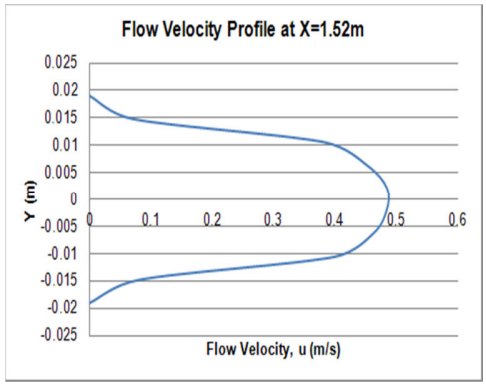
Flow Velocity Profile at X=1.52m
Y (m)
Flow Velocity, u (m/s)

(continued)

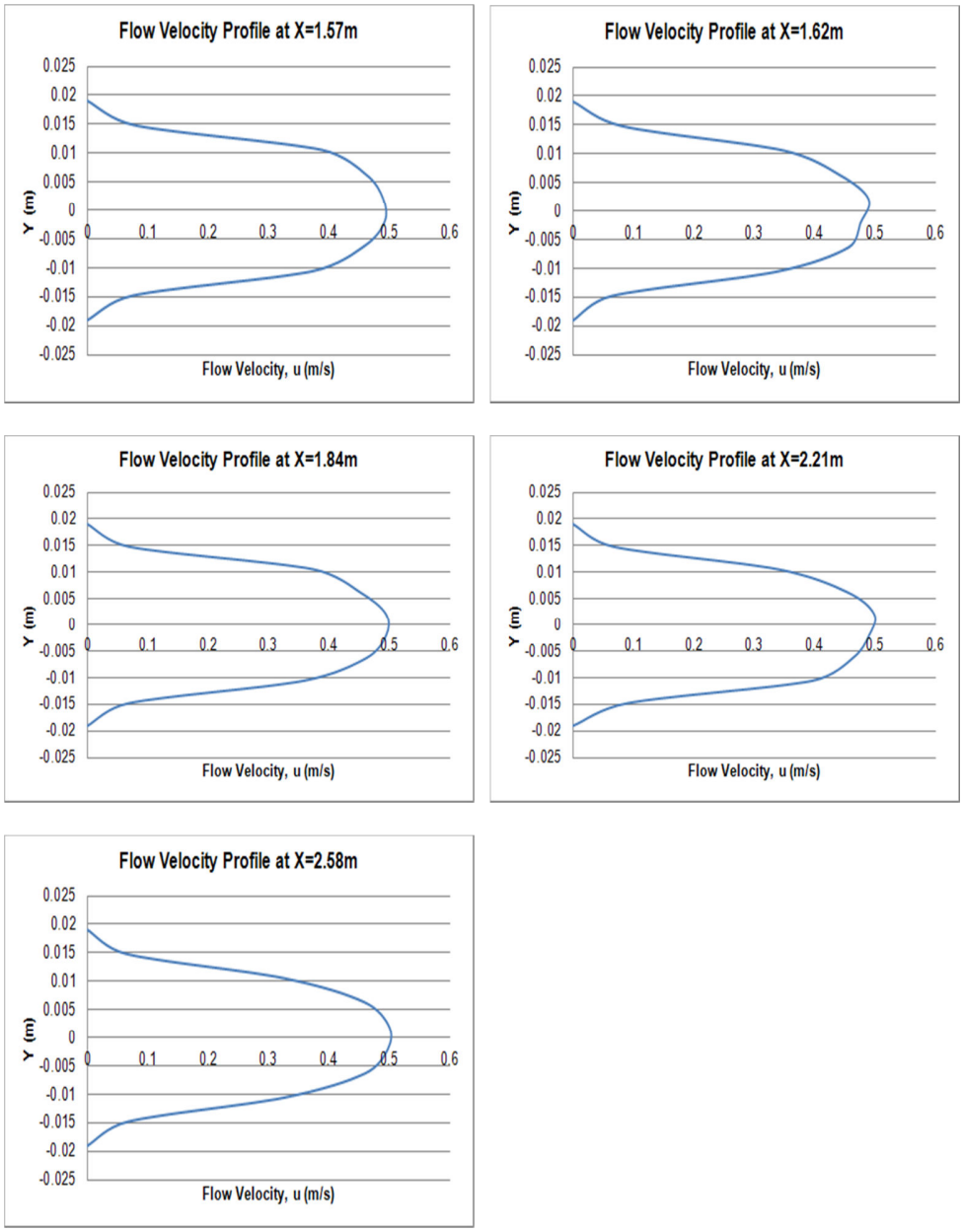

Figure 26. Flow Velocity Profiles at XY Plane at Side of Final Duct Design

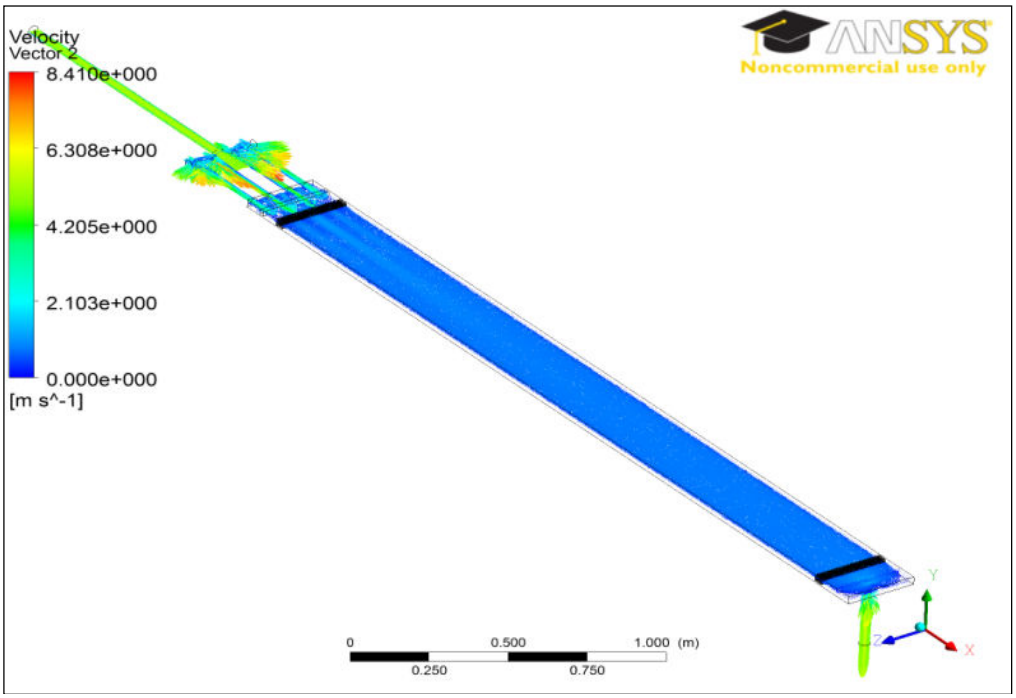

Figure 27. Velocity Vectors at XZ Plane of Final Duct Design

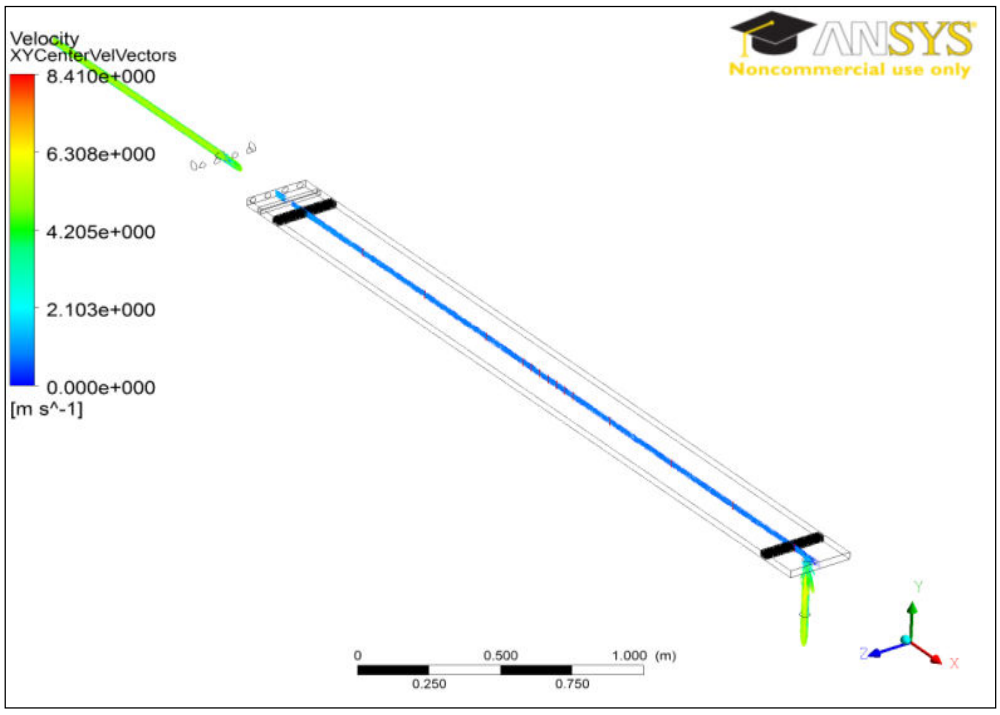

Figure 28. Velocity Vectors at XY Plane at Center of Final Duct Design

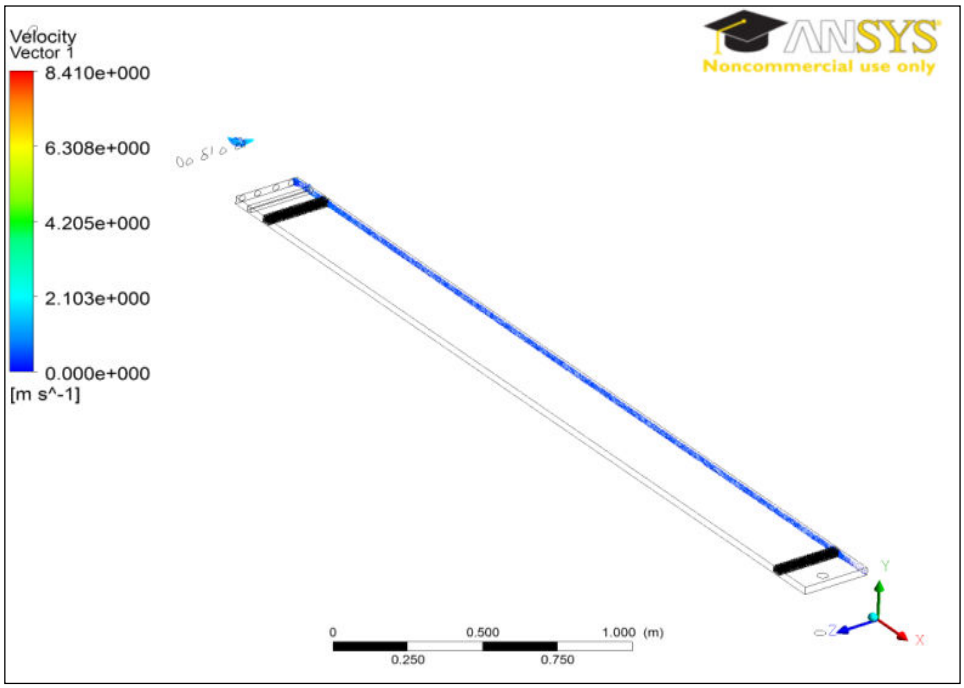

Figure 29. Velocity Vectors at XY Plane at Side of Final Duct Design

From the velocity vectors plot in Figure 27 and various velocity profiles, it was observed that the flow was well distributed and was near fully developed flow as it approaches the half of the duct.

B. SELECTION OF MATERIALS

1. Duct

To allow visualization of the flow, transparent Polymethyl methacrylate (PMMA, Plexiglass) of thickness 0.0127 m was chosen to build the duct, as seen in Figure 30.

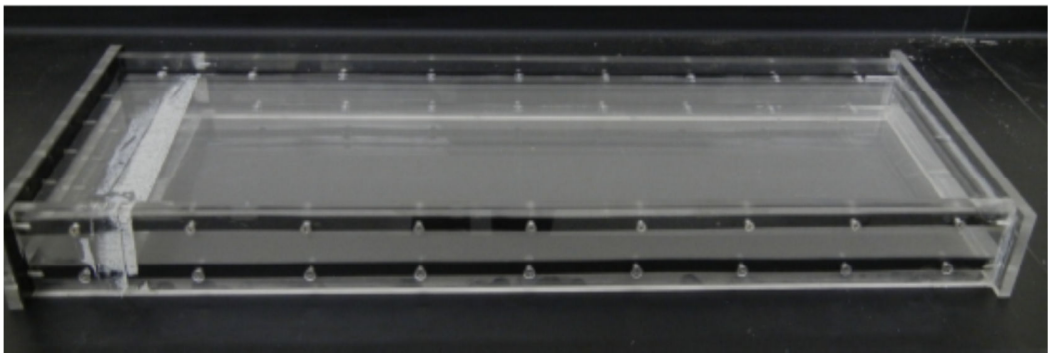

Figure 30. Plexiglass for Construction of Duct

Plexiglass has other advantages such as ease of cutting, joining, low cost and it is inert to the chosen test fluid as well. Due to its transparency, the duct could be used for future work such as flow investigation using laser optical measurement techniques.

2. Test Plate

As the experiment would be a low-pressure application, Aluminum alloy (Al 1100) with a minimum 99% aluminum, was chosen to be the test plate material. It has a Young's Modulus of 68.9 GPa, Poisson ratio of 0.33 and density of 2710 kg/m^3, as shown in Figure 31. The test plate was 0.254 m by 0.305 m and 0.000508 m thick.

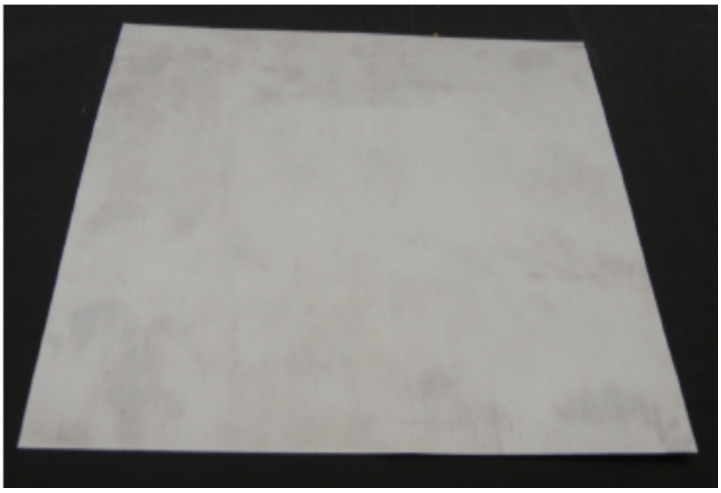

Figure 31. Al 1100 Test Plate

3. Test Fluid

As previously mentioned, the requirement of the project was in the laminar regime, a fluid of high dynamic viscosity needs to be chosen as the test fluid to attain Reynolds numbers (Re) of less than 2300. In this case, Propylene Glycol with a density of 965.3 kg/m^3 and dynamic viscosity of 0.06 kg/m s was selected as the test fluid.

4. Piping System

For flexibility and simplicity, Polyvinyl chloride (PVC) pipes and connectors were chosen to build the piping system, (see Figure 32). In addition, PVC is lightweight, durable, low cost and has low reactivity. The pipes and connectors were assembled using solvent welding.

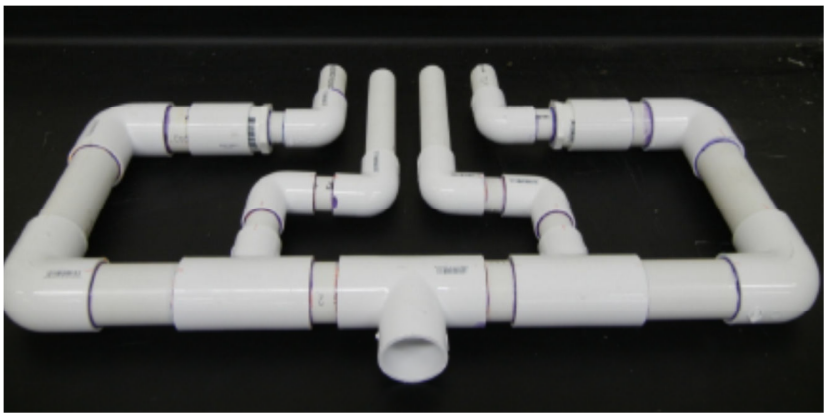

Figure 32. PVC Pipes and Connectors

C. APPARATUS SETUP

1. Construction of Duct

The entire duct consists of three center sections that were each 0.914 m long, 0.254 m wide and 0.0318 m high, and two sections for the entrance and exit sections that were each 0.152 m long, 0.254 m wide and 0.0318 m high. Each section was made out of 0.0127 m thick Plexiglass plates assembled by solvent welding. For examples, see Figure 33.

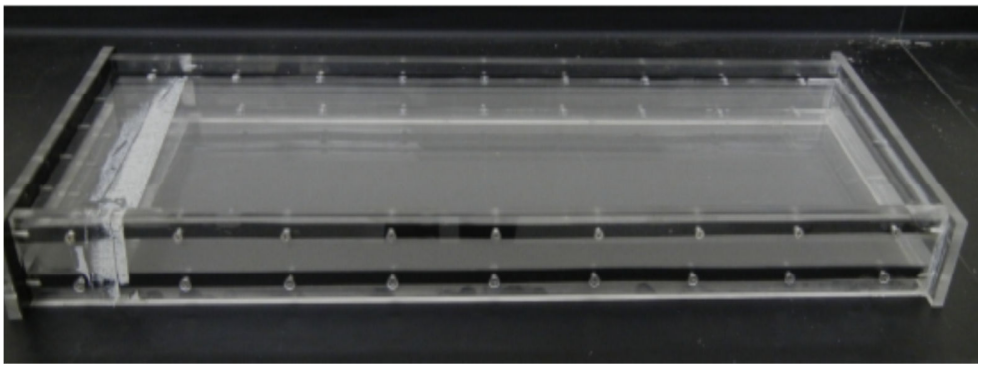

(a) Center Section of Duct

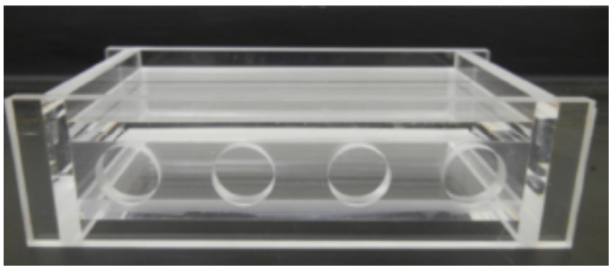

(b) Entrance Section of Duct

Figure 33. Sections of Duct

As previously mentioned, to further distribute the flow, two sets of honeycomb structures were placed 0.152 m from the entrance and exit respectively. The honeycomb structures were made of aluminum and were 0.254 m wide, 0.0508 long and 0.0318 high, see Figure 34.

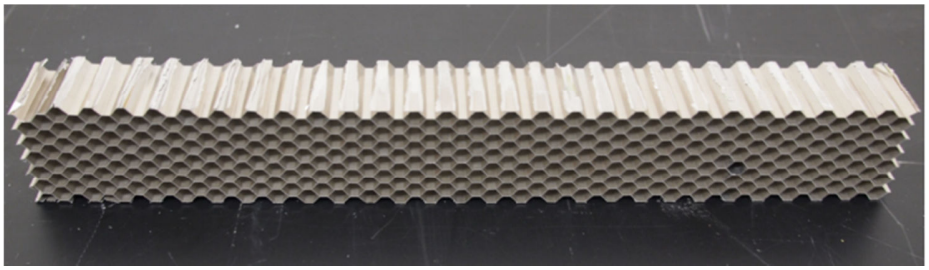

Figure 34. Honeycomb Structures

To ensure that the test plate lied in the region where the flow before and after the test plate was fully developed, it was placed at 1.57 m downstream from

the entrance of the duct. A 0.203 m by 0.203 m window section was cut from the bottom plate of the duct and the test plate was joined to the Plexiglass plate, covering the section, using 3M^{TM} super 77 Multipurpose Spray Adhesive. Edges of the test plate were smoothened with sandpaper to ensure smooth transition of flow. Silicon sealant was applied to prevent leakages. This window section would allow flexing of test plate and therefore the measurement of strain of the plate during the experiment, as seen in Figure 35.

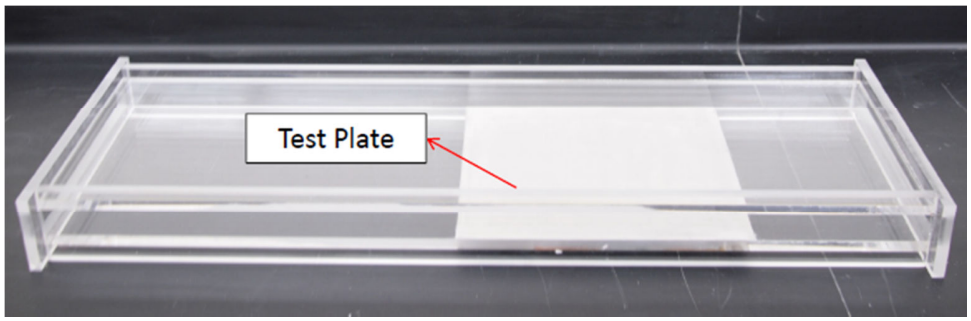

Figure 35. Test Section

Finally, all the sections were assembled using clamps and sealant to form the entire duct, 3.05 m in length, 0.254 m in width and 0.0318 m in height, see Figure 36.

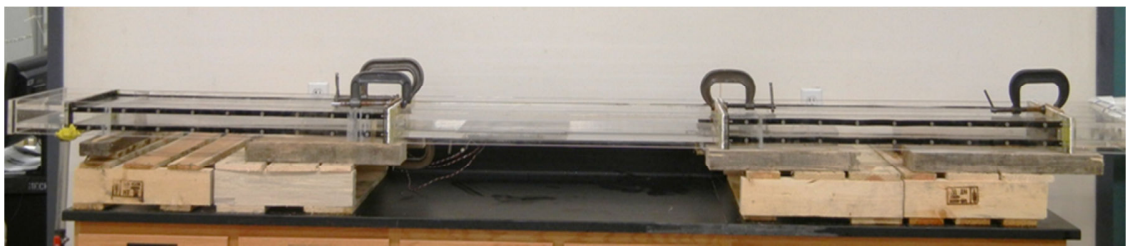

Figure 36. Entire Duct

2. Flow Circuit

Due to the requirement to create a laminar flow with high viscous fluid, a controllable and accurate flow circuit was constructed, see Figure 37.

Figure 37. Flow Circuit

The flow circuit was powered by an Baldor VL3515 AC motor single phase pump, with a maximum flow rate of 70 GPM. Flow diffusers were used to direct excessive flow away from the duct, see Figure 38.

Figure 38. AC Motor Single Phase Pump

3. Instrumentation

a. Strain Gages

Vishay Micro-Measurements CEA-00–250UR-350 rosette strain gages were used to measure the strain. As shown in Figure 39, two gages were fitted to the underside of the test plate.

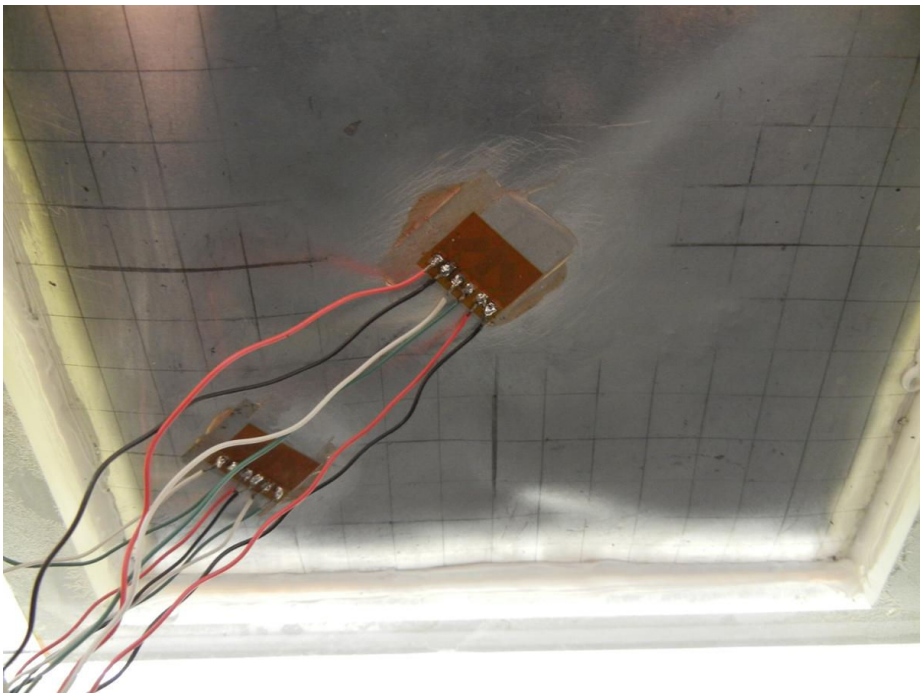

Figure 39. Rosette strain gages

b. Data Analyzer

Measurements from the rosette strain gages were acquired by a data acquisition system. The system consisted of a Pentium™ 4, 2.4 GHz, 512-MB RAM system and National Instruments™ simultaneous sampling multifunction DAQ. This system is shown in Figure 40.

Figure 40. Data Acquisition System

The system had a 16 bit analog-to-digital conversion resolution and was capable of reading a total of 16 channels at a throughput rate of up to 250 kS/s per channel, which was appropriate for the rate of testing used in this study. The data-acquisition process was controlled using the NI-DAQmx driver software and LabVIEW™ interactive data-logging software.

THIS PAGE INTENTIONALLY LEFT BLANK

III. FLUID STRUCTURE INTERACTION MODELING

A. OVERVIEW

In order to understand transient response of the test plate under FSI conditions, computational studies were carried out in ANSYS 13.0 Multi-field (MFX) simulation. Structural analysis of the test plate was set up in Transient Structural analysis system while the flow analysis concerning the test fluid was set up in Fluid Flow (CFX) analysis system. Coupling between the two analysis systems was required throughout the solution to model the FSI between test plate and fluid as time progresses. The geometry used in the simulation consisted of the fluid body and the test plate body that followed the dimensions of the actual experimental setup (see Figure 41).

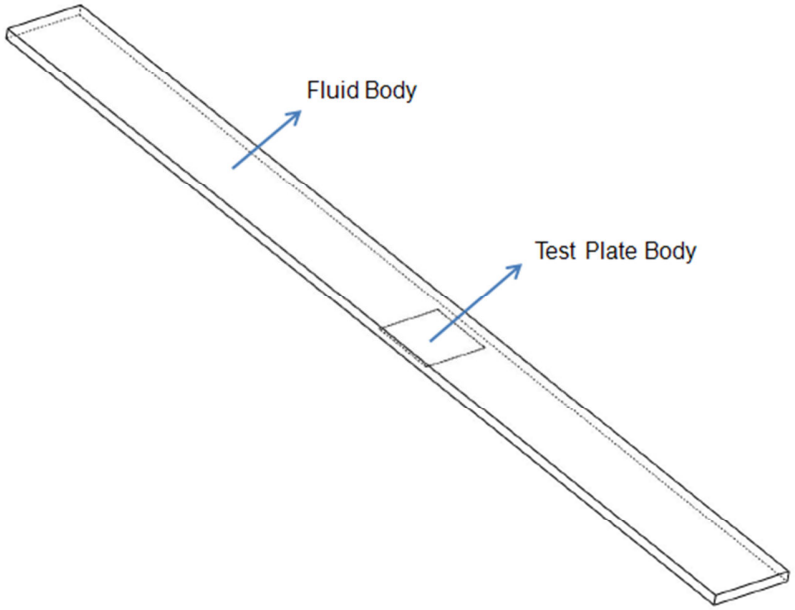

Figure 41. Geometry Used in FSI Modeling

Different sizes of meshes were used for the fluid body and test plate body since the fluid body was much larger than the test plate body. The program was able to handle the mismatch of meshes through an interpolation algorithm. In all

cases, the test plate body had about 1,250 tetrahedron elements while the fluid body had about 500,000 tetrahedron elements. Boundary conditions applied to the test plate body include fixed support at the edges and fluid-solid interface which defined the interface between the fluid body and the test plate body. For the fluid body, inlet velocity, outlet pressure and wall boundary conditions at the interface were applied. The boundary condition at the interface allowed nodal velocity values to be received from the Transient Structural solver and the sending of force values to the Transient Structural solver. The simulations were conducted for a duration of 0.6s and with a time step of 0.005s. Parameters such as nodal displacement, fluid pressure, structural acceleration and velocity were gathered for each simulation. The studies included comparisons of results of different velocities, densities, and Young's Moduli. Propylene Glycol was used as the test fluid in all the cases. The baseline case was set up as close as possible to the actual experiment. Thus, Al 1100 properties were used and a uniform velocity of 1 m/s was prescribed at the inlet.

B. VARIATIONS IN INPUT VELOCITY

In the first example, the inlet velocity was varied for comparison. Inlet velocities of 0.5 m/s and 2 m/s were modeled and compared to the baseline case. Results for nodal displacement, fluid pressure, structural acceleration and velocity were illustrated in Figures 42 to 45. Nodal displacements for both fluid and test plate were similar, thus only one of them is shown here. Undefined data was present in the plot in Figure 43, hence producing a curve that was not sinusoidal in nature.

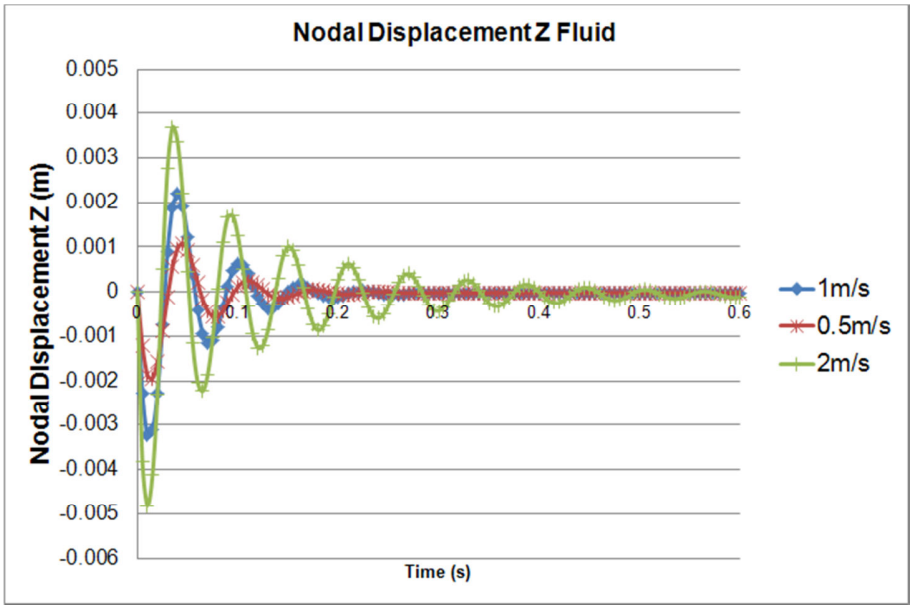

Figure 42. Nodal Displacement Z for Fluid Body for Different Inlet Velocities

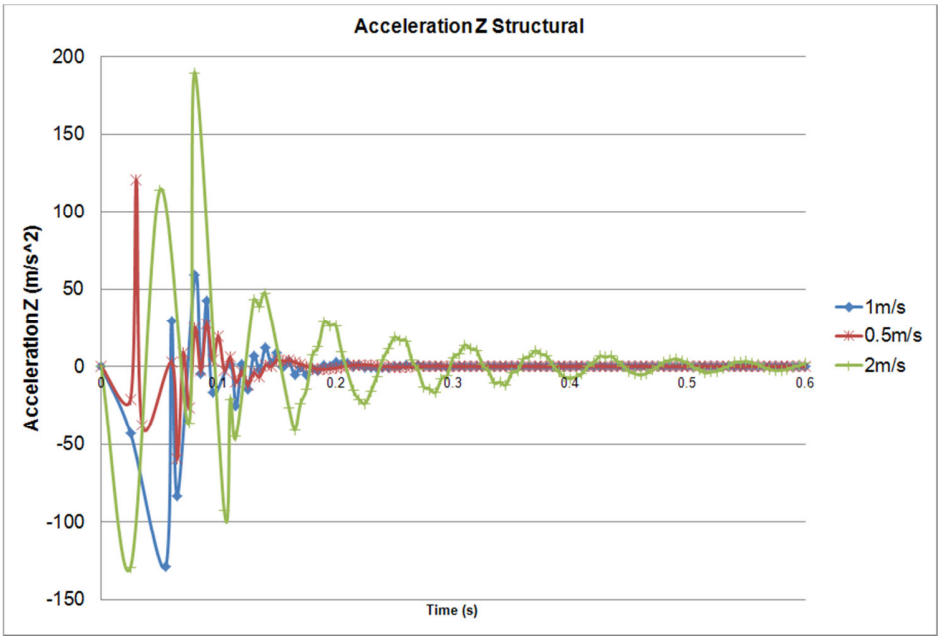

Figure 43. Acceleration Z for Test Plate for Different Inlet Velocities

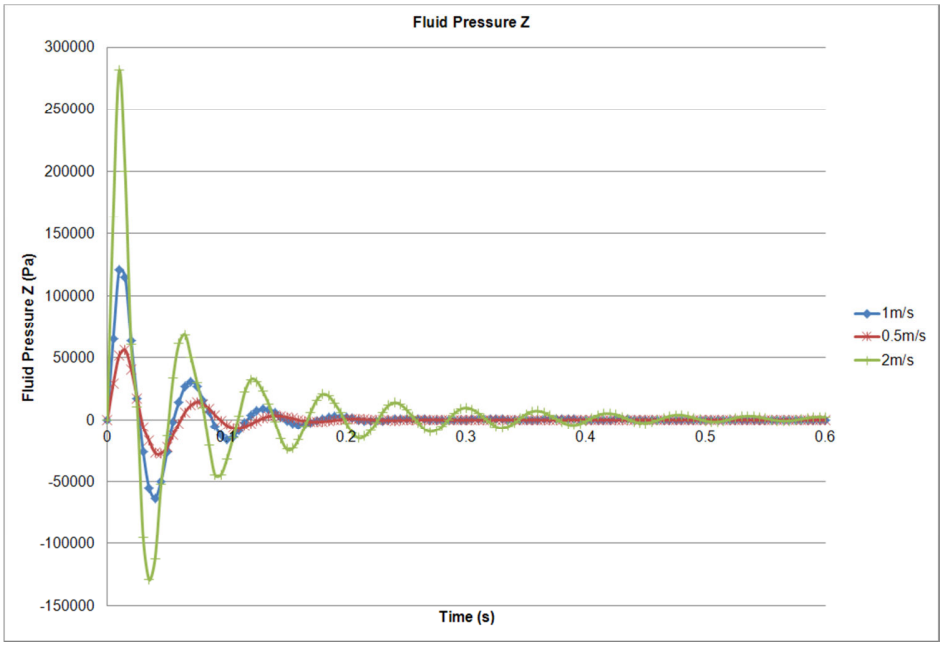

Figure 44. Pressure for Fluid Body for Different Inlet Velocities

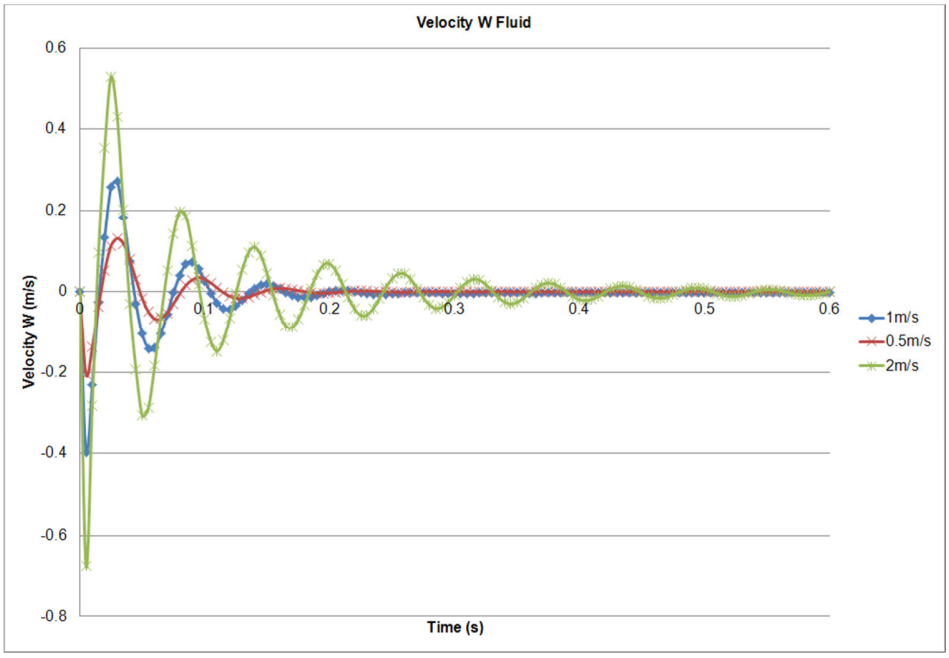

Figure 45. Velocity W for Fluid Body for Different Inlet Velocities

As shown in the preceding group of figures, in all three cases, vibration of the test plate damped out as time progressed because of the FSI effect. Damping out started at about 0.25s for inlet velocity of 0.5 m/s, 0.30s for 1 m/s and beyond 0.60s for 2 m/s. It was observed that the magnitude of displacement, acceleration, pressure and velocity at the interface increased with inlet velocity.

C. VARIATIONS IN DENSITY

In this example, the density of the test plate was varied for the simulations, while all other material properties and experimental conditions remained. Densities of 1335 kg/m^3 (half of Al 1100's density) and 5420 kg/m^3 (twice of Al 1100's density) were modeled. Results for nodal displacement, fluid pressure, structural acceleration and velocity were illustrated in Figures 46 to 49. Nodal displacements for both fluid and test plate were similar, thus only one of them is shown here. Undefined data was present in the plot in Figure 47, hence producing a curve that was not sinusoidal in nature.

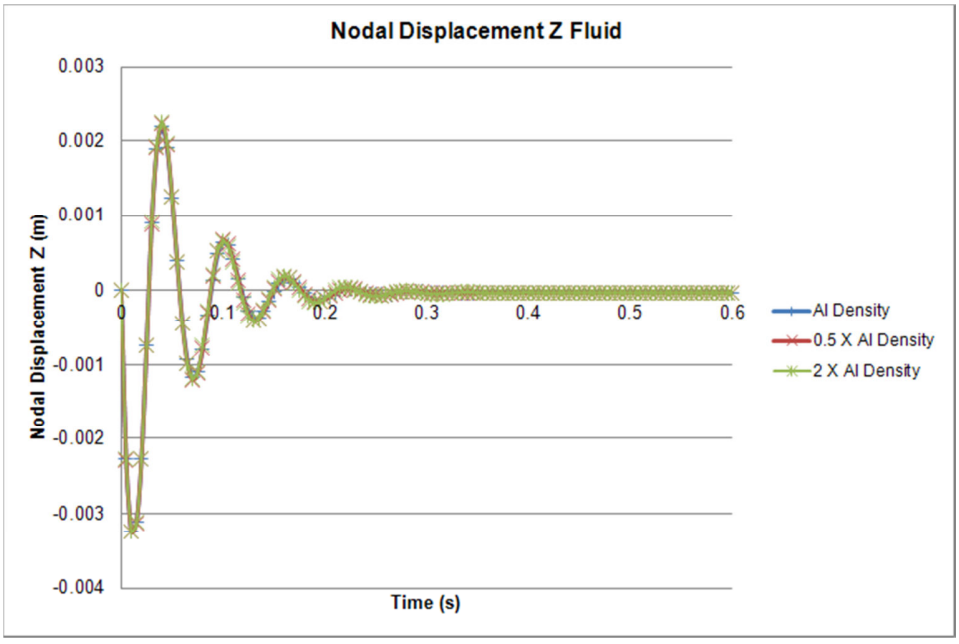

Figure 46. Nodal Displacement Z for Fluid Body for Different Densities

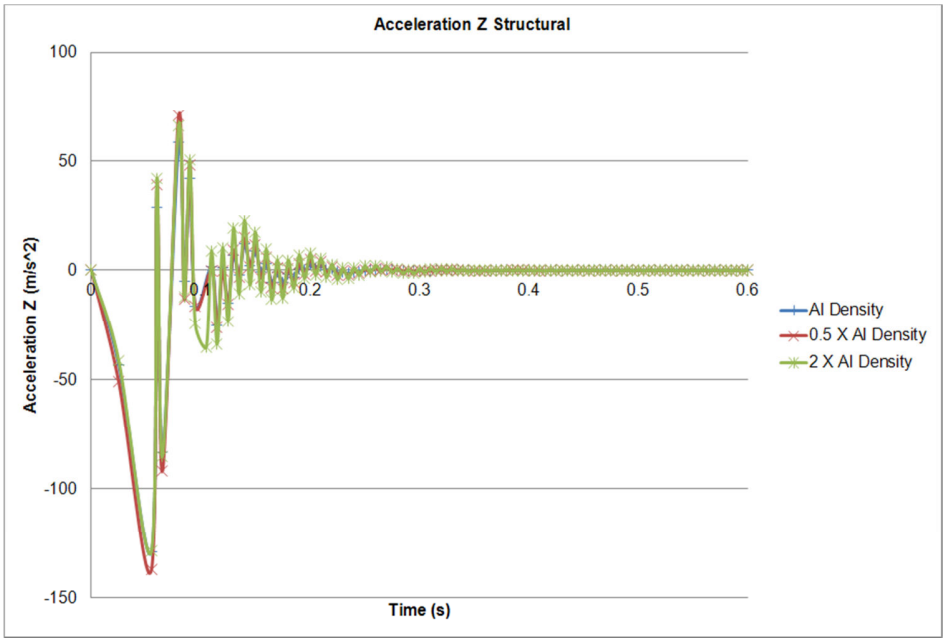

Figure 47. Acceleration Z for Test Plate for Different Densities

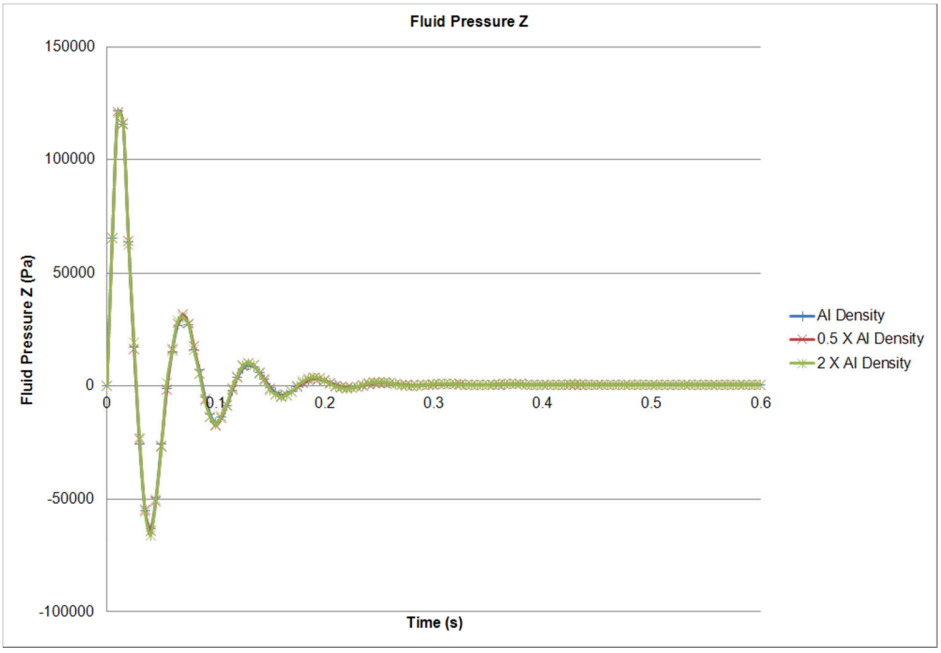

Figure 48. Pressure for Fluid Body for Different Densities

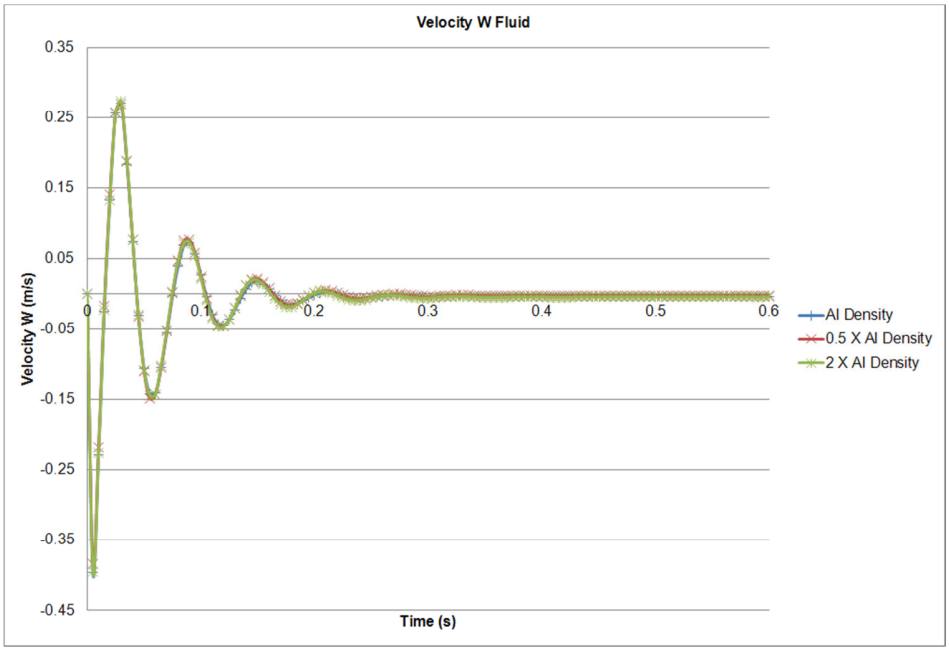

Figure 49. Velocity W for Fluid Body for Different Densities

It could be seen from the results that as density increased, the FSI effect decreased. However, for all the cases, differences in magnitude of the parameters measured were not significant. The vibration for all cases damped out at about 0.25s.

D. VARIATIONS IN YOUNG'S MODULUS

Next, the Young's Modulus of the test plate was varied to investigate its effect on FSI, while all other material properties and experimental conditions remained constant. Young's Moduli of 34.5 GPa (half of Al 1100's Young's Modulus) and 134.9 GPa (twice of Al 1100's Young's Modulus) were modeled in the simulations. Results for total mesh displacement, fluid pressure, structural acceleration and velocity were illustrated in Figures 50 to 53. Nodal displacements for both fluid and test plate were similar, thus only one of them is shown here. Undefined data was present in the plot in Figure 51, hence producing a curve that was not sinusoidal in nature.

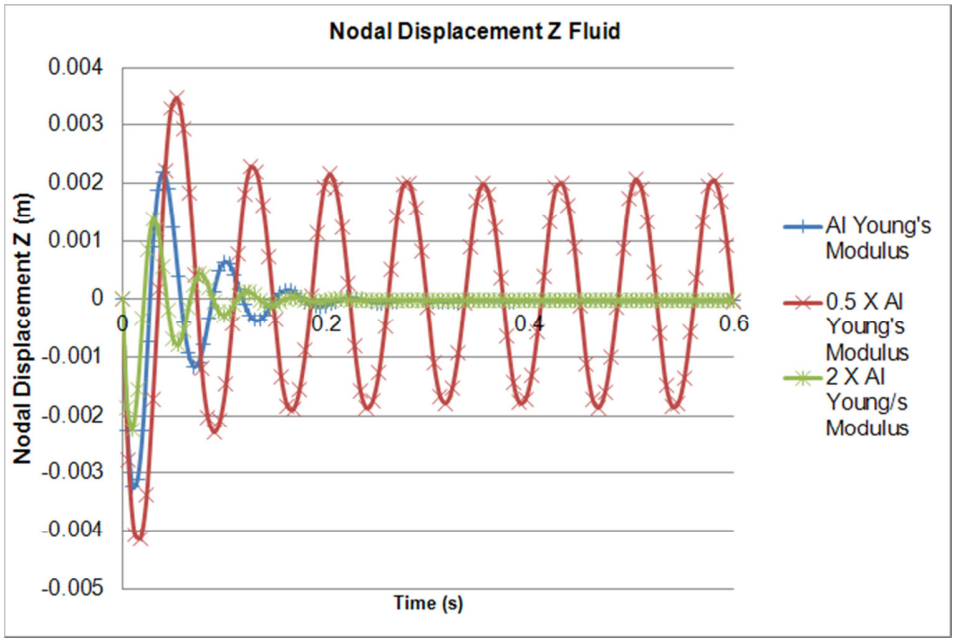

Figure 50. Nodal Displacement Z for Fluid Body for Different Young's Moduli

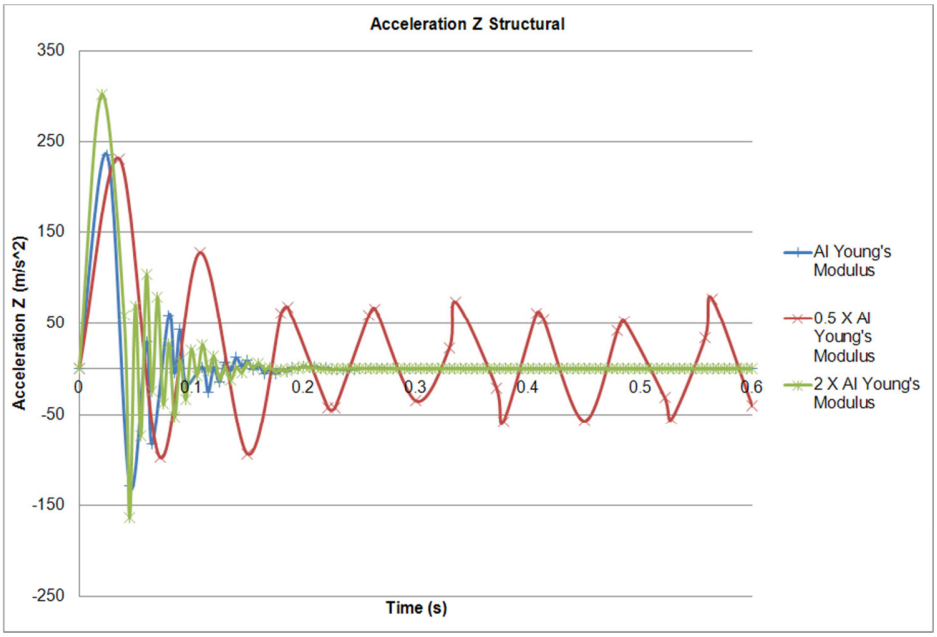

Figure 51. Acceleration Z for Test Plate for Different Young's Moduli

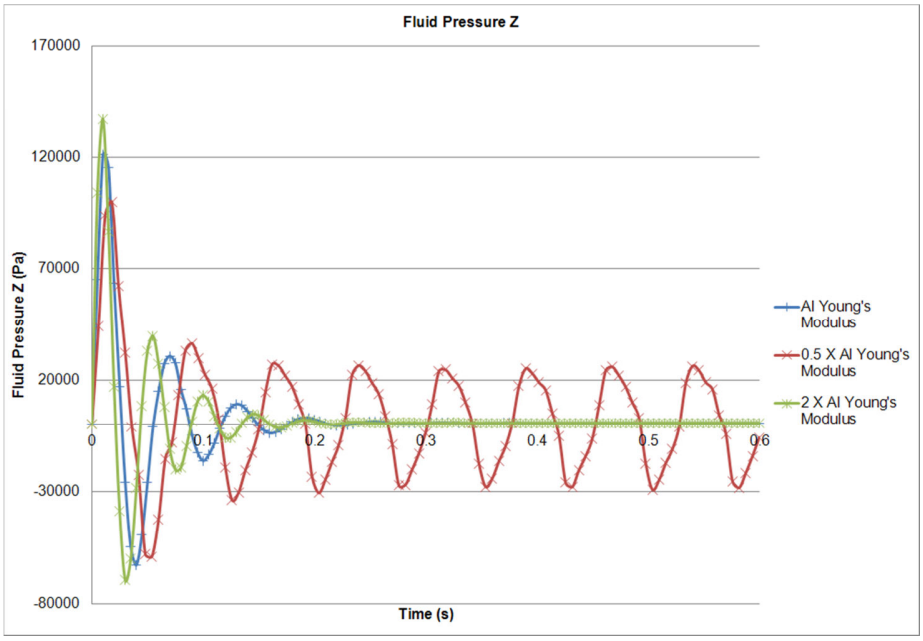

Figure 52. Pressure for Fluid Body for Different Young's Moduli

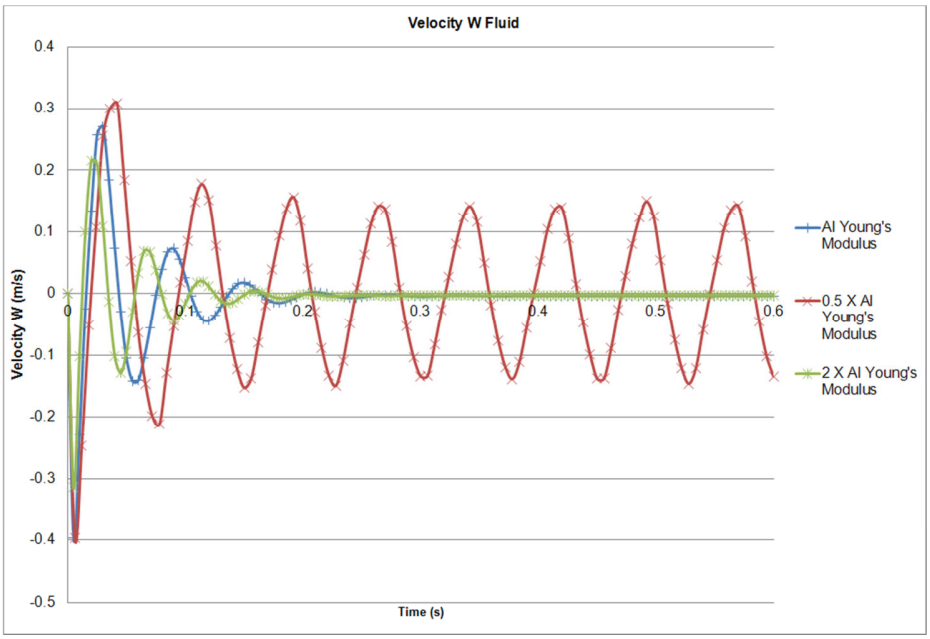

Figure 53. Velocity W for Fluid Body for Different Young's Moduli

As illustrated in the preceding group of figures, under the same input velocity for fluid body, the FSI effect was greater for lower Young's Moduli. This was exemplified by the results for Young's Modulus of 34.5 GPa. The magnitude of parameters measured was much larger than the other two simulations. The FSI effect damped out at about 0.25s for both Young's Modulus of 68.9 GPa and 134.9 GPa. On the other hand, for the lowest Young Modulus of 34.5 GPa, the FSI effect did not showed any signs of damping out for the duration of simulation. These results were consistent with the physical meaning of Young's Modulus as a measure of stiffness.

IV. EXPERIMENTAL RESULTS

A. OVERVIEW

The experiment was performed using the designed and constructed duct and flow circuit. Many pre-tests were conducted to detect and prevent leakages and to ensure that the flow circuit was in appropriate working conditions for the experiment. Measurements of strains were recorded for a period of 120 sec with a sampling rate of 100/s and resulting in 12,000 data per strain gage. The gages and pump were initiated together to synchronize the measurements. The flow was able to fill up the whole duct and became steady after about 25 sec. The pump was switched off after the flow had reached an equilibrium state. Due to the lack of instrumentation, pressure and velocity of flow were not measured. Five tests were conducted to confirm repeatability of the testing data.

B. RESULTS

The strain values were measured from the gages on the underside of the test plate, with the positions and naming shown in Figure 54.

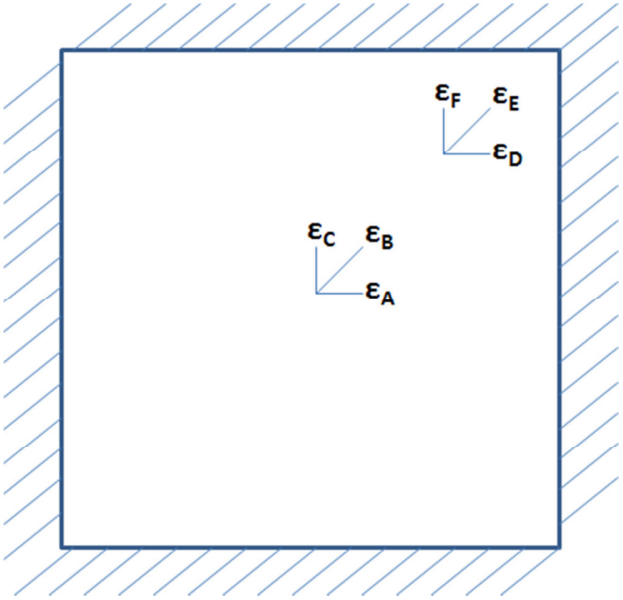

Figure 54. Positions and Naming of Strain Values

1. Experimental Results

Figures 55 to 61 illustrated a representative sample of the experimental results from the strain gages' measurement for one of the runs. Results were consistent for all the runs.

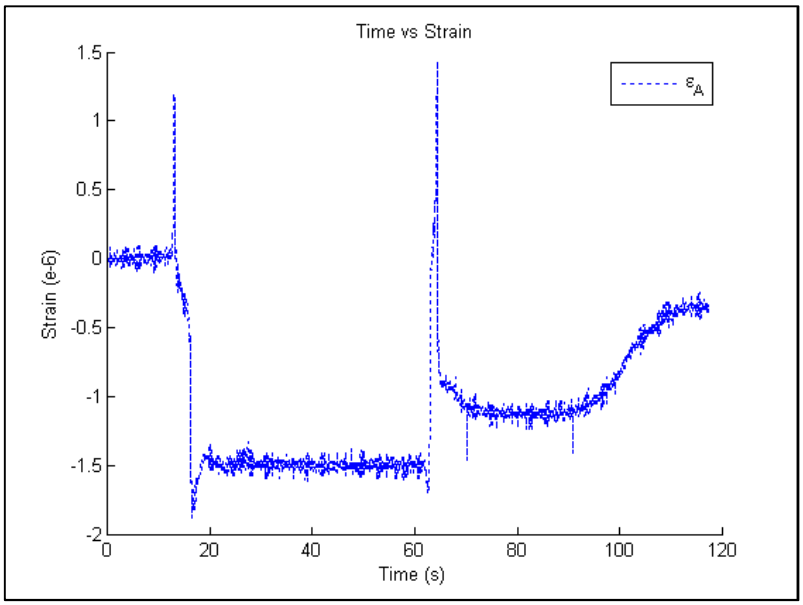

Figure 55. ε_A Response

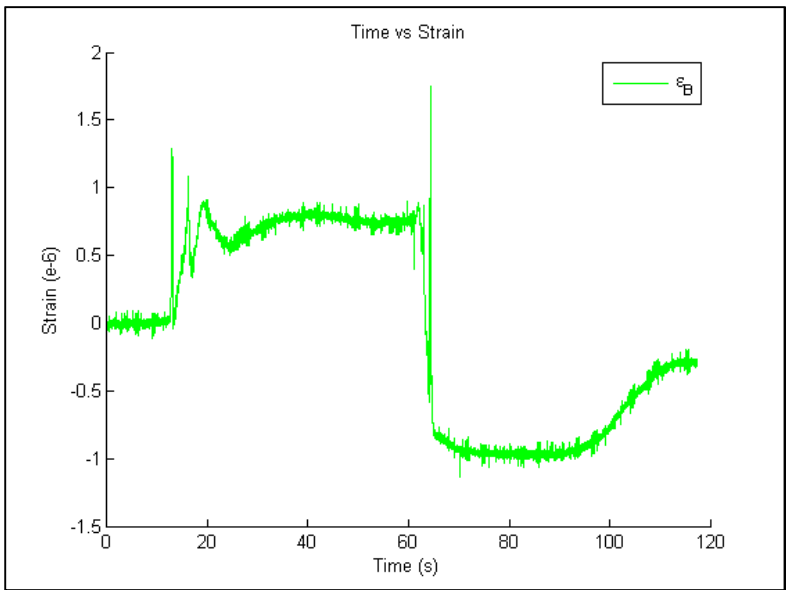

Figure 56. ε_B Response

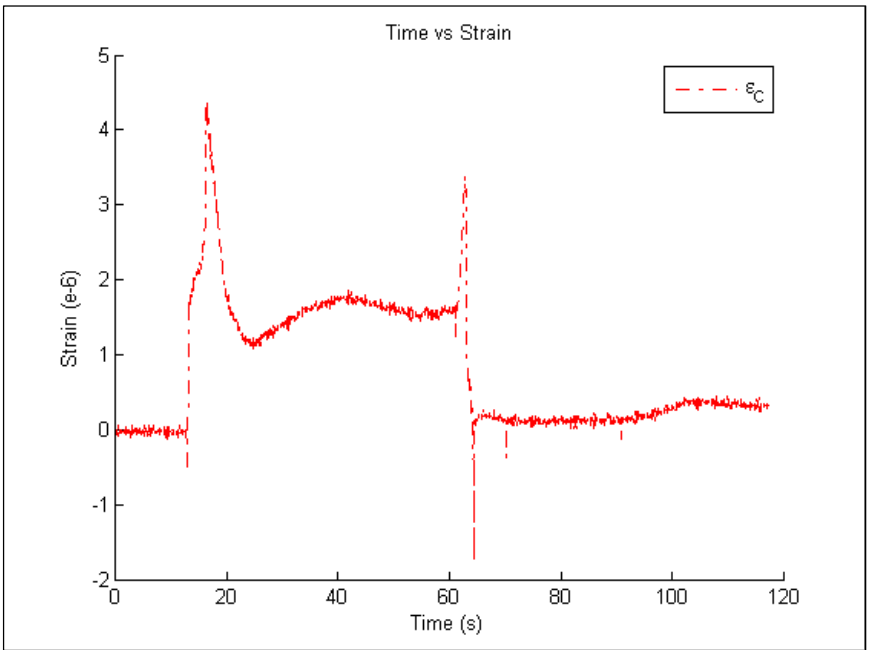

Figure 57. ε_C Response

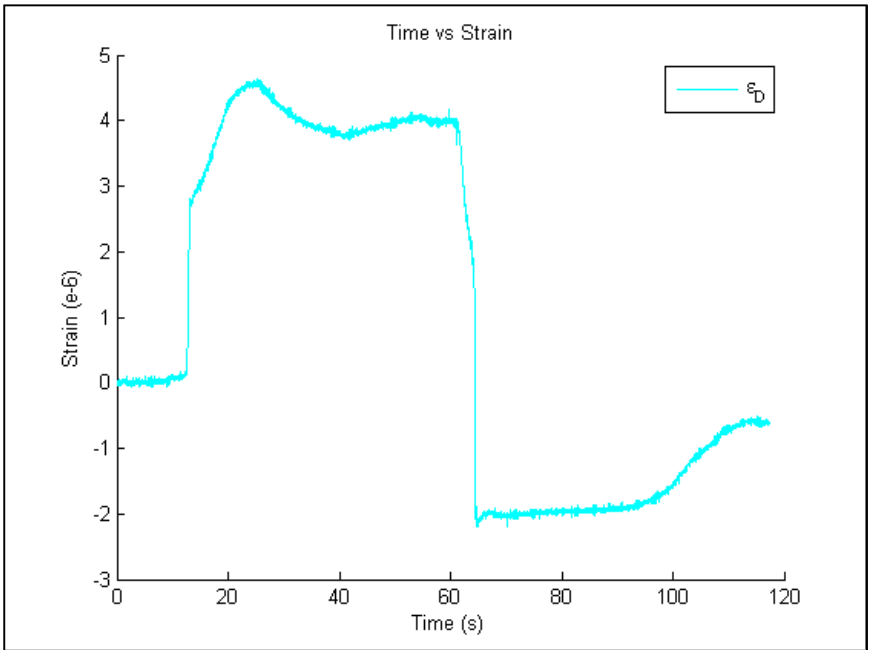

Figure 58. ε_D Response

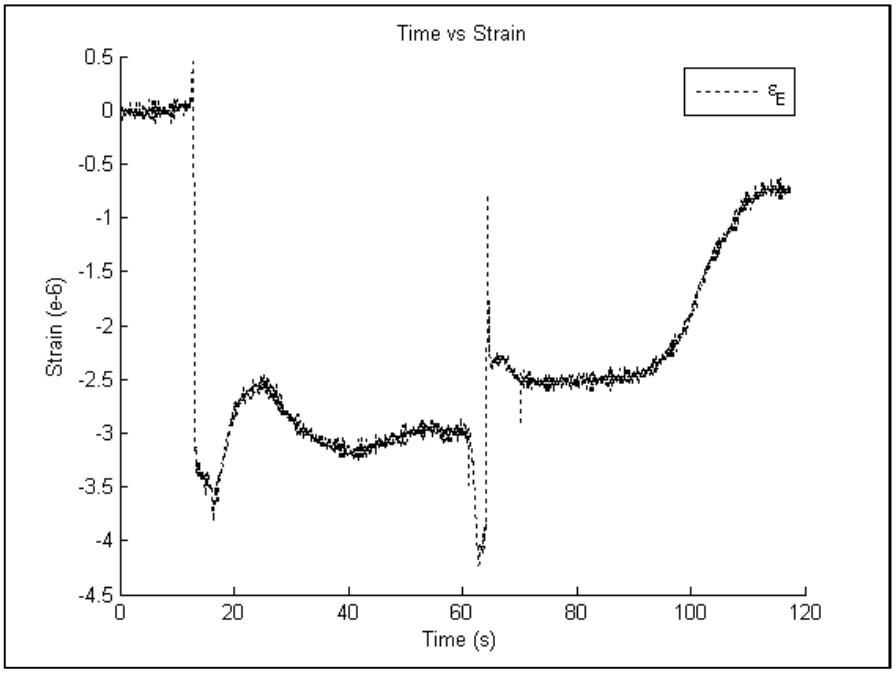

Figure 59. ε_E Response

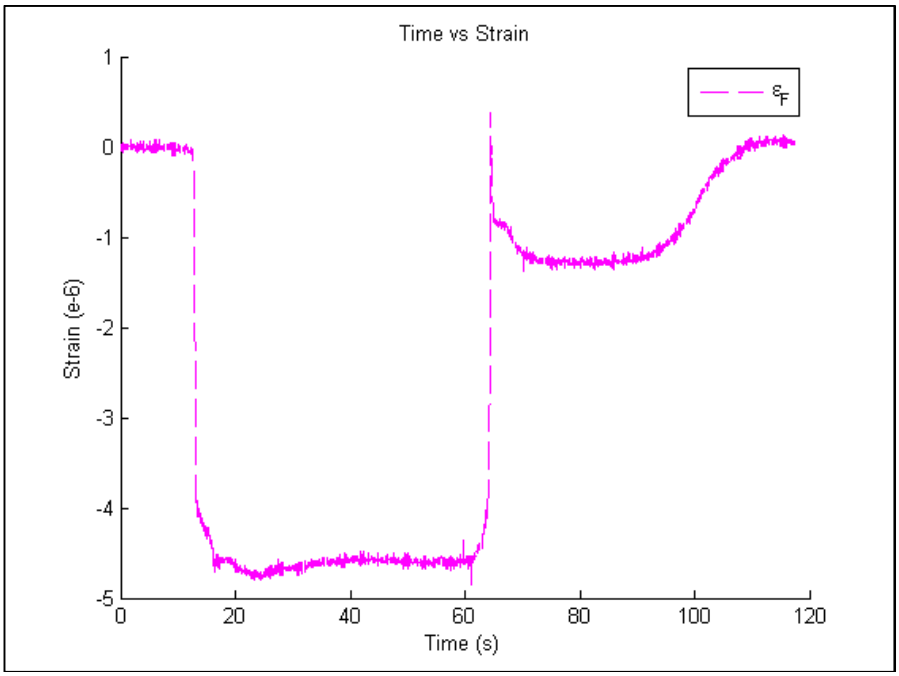

Figure 60. ε_F Response

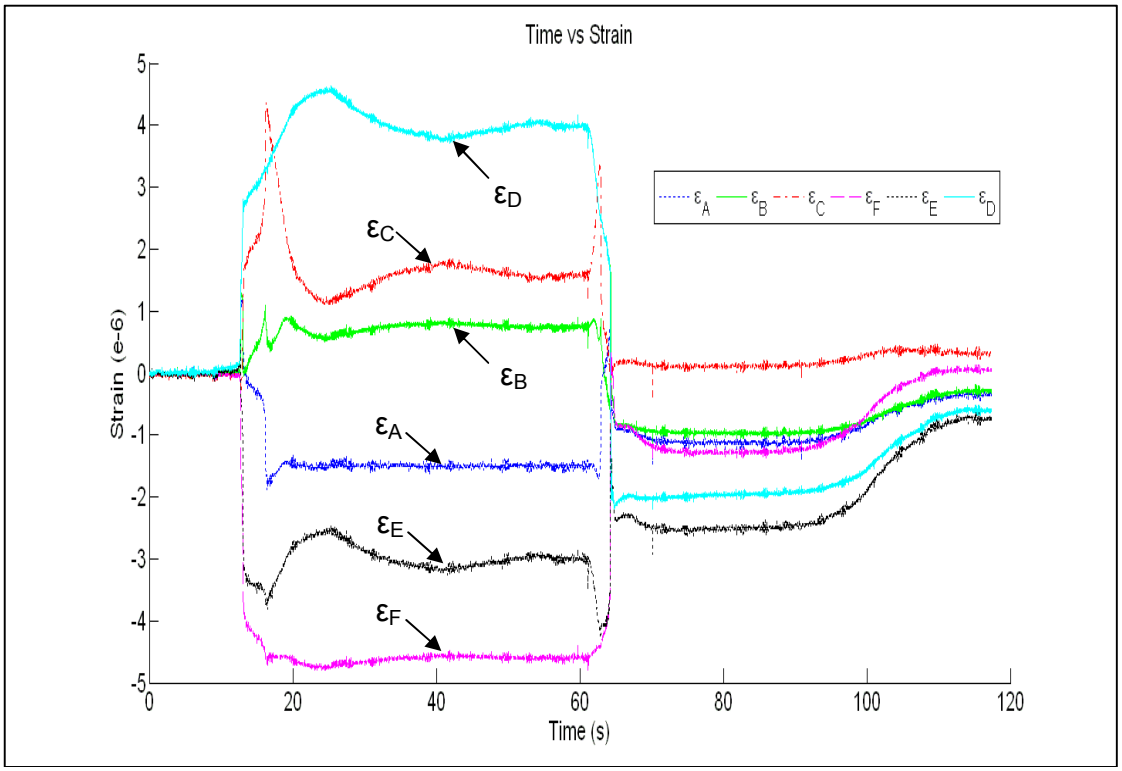

Figure 61. Combining Results for Strains

From the preceding group of figures, the following trend could be observed generally. At about 15 sec., the strain values ε_A, and ε_D started to increase sharply while strain values ε_C and ε_F decreased sharply as the fluid started to fill up the duct. Between 20 sec to 60 sec, the strain values were oscillating about some equilibrium point as the flow approaches steady state. At about 60 sec, the pump was switched off intentionally to observe changes in the results. The strain values decreased sharply before damping out as the flow slowed down from 60 sec. onwards. The decay of ε_D and ε_F were the greatest.

The strain values (ε_A and ε_C) from the gage at center of the plate were smaller than the strain values (ε_D and ε_F) from the gage nearer to the boundary in terms of magnitude, as expected. Comparing the strains along x-axis and y-axis, the magnitudes at each gage were different in signs. This was due to the uneven surface of the test plate where local warping and kinking existed.

Lastly, results across the five runs were consistent, illustrating the repeatability of the experiment.

2. Comparison to Computational Results

Strain data from the previous FSI computational modeling of the baseline case are shown from Figures 62 to 65 for comparison.

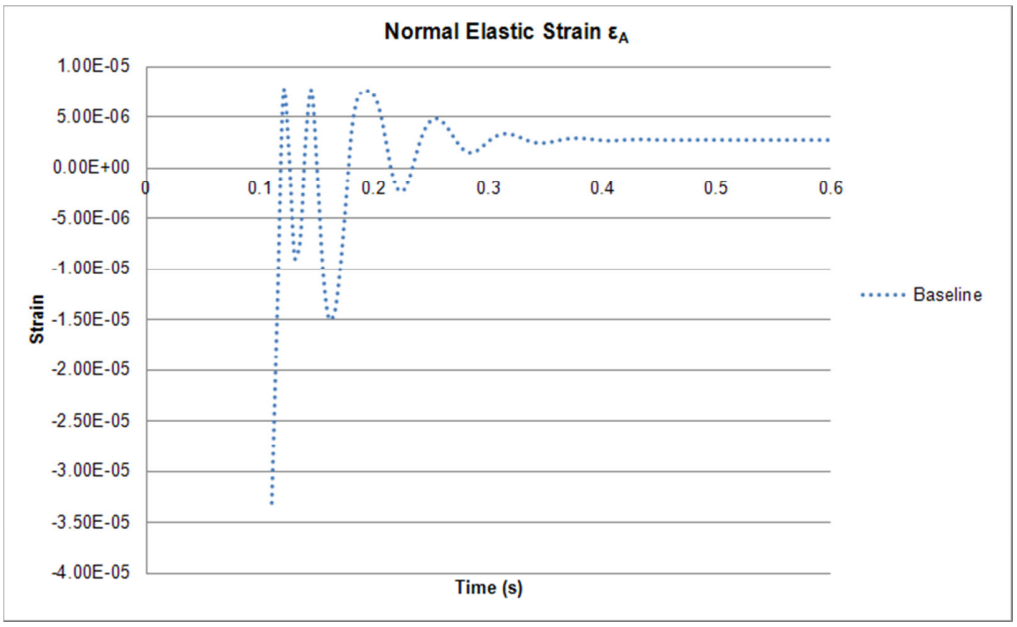

Figure 62. ε_A Response from Computational Modeling of Baseline Case

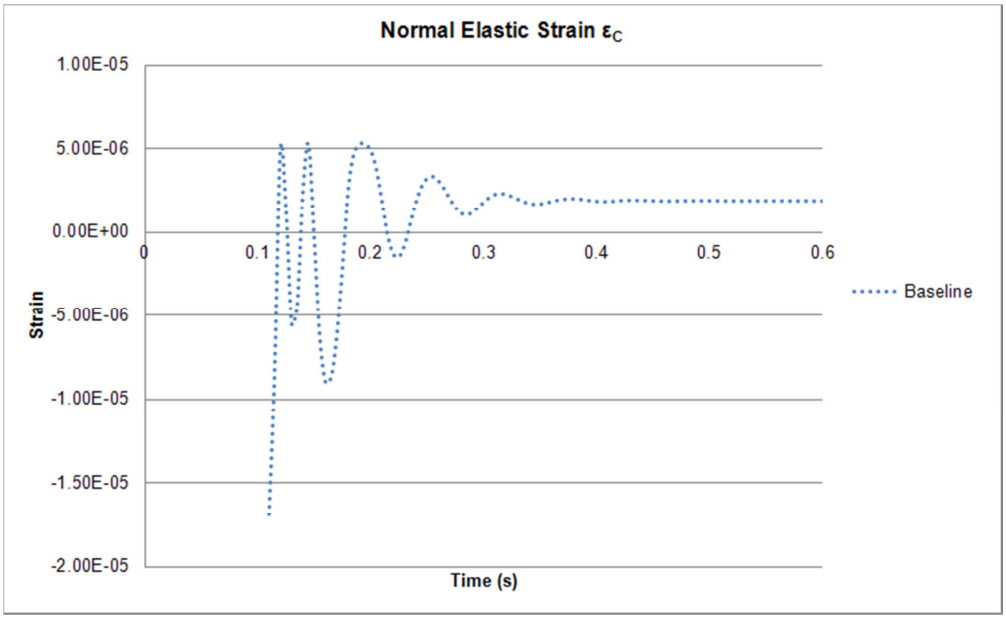

Figure 63. ε_C Response from Computational Modeling of Baseline Case

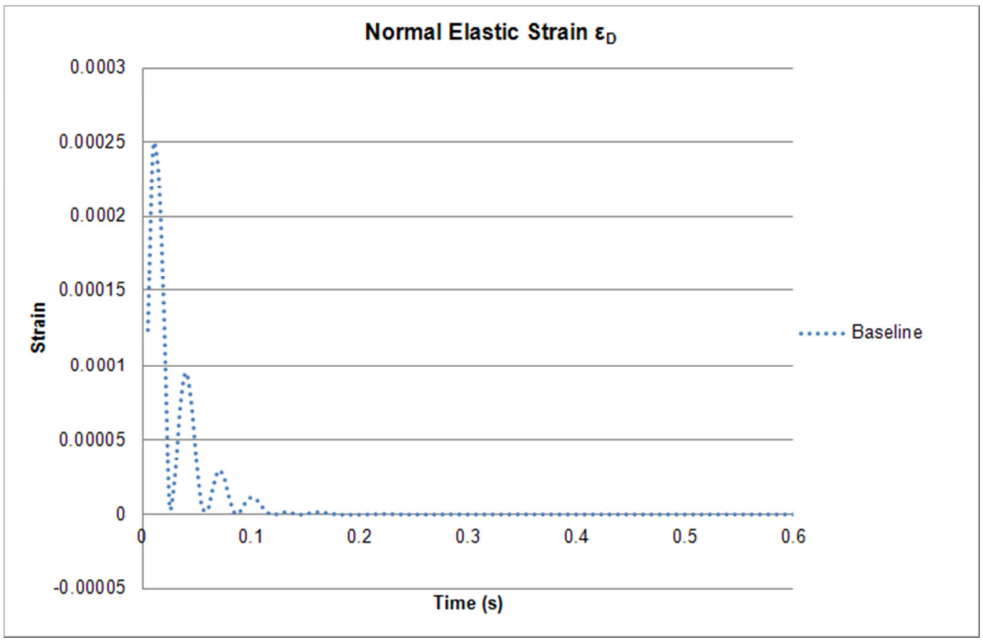

Figure 64. ε_D Response from Computational Modeling of Baseline Case

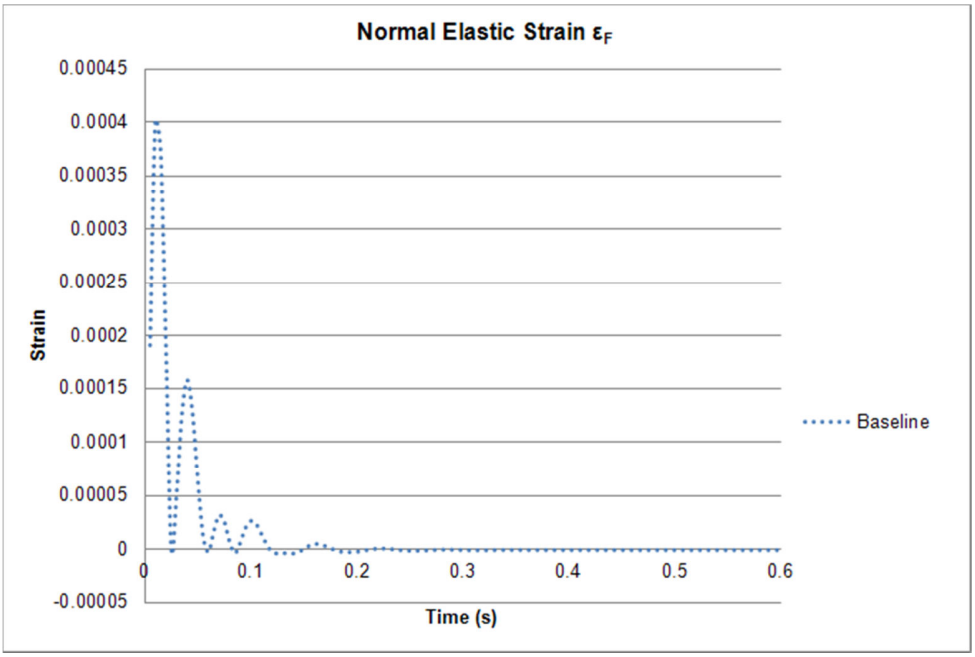

Figure 65. ε_F Response from Computational Modeling of Baseline Case

From the comparison between the experimental strain values and strain values from the computational modeling of the baseline case, it was observed that the order of magnitude for the strain values differed by about $1x10^{-1}$. Because pressures and/or inlet and outlet velocities could not be measured, more quantitative comparison could not be made. In addition, for ε_C and ε_F, the trend of response from the experiment was reasonably similar as compared to the computational values.

To explore the possibility of creating larger deflections on the test plate, the current model was modified and simulated in ANSYS for analysis. The fluid body was lengthened for in the -Z direction above the test plate in an attempt to create a swirling motion in a cavity, as shown in Figure 66. Two models with extensions of 0.102m and 0.203m were simulated, respectively. A sample velocity vectors plot at 0.03 sec was illustrated in Figure 67.

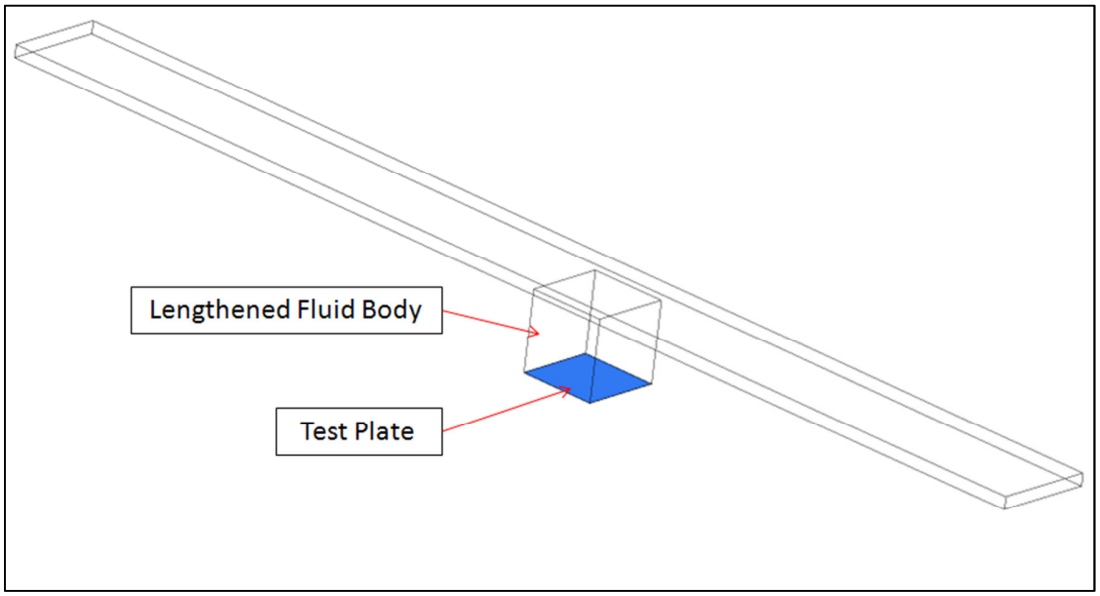

Figure 66. Modified Model for Simulation

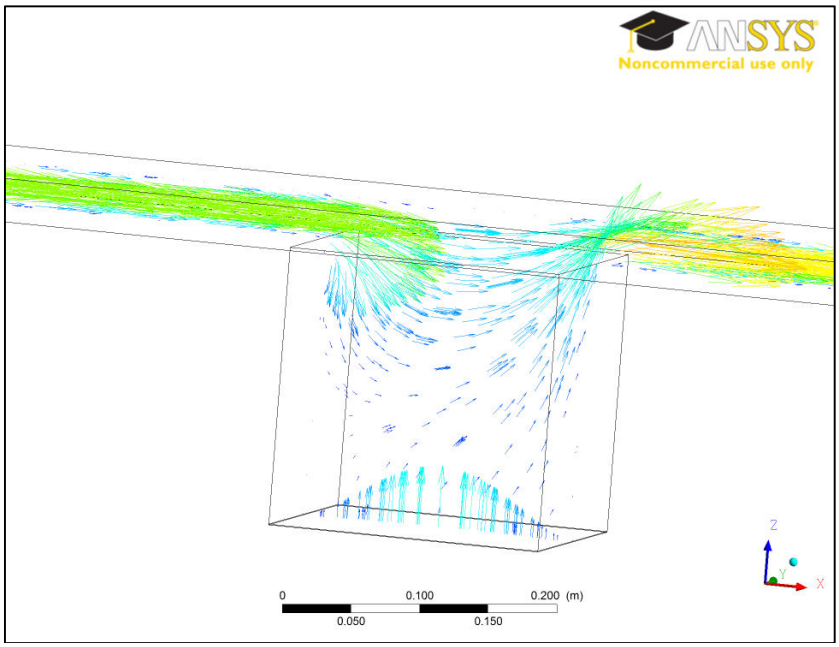

Figure 67. Velocity Vector Plot of Modified Model

As shown in Figure 67, swirling motion did occur in the fluid body inside the cavity box. However, as illustrated in Figures 68 to 71, an examination of the

strain values at the test plate did not show significant increases in magnitude. Further investigations would be necessary to verify these results.

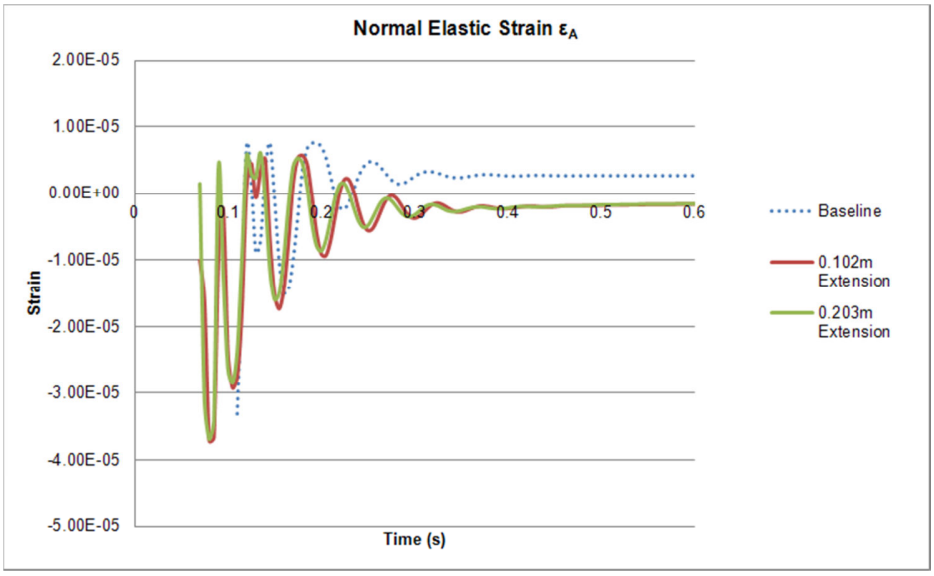

Figure 68. Comparing ε_A Responses

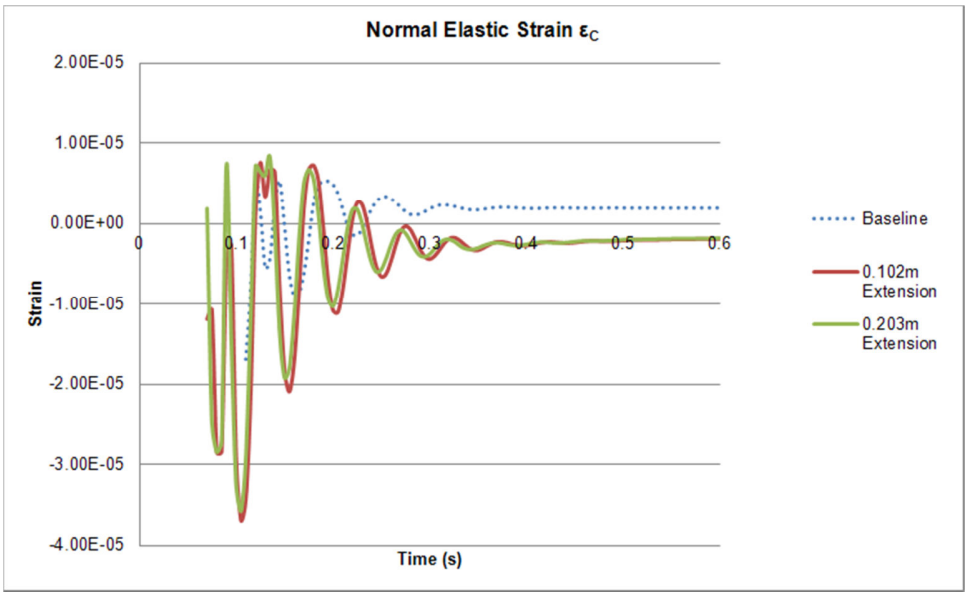

Figure 69. Comparing ε_C Responses

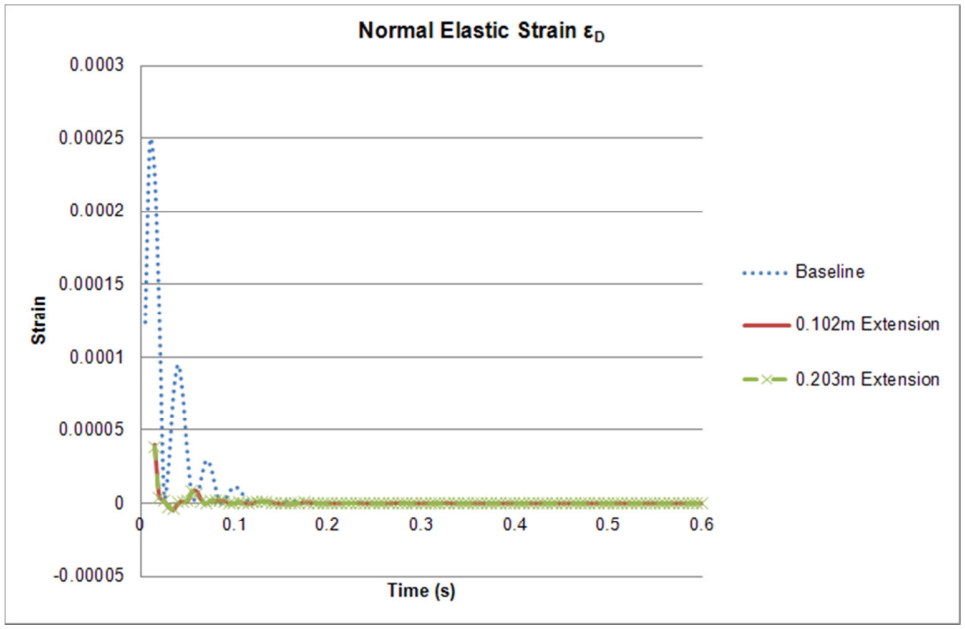

Figure 70. Comparing ε_D Responses

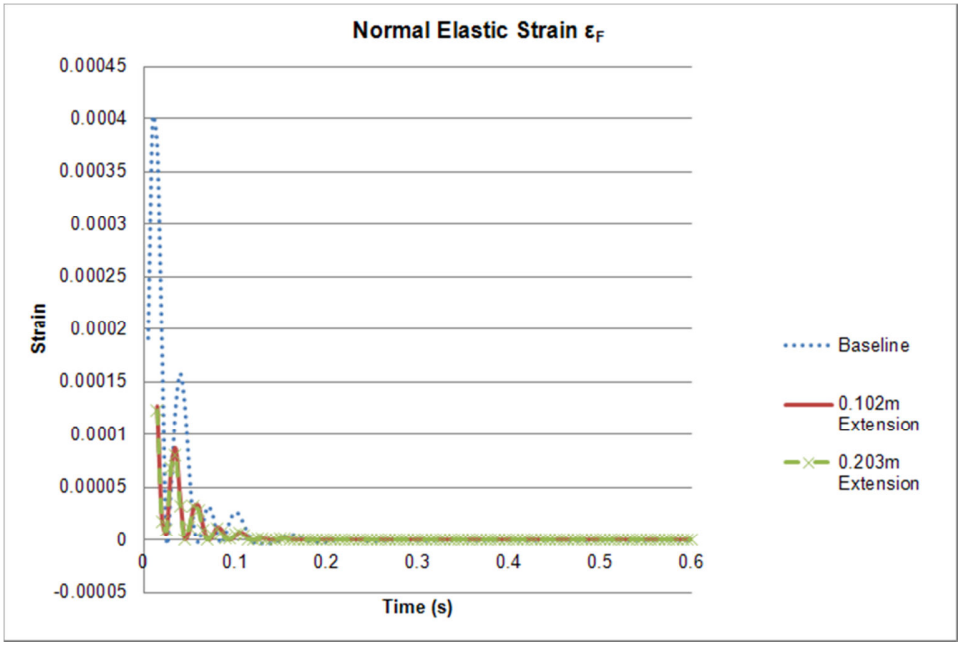

Figure 71. Comparing ε_F Responses

THIS PAGE INTENTIONALLY LEFT BLANK

V. CONCLUSIONS AND RECOMMENDATIONS

In this study, a new experimental facility was designed and developed for the investigation of FSI effect between a metal plate and fully developed laminar flow through a duct. Appropriate dimensions of the duct were obtained through a series of modeling and simulations. The construction of the facility was carried out after a careful selection of materials. The experiment was performed and strain data were collected. As a parametric study, fully coupled computational simulations were conducted to understand the transient response of the metal plate under FSI conditions. From the study, it was found that the magnitude of displacement, acceleration, pressure and velocity at the interface increased with inlet velocity. FSI effect was also observed to decrease as density and Young's Modulus increased.

Results from the experiments proved that the facility developed was capable of maintaining constant flow through the duct when operating with a fluid of high viscosity and high reproducibility of results.

An additional computational study was conducted to examine the likelihood of generating larger deflections by including a cavity box above the test plate. Results of the study showed that a swirling motion occurred in the fluid body in the cavity box as flow past through, but it did not increase deflection of the test plate. This could be verified in further investigations.

Other future studies could include more measurement techniques to investigate other critical FSI parameters such as displacement, velocity, fluid pressure and frequency. For example, using non-contact inductive distance sensors or digital correlation technique for displacement measurement and differential pressure sensors for the assessment of fluid pressure and velocity. Investigations with other plate materials, different plate, other duct geometries

and fluids with different viscosities could be conducted to gain more insight into the FSI effect, hence building a database of results that could be easily validated and verified.

LIST OF REFERENCES

[1] E. H. Dowell and K. C. Hall, “Modeling of fluid-structure interaction,” *Annual Review of Fluid Mechanics*, vol. 33, iss. 1, pp. 445–490, 2001.

[2] Y. W. Kwon and P. K. Fox, “Underwater shock response of a cylinder subjected to a side on explosion,” *Computers and Structures*, vol. 48 iss. 4 pp. 637–646, 1993.

[3] Y. W. Kwon, J. K. Bergensen and Y. S. Shin, “Effect of surface coatings on cylinders exposed to underwater shock,” *Shock and Vibration*, vol. 1 iss. 3, pp. 253–265, 1994.

[4] V. S. Deshpande, A. Heaver and N. A. Fleck, “An underwater shock simulator,” *in Proceedings of Royal Society (London): Mathematical, Physical and Engineering Sciences,* vol. 462, iss: 2067 pp. 1021–1041, 2006.

[5] K. J. Bathe and H. Zhang, “Finite element developments for general fluid flows with structural interactions,” *International Journal For Numerical Methods in Engineering*, vol. 60, iss. 1, pp. 213–232, 2004.

[6] L. Gaul and W. Wenzel, “A coupled symmetric BE-FE method for acoustic fluid-structure interaction,” *Engineering Analysis With Boundary Elements*, vol. 26, iss. 7, pp. 629–636, 2002.

[7] J. Sarrate, A. Huerta and J. Donea, “Arbitrary Lagrangian-Eulerian formulation for fluid-rigid body interaction,” *Computer Methods Applied Mechanics and Engineering*, vol. 190, iss. 24–25, pp. 3171–3188, 2001.

[8] Y. W. Kwon, “Coupling of Lattice Boltzmann and finite element methods for fluid-structure interaction application,” *Journal of Pressure Vessel Technology*, vol. 130, pp. 011302–1 – 011302–6, 2008.

[9] J. P. Gomes and H. Lienhart, “Experimental study on a fluid-structure interaction reference test case,” *Lecture Notes in Computational Science and Engineering*, vol. 53, pp. 356–370, 2006.

[10] S. M. Soedal and W. Sodel, “On the free and forced vibration of a plate supporting a freely sloshing surface liquid,” *Journal of Sound and Vibrations*, vol. 171, iss. 2, pp. 159–171, 1994.

[11] M. K. Kwak, “Hydroelastic vibration of rectangular plates,” *Journal of Applied Mechanics,* vol. 63, pp. 110–115, 1996.

[12] D. Zhou and Y. K. Cheung, “Vibration of vertical rectangular plate in contact with water,” *Earthquake Engineering and Structural Dynamics*, vol. 29, iss. 5, pp. 693–710, 2000.

[13] K. Wang, R. J. Hosking and F. Milinazzo, “Time-dependent response of a floating viscoelastic plate to an impulsively started moving load,” *Journal of Fluid Mechanics*, vol. 521, pp. 319–342, 2004.

[14] W. Zhang, A. Wang, N. Vlahopoulos and K. Wu, “High-frequency vibration analysis of thin elastic plates under heavy fluid loading by an energy finite element formulation,” *Journal of Sound and Vibrations*, vol. 263, iss. 1, pp. 21–6, 2003.

INITIAL DISTRIBUTION LIST

1. Defense Technical Information Center
   Ft. Belvoir, Virginia

2. Dudley Knox Library
   Naval Postgraduate School
   Monterey, California

3. Young W. Kwon
   Naval Postgraduate School
   Monterey, California

4. Jarema M. Didoszak
   Naval Postgraduate School
   Monterey, California

5. Chee Chew Wong
   Singapore Technologies Kinetics Ltd
   Singapore

6. Tat Soon Yeo
   Temasek Defence Systems Institute, National University of Singapore
   Singapore

7. Lai Poh Tan
   Temasek Defence Systems Institute, National University of Singapore
   Singapore